The Pendulum

a case study in physics

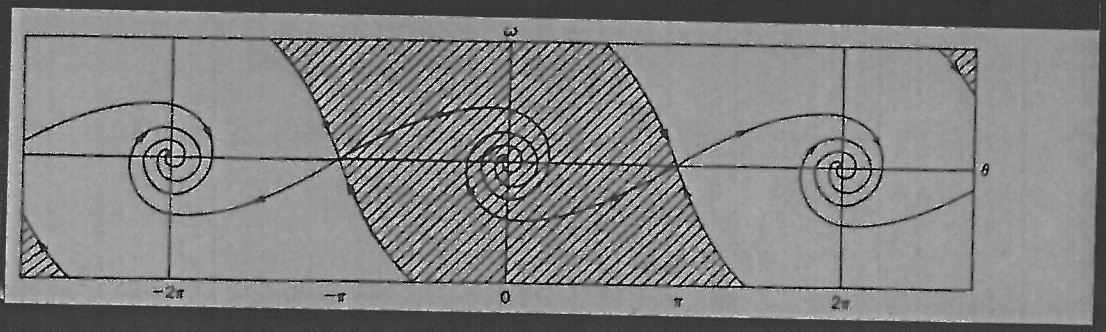

GREGORY L. BAKER • JAMES A. BLACKBURN

Contents

2 Pendulums somewhat simple

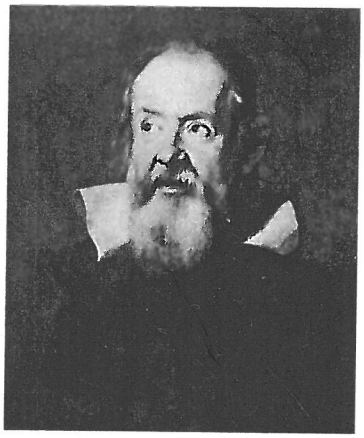

Fig. 2.1
Portrait of Galileo. ©Bettmann/Corbis/Magma.

Fig. 2.2
Cathedral at Pisa. The thin vertical wire indicates a hanging chandelier.

There are many kinds of pendulums. In this chapter, however, we introduce a simplified model; the small amplitude, linearized pendulum. For the present, we ignore friction and in doing so obviate the need for energizing the pendulum through some forcing mechanism. Our initial discussion will therefore assume that the pendulum's swing is relatively small; and this approximation allows us to linearize the equations and readily determine the motion through solution of simplified model equations. We begin with a little history.

2.1 The beginning

Probably no one knows when pendulums first impinged upon the human consciousness. Undoubtedly they were objects of interest and decoration after humankind learnt to attend routinely to more basic needs. We often associate the first scientific observations of the pendulum with Galileo Galilei (1564–1642; Fig. 2.1).

According to the usual story (perhaps apocryphal), Galileo, in the cathedral at Pisa, Fig. 2.2 observed a lamplighter push one of the swaying pendular chandeliers. His earliest biographer Viviani suggests that Galileo then timed the swings with his pulse and concluded that, even as the amplitude of the swings diminished, the time of each swing was constant. This is the origin of Galileo's apparent discovery of the approximate isochronism of the pendulum's motion. According to Viviani these observations were made in 1583, but the Galileo scholar Stillman Drake (Drake 1978) tells us that guides at the cathedral refer visitors to a certain lamp which they describe as "Galileo's lamp," a lamp that was not actually installed until late in 1587. However, there were undoubtedly earlier swaying lamps. Drake surmises that Galileo actually came to the insight about isochronism in connection with his father's musical instruments and then later, perhaps 1588, associated isochronism with his earlier pendulum observations in the cathedral. However, Galileo did make systematic observations of pendulums in 1602. These observations confirmed only approximately his earlier conclusion of isochronism of swings of differing amplitude. Erlichson (1999) has argued that, despite the nontrivial empirical evidence to the contrary, Galileo clung to his earlier conclusion,

in part, because he believed that the universe had been ordered so that motion would be simple and that there was "no reason" for the longer path to take a longer time than the shorter path. While Galileo's most famous conclusion about the pendulum has only partial legitimacy, its importance resides (a) in it being the first known scientific deduction about the pendulum, and (b) in the fact that the insight of approximate isochronism is part of the opus of a very famous seminal character in the history of physical science. In these circumstances, the pendulum begins its history as a significant model in physical science and, as we will see, continues to justify its importance in science and technology during the succeeding centuries.

2.2 The simple pendulum

The simple pendulum is an idealization of a real pendulum. It consists of a point mass, m, attached to an infinitely light rigid rod of length l that is itself attached to a frictionless pivot point. See Fig. 2.3. If displaced from its vertical equilibrium position, this idealized pendulum will oscillate with a constant amplitude forever. There is no damping of the motion from friction at the pivot or from air molecules impinging on the rod. Newton's second law, mass times acceleration equals force, provides the equation of motion:

$$ml\frac{d^2\theta}{dt^2} = -mg\sin\theta, \tag{2.1}$$

where θ is the angular displacement of the pendulum from the vertical position and g is the acceleration due to gravity. Equation (2.1) may be simplified if we assume that amplitude of oscillation is small and that $\sin\theta \approx \theta$. We use this *linearization* approximation throughout this chapter. The modified equation of motion is

$$\frac{d^2\theta}{dt^2} + \frac{g}{l}\theta = 0. \tag{2.2}$$

The solution to Eq. (2.2) may be written as

$$\theta = \theta_0 \sin(\omega t + \phi_0), \tag{2.3}$$

where θ_0 is the angular amplitude of the swing,

$$\omega = \sqrt{\frac{g}{l}} \tag{2.4}$$

is the angular frequency, and ϕ_0 is the initial phase angle whose value depends on how the pendulum was started—its initial conditions. The period of the motion, *in this linearized approximation*, is given by

$$T = 2\pi\sqrt{\frac{l}{g}}, \tag{2.5}$$

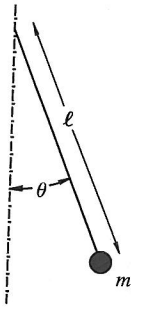

Fig. 2.3
The simple pendulum with a point mass bob.

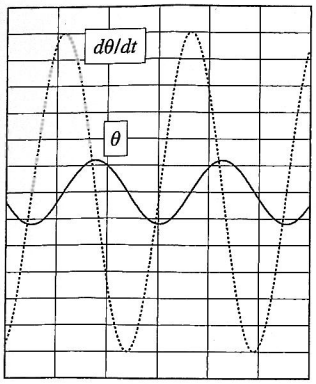

Fig. 2.4
Time series for the angular displacement θ and the angular velocity, $\dot{\theta}$.

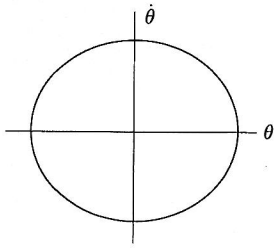

Fig. 2.5
Phase plane diagram. As time increases the phase point travels around the ellipse.

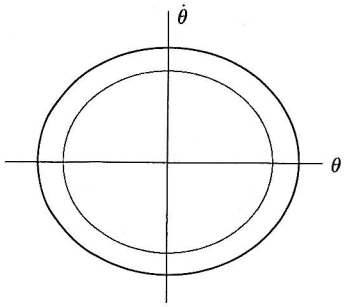

Fig. 2.6
Phase orbits for pendulums with different energies, E_1 and E_2.

which is a constant for a given pendulum, and therefore lends support to Galileo's conclusion of isochronism.

The dependence of the period on the geometry of the pendulum and the strength of gravity has very interesting consequences which we will explore. But for the moment we consider further some of the mathematical relationships. Figure 2.4 shows the angular displacement $\theta = \theta_0 \sin(\omega t + \phi_0)$ and the angular velocity $\dot{\theta} = \theta_0 \omega \cos(\omega t + \phi_0)$, respectively, as functions of time. We refer to such graphs as time series. The displacement and velocity are 90 degrees out of phase with each other and therefore when one quantity has a maximum absolute value the other quantity is zero. For example, at the bottom of its motion the pendulum has no angular displacement yet its velocity is greatest.

The relationship between angle and velocity may be represented graphically with a *phase plane diagram.* In Fig. 2.5 angle is plotted on the horizontal axis and angular velocity is plotted on the vertical axis. As time goes on, a point on the graph travels around the elliptically shaped curve. In effect, the equations for angle and angular velocity are considered to be parametric equations for which the parameter is proportional to time. Then the *orbit* of the *phase trajectory* is the ellipse

$$\frac{\theta^2}{\theta_0^2} + \frac{\dot{\theta}^2}{(\omega\theta_0)^2} = 1. \tag{2.6}$$

Since the motion has no friction nor any forcing, energy is conserved on this phase trajectory. Therefore the sum of the kinetic and potential energies at any time can be shown to be constant as follows. In the linearized approximation,

$$E = \frac{1}{2} ml^2 \dot{\theta}^2 + \frac{1}{2} mgl\theta^2 \tag{2.7}$$

and, using Eqs. (2.3) and (2.4), we find that

$$E = \frac{1}{2} mgl\theta_0^2, \tag{2.8}$$

which is the energy at maximum displacement.

The *phase plane* is a useful tool for the display of the dynamical properties of many physical systems. The linearized pendulum is probably one of the simplest such systems but even here the phase plane graphic is helpful. For example, Eq. (2.6) shows that the axes of the ellipse in Fig. 2.5 are determined by the amplitude and therefore the energy of the motion. A pendulum of smaller energy than that shown would exhibit an ellipse that sits inside the ellipse of the pendulum of higher energy. See Fig. 2.6. Furthermore the two ellipses would never intersect because such intersection implies that a pendulum can jump from one energy to another without the agency of additional energy input. This result leads to a more general conclusion called the *no-crossing theorem*; namely, that orbits in phase space never cross. See Fig. 2.7.

Why should this be so? Every orbit is the result of a deterministic equation of motion. Determinism implies that the orbit is well defined and that there would be no circumstance in which a well determined particle would arrive at some sort of ambiguous junction point where its path would be in doubt. (Later in the book we will see *apparent* crossing points but these false crossings are the result of the system arriving at the same phase coordinates at *different* times.)

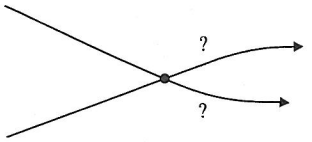

Fig. 2.7
If two orbits in phase space intersect, then it is uncertain which orbit takes which path from the intersection. This uncertainty violates the deterministic basis of classical mechanics.

We introduce one last result about orbits in the phase plane. In Fig. 2.6 there are phase trajectories for two pendulums of different energy. Now think of a large collection of pendulums with energies that are between the two trajectories such that they have very similar, but not identical, angles and velocities. This cluster of pendulums is represented by a set of many *phase points* such that they appear in the diagram as an approximately solid block between the original two trajectories. As the group of pendulums executes their individual motions the set of phase points will move between the two ellipses in such a way that the area defined by the boundaries of the set of points is preserved. This preservation of *phase area*, known as Liouville's theorem (after Joseph Liouville (1809–1882)) is a consequence of the conservation of energy property for each pendulum. In the next chapter we will demonstrate how such areas decrease when energy is lost in the pendulums. But for now let us show how phase area conservation is true for the very simple case when $\theta_0 = 1, \phi = 0$, and $\omega = 1$. In this special case, the ellipses becomes circles since the axes are now equal. See Fig. 2.8. A block of points between the circles is bounded by a small polar angle interval $\Delta\alpha$, in the phase space, that is proportional to time. Each point in this block rotates at the same rate as the motion of its corresponding pendulum progresses. Therefore, after a certain time, all points in the original block have rotated, by the same polar angle, to new positions again bounded by the two circles. Clearly, the size of the block has not changed, as we predicted.

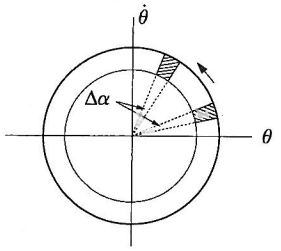

Fig. 2.8
Preservation of area for conservative systems. A block of phase points keeps its same area as time advances.

The motion of the pendulum is an obvious demonstration of the alternating transformation of kinetic energy into potential energy and the reverse. This phenomenon is ubiquitous in physical systems and is known as *resonance*. The pendulum resonates between the two states (Miles 1988*b*). Electrical circuits in televisions and other electronic devices resonate. The terms *resonate* and *resonance* may also refer to a sympathy between two or more physical systems, but for now we simply think of resonance as the periodic swapping of energy between two possible formats.

We conclude this section with the introduction of one more mathematical device. Its use for the simple pendulum is hardly necessary but it will be increasingly important for other parts of the book. Almost two hundred years ago, the French mathematician Jean Baptiste Fourier (1768–1830) showed that periodic motion, whether that of a simple sine wave like our pendulum, or more complex forms such as the triangular wave that characterizes the horizontal sweep on a television tube, are simple linear sums of sine and cosine waves now known as *Fourier Series*. That is, let $f(t)$

be a periodic function such that $f(t) = f(t + (2\pi)/\omega_0)$, where $T = (2\pi)/\omega_0$ is the basic periodicity of the motion. Then Fourier's theorem says that this function can be expanded as

$$f(t) = \sum_{n=1}^{\infty} b_n \cos n\omega_0 t + \sum_{n=1}^{\infty} c_n \sin n\omega_0 t + d, \tag{2.9}$$

where the coefficients b_n and c_n give the strength of the respective cosine and sine components of the function and d is constant. The coefficients are determined by integrating $f(t)$ over the fundamental period, T. The appropriate formulas are

$$\begin{aligned} d &= \frac{1}{T}\int_{-T/2}^{T/2} f(t)\,dt, \quad b_n = \frac{1}{T}\int_{-T/2}^{T/2} f(t)\cos n\omega_0 t\,dt, \\ c_n &= \frac{1}{T}\int_{-T/2}^{T/2} f(t)\sin n\omega_0 t\,dt. \end{aligned} \tag{2.10}$$

These Fourier coefficients are sometimes portrayed crudely on stereo equipment as dancing bars in a dynamic bar chart that is meant to portray the strength of the music in various frequency bands.

The use of complex numbers allows Fourier series to be represented more compactly. Then Eqs. (2.9) and (2.10) become

$$f(t) = \sum_{n=-\infty}^{n=\infty} a_n e^{in\omega_0 t}, \quad \text{where } a_n = \frac{\omega_0}{2\pi}\int_{-\pi/\omega_0}^{\pi/\omega_0} f(t)e^{-in\omega_0 t}dt. \tag{2.11}$$

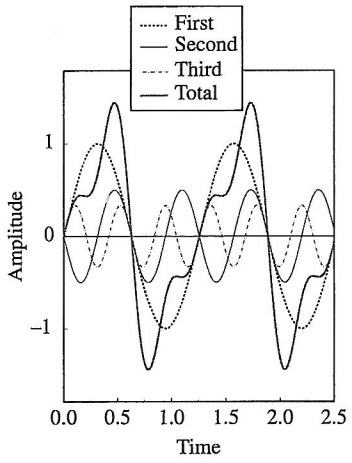

Fig. 2.9
The first three Fourier components of the sawtooth wave. The sum of these three components gives an approximation to the sawtooth shape.

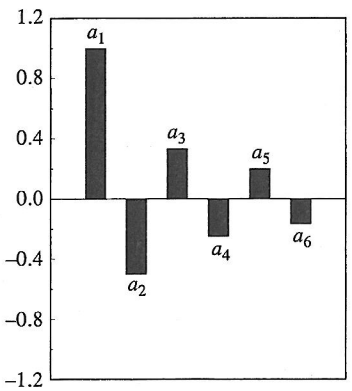

Fig. 2.10
The amplitudes of several Fourier components for the sawtooth waveform.

Example 1 *Consider the time series known as the "sawtooth," $f(t) = t$ when $-\frac{T}{2} < t < \frac{T}{2}$, with the pattern repeated every period, T. Using Eq. (2.11) it can be shown that*

$$a_n = 0 \text{ for } n = 0,$$

$$a_n = \tfrac{1}{in\omega_0} \text{ for } n = \text{odd integer, and}$$

$$a_n = \tfrac{-1}{in\omega_0} \text{ for } n = \text{even integer.}$$

Through substitution and appropriate algebraic manipulation we obtain the final result:

$$f(t) = \frac{2}{\omega_0}\left[\sin\omega_o t - \frac{1}{2}\sin 2\omega_0 t + \frac{1}{3}\sin 3\omega_0 t + \cdots\right]. \tag{2.12}$$

The original function and the first three frequency components are shown in Figs. 2.9 and 2.10.

The time variation of the motion of the linearized version of the simple pendulum is just that of a single sine or cosine wave and therefore one frequency, the resonant frequency ω_0 is present in that motion. Obviously, the machinery of the Fourier series is unnecessary to deduce that result.

However, we now have it available as a tool for more complex periodic phenomena.

Fourier, like other contemporary French mathematicians, made his contribution to mathematics during a turbulent period of French history. He was active in politics and as a student during the "Terror" was arrested although soon released. Later when Napoleon went to Egypt, Fourier accompanied the expedition and coauthored a massive work on every possible detail of Egyptian life, *Description de l'Egypt*. This is multivolume work included nine volumes of text and twelve volumes of illustrations. During that same campaign, one of Napoleon's engineers uncovered the Rosetta Stone, so-named for being found near the Rosetta branch of the Nile river in 1799. The significance of this find was that it led to an understanding of ancient Egyptian Hieroglyphics. The stone, was inscribed with the same text in three different languages, Greek, demotic Egyptian, and Hieroglyphics. Only Greek was understood, but the size and the juxtaposition of the texts allowed for the eventual understanding of Hieroglyphics and the ability to learn much about ancient Egypt. In 1801, the victorious British, realizing the significance of the Rosetta stone, took it to the British Museum in London where it remains on display and is a popular artifact. Much later, the writings from the Rosetta Stone become the basis for translating the hieroglyphics on the Rhind Papyrus and the Golenischev Papyrus; these two papyri provide much of our knowledge of early Egyptian mathematics. The French Egyptologist Jean Champollion (1790–1832) who did much of the work in the translation of Hieroglyphics is said to have actually met Fourier when the former was only 11 years old, in 1801. Fourier had returned from Egypt with some papyri and tablets which he showed to the boy. Fourier explained that no one could read them. Apparently Champollion replied that he would read them when he was older—a prediction that he later fulfilled during his brilliant career of scholarship (Burton 1999). After his Egyptian adventures, Fourier concentrated on his mathematical researches. His 1807 paper on the idea that functions could be expanded in trigonometric series was not well received by the Academy of Sciences of Paris because his presentation was not considered sufficiently rigorous and because of some professional jealousy on the part of other Academicians. But eventually Fourier was accepted as a first rate mathematician and, in later life, acted a friend and mentor to a new generation of mathematicians (Boyer and Merzbach 1991).

We have now developed the basic equations for the linearized, undamped, undriven, very simple harmonic pendulum. There are an amazing number of applications of even this simple model. Let us review some of them.

2.3 Some analogs of the linearized pendulum

2.3.1 The spring

The linearized pendulum belongs to a class of systems known as harmonic oscillators. Probably the most well known realization of a harmonic

oscillator is that of a mass suspended from a spring whose restoring force is proportional to its stretch. That is

$$F_{\text{restoring}} = -kx, \tag{2.13}$$

where k is the spring constant and rate at which the spring's response increases with stretch, x. This force law was discovered by Robert Hooke in 1660. The equation of motion

$$m\frac{d^2x}{dt^2} + kx = 0 \tag{2.14}$$

is identical in form to that of the linearized pendulum and therefore its solution has corresponding properties: single frequency periodic motion, resonance, energy conservation and so forth. A schematic drawing of the spring and a graph of its force law are shown in Fig. 2.11.

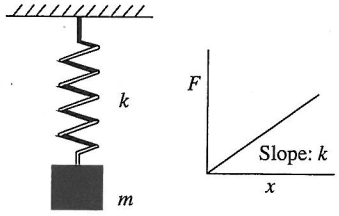

Fig. 2.11
A mass hanging from a spring. The graph shows the dependence of the extension of the spring on the force (weight). The linear relationship is known as "Hooke's law."

The functional dependence of the spring force (Eq. (2.13)) can be viewed more generally. Consider any force law that is derived from a smooth potential energy $V(x)$; that is $F(x) = -dV/dx$. The potential energy may be expanded in a power series about some arbitrary position x_0 which, for simplicity, we will take as $x_0 = 0$. Then the series becomes

$$V(x) = V(0) + V'(0)x + \frac{1}{2}V''(0)x^2 + \frac{1}{6}V'''(0)x^3 + \cdots . \tag{2.15}$$

The first term on the right side is constant and, as the reference point of a potential energy, is typically arbitrary and may be set equal to zero. The second, linear, term contains $V'(0)$ which is the negative of the force at the reference point. Since this reference point is, again typically, chosen to be a point of stable equilibrium where the forces are zero, this second term also vanishes. For the spring, this would be the point where the mass attached to the spring hangs when it is not in motion. Thus, the first nonvanishing term in the series is the quadratic term $\frac{1}{2}V''(0)x^2$ and comparison of it with the spring's restoring force (Eq. 2.13) leads to the identification

$$k = V''(0). \tag{2.16}$$

The spring constant is the second derivative of any smooth potential.

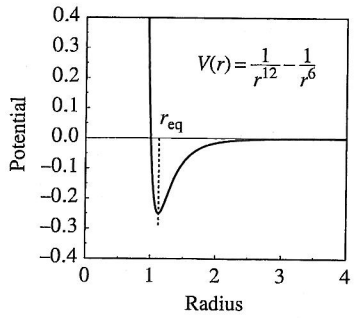

Fig. 2.12
A typical Lennard–Jones potential curve that can effectively model, for example, intermolecular interactions. For this illustration, $a = b = 1$.

Example 2 *The Lennard–Jones potential energy is often used to describe the electrostatic potential energy between two atoms in a molecule or between two molecules. Its functional form is displayed in Fig. 2.12 and is given by the equation*

$$V(r) = \frac{a}{r^{12}} - \frac{b}{r^6}, \tag{2.17}$$

where a and b are constants appropriate to the particular molecule. The positive term describes the repulsion of the atoms when they are too close and the negative term describes the attraction if the atoms stray too far from each other. Hence, the two terms balance at a stable equilibrium point as shown in the figure, $r_{eq} = (\frac{2a}{b})^{1/6}$. *The second derivative of the potential energy may*

be evaluated at r_{eq} to yield the spring constant of the equivalent harmonic oscillator,

$$V''(r_{eq}) = \frac{18b^2}{a}\left(\frac{b}{2a}\right)^{1/3} = k. \tag{2.18}$$

Knowledge of the molecular bond length provides r_{eq} and observation of the vibrational spectrum of the molecule will yield a value for the spring constant, k. With just these two pieces of information, the parameters, a and b of the Lennard–Jones potential energy may be determined.

The linearized pendulum is therefore equivalent to the spring in that they both are simple harmonic oscillators each with a single frequency and therefore a single spectral component. Occasionally we will refer to a pendulum's equivalent oscillator or equivalent spring, and by this terminology we will mean the linearized version of that pendulum.

2.3.2 Resonant electrical circuit

We say that a function $f(t)$ or operator $L(x)$ is linear if

$$\begin{aligned} L(x+y) &= L(x) + L(y) \\ L(\alpha x) &= \alpha L(x). \end{aligned} \tag{2.19}$$

Examples of linear operators include the derivative and the integral. But functions such as $\sin x$ or x^2 are nonlinear. Because linear models are relatively simple, physics and engineering often employ linear mathematics, usually with great effectiveness. Passive electrical circuits, consisting of resistors, capacitors, and inductors are realistically modeled with linear differential equations. A circuit with a single inductor L and capacitor C, is shown in Fig. 2.13. The sum of the voltages measured across each element of a circuit is equal to the voltage provided to a circuit from some external source. In this case, the external voltage is zero and therefore the sum of the voltages across the elements in the circuit is described by the linear differential equation

$$L\frac{d^2q}{dt^2} + \frac{1}{C}q = 0, \tag{2.20}$$

where q is the electrical charge on the capacitor. The form of Eq. (2.20) is exactly that of the linearized pendulum and therefore a typical solution is

$$q = q_0 \sin(\omega t + \phi), \tag{2.21}$$

where the resonant frequency depends on the circuit elements:

$$\omega = \sqrt{\frac{1}{LC}}. \tag{2.22}$$

The charge q plays a role analogous to the pendulum's angular displacement θ and the current $i = dq/dt$ in the circuit is analogous to the pendulum's angular velocity, $d\theta/dt$. All the same considerations, about the motion in phase space, resonance, and energy conservation, that previously held

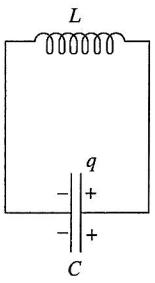

Fig. 2.13
A simple LC (inductor and capacitor) circuit.

for the linearized pendulum, also apply for this simple electrical circuit. In a (q, i) phase plane, the point moves in an elliptical curve around the origin. The charge and current oscillate out of phase with each other. The capacitor alternately fills with positive and negative charge. The voltage across the inductor is always balanced by the voltage across the capacitor such that the total voltage across the circuit always adds to zero as expressed by Eq. (2.20). As with the spring, we will return to this electrical analog with additional complexity. For now, we turn to some applications and complexities of the linearized pendulum.

2.3.3 The pendulum and the earth

From ancient times thinkers have speculated about, theorized upon, calculated, and measured the physical properties of the earth (Bullen 1975). About 900BC, the Greek poet Homer suggested that the earth was a convex dish surrounded by the Oceanus stream. The notion that the earth was spherical seems to have made its first appearance in Greece at the time of Anaximander (610–547BC). Aristotle, the universalist thinker, quoted contemporary mathematicians in suggesting that the circumference of the earth was about 400,000 stadia—one stadium being about 600 Greek feet. Mensuration was not a precise science at the time and the unit of the stadium has been variously estimated as 178.6 meters (olympic stadium), 198.4 m (Babylonian–Persian), 186 m (Italian) or 212.6 m (Phoenician–Egyptian). Using any of these conversion factors gives an estimate that is about twice the present measurement of the earth's circumference, 4.0086×10^4 km. Later Greek thinkers somewhat refined the earlier values. Eratosthenes (276–194BC), Hipparchus (190–125BC), Posidonius (135–51BC), and Claudius Ptolemy (AD100–161) all worked on the problem. However the Ptolemaic result was too low. It is rumored that a low estimate of the distance to India, based on the Ptolemy's result, gave undue encouragement to Christopher Columbus 1500 years later.

In China the astronomer monk Yi-Hsing (AD683–727) had a large group of assistants measure the lengths of shadows cast by the sun and the altitudes of the pole star on the solstice and equinox days at thirteen different locations in China. He then calculated the length L of a degree of meridian arc (earth's circumference/360) as 351.27 li (a unit of the Tang Dynasty) which, with present day conversion, is about 132 km, an estimate that is almost 20% too high.

The pendulum clock, invented by the Dutch physicist and astronomer Christiaan Huygens (1629–1695) and presented on Christmas day, 1657, provided a powerful tool for measurement of the earth's gravitational field, shape, and density. The daily rotation of the earth was, by then, an accepted fact and Huygens, in 1673, provided a theory of centrifugal motion that required the effective gravitational field at the equator to be less than that at the poles. Furthermore, the centrifugal effect should also have the effect of fattening the earth at the equator, thereby further

weakening gravity at the surface near the equator. In 1687 Newton published his universal law of gravity in the *Principia*. It is the existence of the relationship between gravity and the length of the pendulum (Eq. (2.5)), established through the work of Galileo and Huygens, that makes the pendulum a useful tool for the measurement of the gravitational field and therefore a tool to infer the earth's shape and density. The first recorded use of the pendulum in this context is usually attributed to the measurements of Jean Richer, the French astronomer, made in 1672 . Richer (1630–1696) found that a pendulum clock beating out seconds in Paris at latitude 49° North lost about 2(1/2) minutes per day near the equator in Cayenne at 5° North and concluded that Cayenne was further from the center of the earth than was Paris. Newton, on hearing of this result ten years later by accident at a meeting of the Royal Society, used it to refine his theory of the earth's oblateness (Bullen 1975). However, Richer's result also helped lead to the eventual demise of the idea of using a pendulum clock as a reliable timing standard for the measurement of longitude (Matthews 2000).

A clever bit of theory by Pierre Bougeur (1698–1758), a French professor of hydrography and mathematics, allowed the pendulum to be an instrument for estimating the earth's density, σ (Bouguer 1749). In 1735 Bouguer was sent, by the French Academy of Sciences, to Peru, to measure the length of a meridian arc, L near the equator. (A variety of such measurements at different latitudes would help to determine the earth's oblateness.) But while in Peru he made measurements of the oscillations of a pendulum, which in Paris beat out seconds whereas in Quito, (latitude 0.25° South) the period was different. His original memoir is a little confusing as to whether he maintained a constant length pendulum or whether, as his data suggests, he modified the length of the pendulum to keep time with his pendulum clock that he adjusted daily. At any rate, he used the pendulum to measure the gravitational field. But more than this he made measurements of the gravitational field close to sea level and then on top of the Cordilleras mountain range. In this way Bouguer was able to estimate the relative size of the mean density of the earth.

In order to appreciate the cleverness of Bouguer's method, we derive his result. Consider the schematic diagram of the earth with the height increment (the mountain range) shown in Fig. 2.14. The acceleration due to gravity at the surface of the earth is readily shown to be

$$g_0 = \frac{GM_E}{a^2} = \frac{4}{3}\pi G\sigma a, \tag{2.23}$$

where a is the earth's radius, σ is the mean density, and G is the universal gravitational constant. Now consider the acceleration due to gravity on the mountain range. There are two effects. First, the gravitational field is reduced by the fact that the field point is further from the center of the earth, and second, the field is enhanced by the gravitational pull of the mountain range. The first effect is found through a simple ratio using Newton's law of gravity, but the second effect is a little more involved and

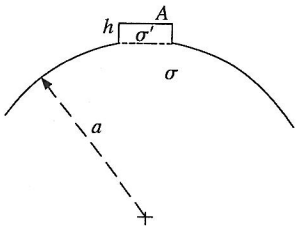

Fig. 2.14
The little "bump" on the earth's surface represents a whole mountain range.

requires the use of a fundamental relation in the theory of gravitational fields; Gauss' law. It is expressed mathematically as

$$\int \mathbf{g} \cdot \mathbf{n}\, dA = 4\pi G \int \sigma\, dV, \tag{2.24}$$

where **g** is the acceleration due to gravity (expressed as a vector) and **n** is the outward unit normal vector. The integral on the left side is calculated over a closed surface and the integral on the right side is a volume integral throughout the inside of the closed surface boundary. Essentially the flux or "amount" of gravitational field coming out of the surface is proportional to the mass contained inside the surface. In the diagram, the mountain range is approximated by a "pill box" with height h and top and bottom areas A. We suppose that h is much less than any lateral dimension and therefore assume that the gravitational field is directed only out of the top and the bottom of the pill box. Then Eq. (2.24) becomes

$$2gA = 4\pi G\sigma' Ah \tag{2.25}$$

or

$$g = 2\pi G\sigma' h, \tag{2.26}$$

where σ' is the density of the mountain range as determined by sampling the local soil materials. With these equations we can now write an expression for the acceleration due to gravity as measured on top of the mountain range:

$$g = \frac{4}{3} G\pi\sigma \frac{a^3}{(a+h)^2} + 2\pi G\sigma' h. \tag{2.27}$$

Since $h \ll a$, the first term on the right can be approximated using the binomial expansion and then the ratio of the two measurements of the gravitational field is found to be

$$\frac{g}{g_0} \approx 1 - \frac{2h}{a} + \frac{3h}{2a}\frac{\sigma'}{\sigma}. \tag{2.28}$$

The two corrections terms on the right side of the equation are the first of several corrections that were eventually incorporated into experiments of this or similar types. The first term $2h/a$ is the so-called *free air* term and the other term is referred to as the *Bouguer* term. The point of Eq. (2.28) is that, with data on the relative accelerations due to gravity, it should be possible to calculate the ratio of the density of the mountainous material to that of the rest of the earth. Bouguer's pendulum measurements convinced him that the earth's mean density was about four times that of the mountains, a ratio not too different from a modern value of 4.7. In Bouguer's own words

> Thus it is necessary to admit that the earth is much more compact below than above, and in the interior than at the surface... Those physicists who imagined a great void in the middle of the earth, and who would have us walk on a kind of very thin crust, can think so no longer. We can make nearly the same objections to

Woodward's theory of great masses of water in the interior. (page 33 of (Bouguer 1749)).

Bouguer's experiment was the first of many of this type. A common variant on the mountain range experiment was to measure the difference in gravitational field at the top and the bottom of a mine shaft. In this case, the extra structure was not just a mountain range but a spherical shell above the radius of the earth to the bottom of the shaft. See Fig. 2.15. An equation similar to Eq. (2.28) holds although the *Bouguer* term must be modified as

$$\frac{g_{\text{top}}}{g_{\text{bottom}}} \approx 1 - 2\frac{h}{a} + 3\frac{h}{a}\frac{\sigma'}{\sigma} \tag{2.29}$$

because of the shape of the spherical shell of density σ', and the radius a is measured from the center of the earth to *bottom* of the mine shaft. Coal mines were widely available in England and the seventh astronomer royal and Lucasian professor of mathematics at Cambridge, George Airy (1801–1892) was one of many to attempt this type of experiment. His early efforts in 1826 and 1828 in Cornwall were frustrated by floods and fire. But much later in 1854 he successfully applied his techniques at a Harton coal-pit in Sunderland and obtained a value for the earth's density of $\sigma = 6.6\,\text{gm/cm}^3$ (Bullen 1975, p. 16).

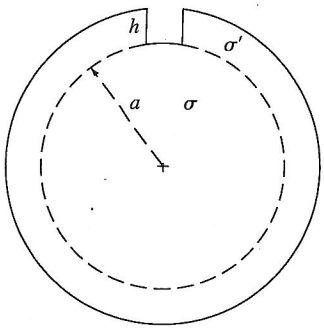

Fig. 2.15
A schematic of the earth with a mine shaft of depth, h.

Pendulum experiments continued to be improved. Von Sterneck explored gravitational fields at various depths inside silver mines in Bohemia and in 1887 invented a four pendulum device. Two pairs of 1/2 second pendulums were placed at right angles. Each pendulum in a given pair oscillated out of phase with its partner, thereby reducing flexure in the support structure that ordinarily contributed a surprising amount of error to measurements. The two mutually perpendicular pairs provided a check on each other. Von Sterneck's values for the mean density of the earth ranged from 5.0 to 6.3 gm/cm^3. The swing of the pendulums in a pair is compared with a calibrated 1/2 second pendulum clock by means of an arrangement of lights and mirrors as observed through a telescope. Because they are slightly out of phase, the gravity pendulum and the clock pendulum eventually get out of phase by a whole period. The number of counts between such "coincidences" is observed and used in calculating the precision of the gravity pendulum period. Accuracies as high as 2×10^{-7} were claimed for the apparatus.

Other types of pendulums have also been used in geological exploration, but they are based upon pendulums that are more involved than the simple pendulum that is the fundamental ingredient of the experiments and equipment described above.

2.3.4 The military pendulum

Since the mid-twentieth century physics has had a strong relationship with the engineering of military hardware. Yet there are precursors to this modern connection. Benjamin Robin (1707–1751), a British mathematician

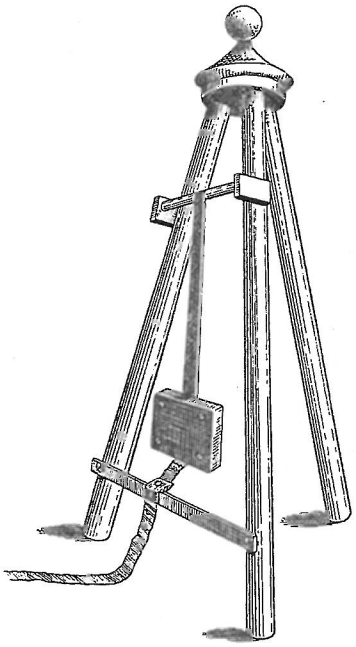

Fig. 2.16
Robin's 1742 ballistic pendulum. (From Taylor (1941) with permission from Dover).

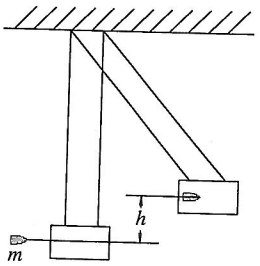

Fig. 2.17
Schematic diagram of the Blackwood ballistic pendulum used in undergraduate laboratories.

and military engineer gave a giant boost to the "modern" science of artillery with the 1742 publication of his book, "New Principles of Gunnery." One of his contributions was a method for determining the muzzle velocity of a projectile; the apparatus is illustrated in Fig. 2.16. (Even today, undergraduate physics majors do an experiment with a version of this method using an apparatus known as the Blackwood ballistic pendulum—Blackwood was a professor of physics in the early twentieth century at the University of Pittsburgh.)

With a relatively modern apparatus a "bullet" is fired into a pendulum consisting of a large wooden bob suspended by several ropes. The projectile is trapped in the bob, causing the bob to pull laterally against the ropes and therefore rise to some measurable height. See Fig. 2.17. Application of the elementary laws of conservation of energy and momentum produce the required value of projectile muzzle velocity.

Here is the simple analysis. Prior to the moment of collision between the projectile of mass m and the pendulum bob of mass M, the projectile has a velocity v. After the collision, the projectile quickly embeds in the bob and imparts a velocity V to the bob. Momentum before and after the collision is preserved so that

$$mv = (M + m)V. \tag{2.30}$$

After the particle is embedded in the bob, the kinetic energy of the combination of projectile and bob thrusts the pendulum outward and upward to a height h. All the kinetic energy is transformed to potential energy and therefore

$$\frac{1}{2}(M + m)V^2 = (M + m)gh. \tag{2.31}$$

Mutual solution of Eqs. (2.30) and (2.31) yields the muzzle velocity of the projectile,

$$v = \frac{M + m}{m}\sqrt{2gh}. \tag{2.32}$$

The beauty of this result is that it bypasses the need to have any sort of measure of the energy lost as the projectile is trapped by the pendulum bob. That lost kinetic energy simply produces heat in the pendulum.

One wonders if the many students who perform this laboratory experiment each year are aware that they are replicating early military research.

2.3.5 Compound pendulum

The model of a simple pendulum requires that all mass be concentrated at a single point. Yet a real pendulum will have some extended mass distribution as indicated in Fig. 2.18. Such a pendulum is called a *compound* pendulum. If I_p is the moment of inertia about the pivot point, l is the distance from the pivot to the center of mass, and m is the mass of the

pendulum, then Newton's second law prescribes the following equation of motion:

$$I_p \frac{d^2\theta}{dt^2} + mgl \sin\theta = 0, \tag{2.33}$$

and for small angular displacements we again substitute θ for $\sin\theta$ The linearized equation of motion is

$$I_p \frac{d^2\theta}{dt^2} + mgl\theta = 0 \tag{2.34}$$

with period equal to

$$T = \frac{1}{2\pi}\sqrt{\frac{I_p}{mgl}}. \tag{2.35}$$

This expression reverts to that for the simple pendulum when all the mass is concentrated at the lowest point.

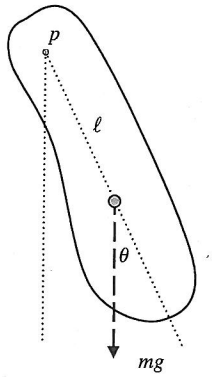

Fig. 2.18
A compound pendulum with an arbitrary distribution of mass.

2.3.6 Kater's pendulum

The formulas for the period of the simple pendulum and the compound pendulum both contain a term for g, the acceleration due to gravity, and therefore one should be able to time the oscillations of the small amplitude pendulum and arrive at an estimate of the local gravitational field. Yet without special effort the results obtained tend to be inaccurate. For example, it is often difficult to determine the appropriate length of the pendulum as there is ambiguity in the measurement at the pivot or at the bob. At the suggestion of the German astronomer F. W. Bessel (1784–1847), Captain Henry Kater (1777–1835) of the British Army invented a reversible pendulum in 1817 that significantly increased the accuracy of the measurement of g Kater's pendulum, shown schematically in Fig. 2.19, consists of a rod with two pivot points whose positions along the rod are adjustable. In principle, the determination of g is made by adjusting the pivot points until the periods of small oscillation about both positions are equal. In practice, it is difficult to adjust the pivot points—usually knife edges—and instead counterweights are attached to the rod and are easily positioned along the rod until the periods are equal. In this way, the pivot positions are defined by fixed knife edges that provide the possibility of accurate measurement. Once the periods are found to be equal and measured, the acceleration due to gravity is calculated from the formula

$$T = 2\pi\sqrt{\frac{h_1 + h_2}{g}}, \tag{2.36}$$

where h_1 and h_2 are the respective distances from the pivots to the center of mass of the pendulum. But more importantly their *sum* $(h_1 + h_2)$ is easily measurable as the distance between the two knife edge pivot points.

Equation (2.36) is not obvious and its derivation is of some interest. Referring to Fig. 2.19, the pendulum, of mass m, may be suspended about

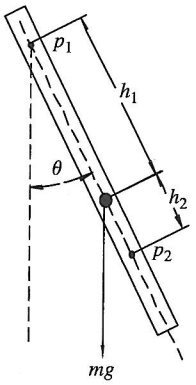

Fig. 2.19
The Kater reversing pendulum.

either point P_1 or point P_2. The distances of these suspension points from the center of mass are h_1 and h_2, respectively. The moments of inertia of the pendulum about each of the pivots are denoted as I_1 and I_2. Therefore the linearized equations of motion corresponding to the two pivot points are

$$I_1 \frac{d^2\theta}{dt^2} + mgh_1\theta = 0 \quad I_2 \frac{d^2\theta}{dt^2} + mgh_2\theta = 0. \tag{2.37}$$

The moments of inertia may be expanded using the parallel axis theorem such that

$$I_1 = mk^2 + mh_1^2 \qquad I_2 = mk^2 + mh_2^2, \tag{2.38}$$

where k is the *radius of gyration*, an effective radius of the system about the center of mass such that mk^2 is equal to the moment of inertia about the center of mass. Solution of Eq. (2.37) leads to periods of

$$T_1 = 2\pi\sqrt{\frac{k^2 + h_1^2}{gh_1}} \qquad T_2 = 2\pi\sqrt{\frac{k^2 + h_2^2}{gh_2}}. \tag{2.39}$$

With a little algebra we see that the periods are equal if

$$h_1h_2(h_1 - h_2) = k^2(h_1 - h_2). \tag{2.40}$$

While it would seem easiest to set h_1 equal to h_2, realization of this condition is difficult to achieve with good accuracy in a physical configuration. Instead, the counterweights are used to establish the other algebraic condition;

$$k^2 = h_1h_2 \tag{2.41}$$

and therefore

$$T_1 = T_2 = 2\pi\sqrt{\frac{h_1 + h_2}{g}}. \tag{2.42}$$

Example 3 *Consider a Kater pendulum in the form of a rod of length L and mass m. Suppose, not very realistically, that we can arbitrarily position the pivot points rather than achieve equality of swing periods with counter weights. Now let us suppose that the pendulum is swung about a pivot located at one end of the rod. We ask ourselves where the other pivot (on the other half of the rod) could be located that would give an equal swing period. (This example is due to Peters (1999).) The moment of inertia of the rod is* $(1/12)\,mL^2$ *about its center. By the parallel axis theorem the moment of inertia about one end is* $(1/12)\,mL^2 + m(L/2)^2 = (1/3)\,mL^2$. *Referring to Eq. (2.35), the period of an oscillation for the pivot located at one end becomes* $T_A = (1/2\pi)\sqrt{(I/mgL/2)} = (1/2\pi)\sqrt{(2L/3g)}$. *Let x be the distance from the center along the other half of the rod where the other pivot point is located. By the parallel axis theorem, the moment of inertia about this point is* $(1/12)\,mL^2 + mx^2$ *so that the period is* $T_B = (1/2\pi)\times\sqrt{((1/12)\,mL^2 + mx^2)/mgx}$. *Setting* $T_A = T_B$ *leads to a quadratic expression for x with the two roots L/2 and L/6. The root at L/2 is obvious and uninteresting and therefore we choose* $x = L/6$. *Substitution of this root*

into the equation leads to $T_B = (1/2\pi)\sqrt{((1/12)\,m\,L^2 + mx^2)/mgx} = (1/2\pi)\sqrt{(2L/3g)} = T_A$ *as expected. As noted previously, the pivot points can not be set exactly and some adjustments are required, using small counter weights, in order to obtain equality of periods.*

In practice, the lengths in Eq. (2.41) are difficult to predict accurately and the experimenter uses a convergence process to arrive at equality of periods. The counterweights are moved systematically until equality is achieved. With this type of pendulum the National Bureau of Standards, in 1936, determined the acceleration due to gravity at Washington, DC as $g = 980.080 \pm 0.003$ cm/s^2 (Daedalon 2000).

After its invention, many of the pendulum gravity experiments were done with the Kater "reversing" pendulum. One of the original pendulums, number 10, constructed by a certain Thomas Jones, rests in the Imperial Science Museum in London. The display card reads as follows.

This pendulum was taken together with No. 11, which was identical, ... on a voyage lasting from 1828–1831. During this time Captain Henry Foster swung it at twelve locations on the coasts and islands of the South Atlantic. Subsequently it was used in the Euphrates Expedition, of 1835–6, then taken to Antarctic by James Ross in 1840.

2.4 Some connections

One of the fascinating aspects of the history of the pendulum is the remarkable number of famous and not-so-famous physical scientists that have some connection to the pendulum. This phenomenon will come into sharper relief as our story unfolds. We have mentioned a few of these people; here are some others. Marin Mersenne (1588–1648) , a friar of the order of Minims in Paris, proposed the use of the pendulum as a timing device to Christiaan Huygens thereby inspiring the creation of Huygen's pendulum clock. Mersenne is perhaps better known as the inventor of Mersenne numbers. These numbers are generated by the formula

$$2^p - 1, \tag{2.43}$$

where p is prime. Most, but not all, of the numbers generated by this formula are also prime. Jean Picard (1620–1682), a professor of astronomy at the College de France in Paris, introduced the use of pendulum clocks into observational astronomy and thereby enhanced the precision of astronomical data. Picard is perhaps better known for being the first to accurately measure the meridian distance L and his observations, like Richer's observations were used by Newton in calculating the earth's shape. Robert Hooke (1635–1703) well known for the linear law of elasticity, Eq. (2.13), for his invention of the microscope, a host of other inventions, and his controversies with Newton, was one of the first to suggest, in 1666, that the pendulum could be used to measure the acceleration due to gravity. Edmond Halley (1656–1742) , astronomer royal, of Halley's comet fame, was another user of the pendulum. In 1676 Halley sailed to St. Helena's island, the southernmost British possession, located in the south Atlantic, in order

to make a star catalog for the southern hemisphere. As a friend of Hooke, he was aware of Hooke's suggested use of the pendulum to measure gravity and did make such measurements while on St. Helena. (While Halley is famous for having his name applied to the comet, he probably rendered a significantly more important service to mankind by pressing for and financially supporting the publication of Newton's *Principia.*) In the next century, Sir Edward Sabine (1788–1883) , an astronomer with Sir William Parry in the search for the northwest passage (through the Arctic ocean across the north of Canada) spent the years from 1821 to 1825 determining measurements of the gravitational field along the coasts of North America and Africa, and, of course, in the Arctic, with the pendulum.

The American philosopher Charles Saunders Peirce (1839–1914) makes a surprising appearance in this context. Known for his contributions to logic and philosophy, Peirce rarely held academic position in these branches of learning, but made his living with the US Coast and Geodetic Survey. Between 1873 and 1886, Pierce conducted pendulum experiments at a score of stations in Europe and North America in order to improve the determination the earth's ellipticity. However, his relationship with the Survey administration was fractious, and he resigned in 1891. And finally, in the twentieth century, we note the work of Felix Andries Vening Meinesz (1887–1966), a Dutch geophysicist who, as part of his Ph.D. (1915) dissertation, devised a pendulum apparatus which, somewhat like Von Sterneck's device, used the concept of pairs of perpendicularly oriented pendulums swinging out of phase with each other. (See Fig. 2.20).

In this way Vening Meinesz eliminated a horizontal acceleration term due to the vibration of peaty subsoil that seemed to occur in many places where gravity was measured. Vening Meinesz' apparatus was also especially fitted for measurements on or under water and contained machinery that compensated for the motion of the sea. Aside from the interruption caused by the Second World War, some version of this device was used on submarines from 1923 until the late 1950s (Vening 1929).

In the next chapter we add some complexity to the pendulum. We include friction and then compensate for the energy loss with an external source of energy. Eventually, we also relax the condition of small amplitude motion and therefore the equations of motion become nonlinear, a significant complication in our discussion. However the small amplitude motion of the linearized pendulum will predominate in three of the chapters; those on the Foucault pendulum, the torsion pendulum (which is well modeled as linear), and the pendulum clock. Obviously, the linearized pendulum is the basis of important applications.

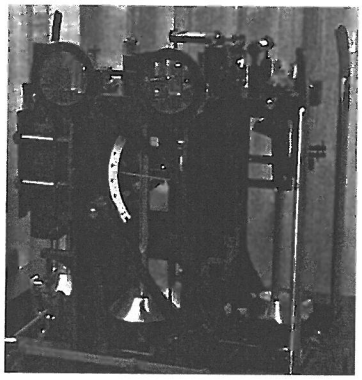

Fig. 2.20
Vening Meinesz pendulum. Four pendulums arranged in mutually perpendicular pairs are visible. (Courtesy of the Society of Exploration Geophysicists Geoscience center. Photo ©2004 by Bill Underwood.)

2.5 Exercises

1. In a later chapter we discuss the Foucault pendulum that was the first explicit demonstration of the rotation of the earth. The original Foucault pendulum was 67 meters in length. Calculate the frequency and period of its motion. The plane of oscillation of the pendulum rotated through a full 360 degrees in 31.88 hours. How many oscillations does the pendulum make in that time?

2. In the early days of gravity measurement by pendulum oscillation, a "seconds" pendulum had a length of about 1 m. This connection between the meter and the second was thought to have some special significance. What was the actual period of the "seconds" pendulum? From your result how do you think the period of the pendulum was initially defined?
3. A particle undergoing uniform acceleration from a standing start at the position $x=0$ has the following parametric equations (or time series) for position and velocity:

$$v = at$$
$$x = \frac{1}{2}at^2.$$

Determine the equation for its orbit in an x, v phase space and sketch the orbit.

4. Consider the phase orbit given by Eq. (2.6). Form the phase space diagram such that the x-axis is θ and the y-axis is $\dot{\theta}/\omega$ Then the phase orbit becomes a circle of radius θ_0. Note also that $\theta=\theta_0\cos\omega t$. Therefore the phase point traces out a circular orbit with a polar angle $\alpha=\omega t$. We are now ready to easily prove that areas in phase space are preserved in time. Proceed as follows. Consider two boundary orbits in phase space defined by two pendulums of different amplitudes (energies), $\theta_0(1)$ and $\theta_0(2)$. These orbits are two concentric circles. Now imagine a region between these two orbits bounded on the other sides by angles $\alpha_1=\omega t_1$ and $\alpha_2=\omega t_2$ Using polar coordinates calculate the area of this region and show that for some later times $t_1+\Delta t$ and $t_2+\Delta t$, the area still only depends upon the difference, t_2-t_1. That is, the area is preserved in time, and the system is conservative. See Fig. 2.21.
5. Find the Fourier series for the periodic function,

$$f(t) = 1 : 0 < t < T/2$$
$$f(t) = -1 : -T/2 < t < T.$$

6. The complete restoring force of the pendulum is $F=-mg\sin\theta$. Various approximations may be obtained using a Taylor series expansion in which the expansion variable is the length along the arc of the pendulum's swing, $s=l\theta$. That is

$$F(s) = F(s_0) + F'(s_0)(s-s_0) + F''(s_0)(s-s_0)^2/2! + F'''(s_0)(s-s_0)^3/3! + \cdots$$

where $F'=dF/ds$. Express F in terms of s. Let $s_0=0$ and show that the first nonvanishing term in the expansion is the usual small angle linear approximation, $F\approx -mg\theta$. Now let $s_0=l\pi/4$, and show that the linear approximation, in the region of $\theta=\pi/4$, is

$$F \approx \frac{mg}{\sqrt{2}}\left[\left(\frac{\pi}{4}-\frac{1}{\sqrt{2}}\right)-\theta\right].$$

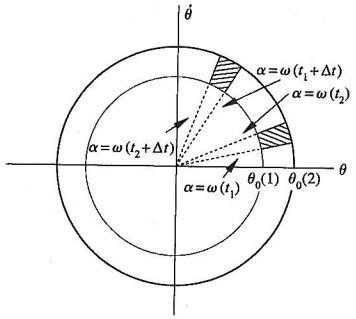

Fig. 2.21
Figure for problem 4.

7. Determine equations for the constants a and b in the Lennard–Jones potential, in terms of given values of the molecular spring constant, k and the equilibrium bond length, r_{eq} Note that the force is zero at $r=r_{eq}$.
8. Derive Eq. (2.29) for the ratio of densities σ'/σ where σ' is the density near the surface of the earth (above the mine shaft), and σ is the average density of the earth. For this derivation try the following sequence of calculations. First calculate g at the bottom of the mine shaft using Gauss' law, and remember that the earth at a radius above that of the bottom of the shaft contributes nothing to the gravitational field. Then use Gauss' law to calculate the gravitational field on top of the earth by dividing the earth into two parts: one at a depth below the shaft with density σ, and the shell above the bottom of the shaft with density σ'. Finally, examine the ratio of g_{top}/g_{bottom} and use the binomial expansion in terms of h/a where needed. Neglect any terms that are more than first degree in the ratio h/a.

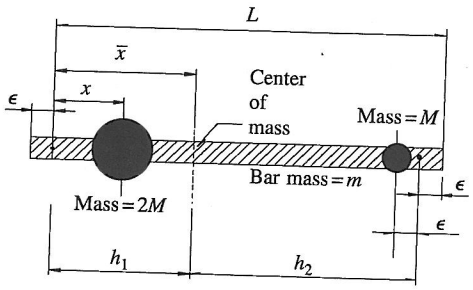

Fig. 2.22
Figure for problem 9.

9. Figure 2.22 shows a Kater pendulum with two attached masses, M and $2M$ The pivot points are just inside the ends of the bar (mass m) at a distance ϵ from the ends. The smaller mass is fixed at a distance of ϵ from the right pivot point. The larger mass is located a variable distance x from the left point. The point of this exercise is to find the location of the mass $2M$ such that the pendulum will oscillate with equal period from either pivot point.

(a) Find the center of mass $\bar{x}$ of the system in terms of the quantities shown in Fig. 2.22.
(b) Find h_1 and h_2.
(c) Check that $h_1 + h_2 = L - 2\epsilon$.
(d) Use the condition that $h_1 = h_2$ to find the appropriate value of x.

10. For the example in the text, $h_1 = L/2$ and $h_2 = L/6$. Using Eq. (2.42) show that these values lead to the correct result for the period.

11. Repeat the analysis for the Kater pendulum example in the text by putting one pivot point half-way between the center and the end of the rod; that is, at $L/4$ from the center. One position for the other pivot is, trivially, a distance $L/4$ from the center on the opposite side of the center line. (a) Using the analysis in the example, show that there is another location for the second pivot point at a distance $L/3$ from the center on the opposite side from the first pivot point. Show that the periods of oscillation for the pendulum from each pivot point are equal.

12. Consider a pendulum that consists of a uniform rod of length L and mass M that hangs from a frictionless peg that passes through a small hole drilled in the rod. The rod is free to oscillate (without friction) and assume that the oscillations are of small amplitude and therefore the equation of motion may be written as

$$I\frac{d^2\theta}{dt^2} + MgD\theta = 0,$$

where I is the moment of inertia and D is the distance between the center of mass of the rod and the pivot point.

(a) What is the frequency of oscillation of this pendulum?
(b) If the pivot point is located very near the top of the rod ($D = L/2$), find the frequency in terms of L and g.
(c) If the pivot point is located 1/3 of the way from the end of the rod, find the frequency of oscillation.
(d) If, in general, the pivot point is located a distance $D = L/k$ from the center of mass where $k \in [2,\infty)$, find a general expression for the frequency in terms of L, g, and k.
(e) For what value of k is the frequency a maximum?
(f) For what value of k is the frequency a minimum?

13. Find the Mersenne primes for $p = 3, 5, 7, 11, 13, 17, 19, 31$.

Pendulums less simple

3

3.1 O Botafumeiro

In the northwest corner of Spain, in the province of Galicia, lies the mist shrouded town of Santiago de Compostela, the birthplace of the cult of Santiago (St. James, the major apostle), and the home of the magnificent cathedral that is presumably built upon the bones of that martyred apostle (Adams 1999) (see Fig. 3.1). For a thousand years, pilgrims have sought out this cathedral as a shrine to Saint James where they might worship and receive salvation. The most famous and unique feature of the celebration of the mass at this cathedral, at least since the fourteenth century, is *O Botafumeiro*, a very large incense burner suspended by a heavy rope from a point seventy feet above the floor of the nave, and swung periodically through a huge arc of about eighty degrees (Sanmartin 1984). The rapid motion through the air fans the hot incense coals, making copious amounts of blue smoke, and the censer itself generates a frightening swooshing sound as it passes through the bottom of its arc. Some of the physics in this chapter is manifested by the remarkable motion of *O Botafumeiro* and therefore we provide some details of its structure and dynamics (Sanmartin 1984).

Fig. 3.1
The cathedral of Santiago de Compostela in northern Spain. Photo by Margaret Walker.

The censer, or incense burner itself, stands more than a meter high and is suspended by a thick rope whose diameter is 4.5 cm. (One can imagine something about the size of a backyard barbecue grill.) Over a period of seven hundred years, a variety of censers have been used. The original censer seems to have been silver, which was later replaced by another silver one, donated by the French king Louis XI. A papal bull from Pope Nicholas V, in 1447, threatened excommunication to anyone who stole it. It was probably this latter censer that was destroyed when it suffered a violent fall in 1499. The censer is sporadically mentioned in records over the next couple of centuries with yet another silver replacement being made as late as 1615. There is some evidence—but not conclusive—that French troops took a silver censer during Napoleon's 1809 campaign. At some point prior to 1852, the censer was made of iron, but at that date it was replaced by a censer of silvered brass, which is the one in use today (see Fig. 3.2). The current censer has a mass of 53 kg and is about 1.5 m in overall height. Its center of mass is about 55 cm above the base. Approximately three meters

Fig. 3.2
O Botafumeiro, the giant censer that hangs in the transept of the cathedral of Santigo de Compostela. (Reproducido con autorización, copyright © 1990. Prensa Científica, S.A. Reservados todos los derechos.)

of rope are used just in tying the heavy knot that secures the rope to the censer.

The other end of the rope is connected, high above the floor of the nave, to rollers on a frame that is supported by an iron structure. The iron structure consists of four large struts, joined at the central frame, that stretch to four posts near the upper part of the tower. The rollers provide the mechanism used for pumping the censer (see Fig. 3.3). In the early days, the complete support structure was wooden; the iron structure was built later, in 1602, in part because the cumbersome wooden support obscured light coming into the tower. The length of rope between the rollers and the top of the knot is 19.4 m. Therefore the length from the rollers to the center of mass of the censer is 20.6 m and the length to the floor is 21.8 m. This means that the bottom of the censer comes within about half a meter of the floor of the nave as it passes through the bottom of its arc.

The censer is pumped by periodically shortening and lengthening the rope as it is wound up and then down around the rollers. This kind of pumping is now known as *parametric* forcing. The pumping action is carried out by a squad of priests, called *tiraboleiros* or ball swingers, grouped to the side and each holding a rope that is a strand of the main rope that goes from the pendulum to the rollers and back down to near the floor. The tiraboleiros periodically pull on their respective ropes in response to orders from the chief verger of the cathedral. Unlike the child on a swing who senses the effect of her pumping, the team must simply act as a unit and follow the timing prescribed by the verger. One of the more terrifying aspects of the pendulum's motion is the fact that the amplitude of its swing is very large—about 82°—and therefore it has a high velocity—about 68 km/h—as it pass through the bottom of its arc, spewing smoke and flames.

How does *O Botafumeiro* differ from the simple pendulum described in Chapter 2? First, the censer is not a point mass or even a mass with spherical symmetry, and therefore it is a *compound* pendulum, a pendulum

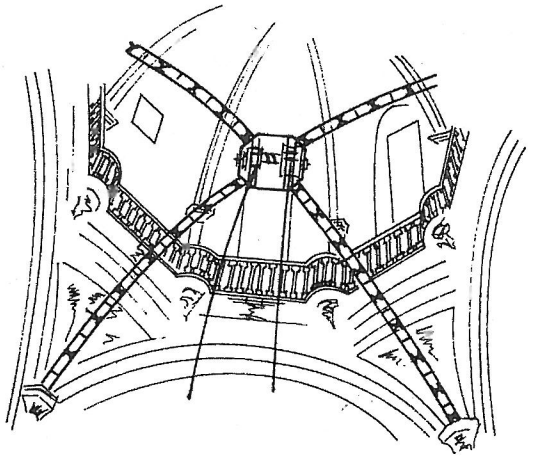

Fig. 3.3
Support structure for the rope holding O Botafumeiro. (Reprinted with permission from Sanmartin (1984, p. 939). ©1984, American Association of Physics Teachers.)

whose bob is an extended nonspherically symmetric mass. Second, the fact that the censer needs to be pumped implies that there is energy *dissipation* in the system and therefore damping of the motion. Third, pumping or *forcing* of the system is a fruitful topic in itself and will be seen to lead to rich dynamical behavior. Fourth, the swing of the pendulum is quite large, and, contrary to Galileo's conclusion of isochronism based upon his crude observations, the period of the motion is *not* independent of the amplitude of the motion. Finally there are some subtle effects associated with the rope itself in the particular case of *O Botafumeiro*. That is, the mass of the rope is not insubstantial and should be included in analysis of the censer's motion as should the fact that the inertia of the system leads to the rope not being stretched straight throughout the oscillation. This latter phenomenon suggests that the motion might be treated as that of a *double pendulum*. (Although we will not do so in this book. See (Sanmartin 1984).) The subject of this chapter is, then, some of the complications to pendulum dynamics suggested by the motion of *O Botafumeiro*.

As a postscript to this introduction, Sanmartin notes that the history of *O Botafumeiro* has not been without mishap and even violence. On July 25, 1499, there was an accident involving the four chains that attach the censer to the rope. The chains broke, thereby sending the censer crashing into one of the side doors. On May 23, 1622, the rope broke. This time, the censer fell approximately vertically since the amplitude of the motion was small at the moment. In a more sinister vein, it has been suggested that the suspending rope was used in the murder of the Archbishop Suero Gomez de Toledo at the entrance to the cathedral on June 29, 1366. Two noblemen, F. Perez Churruchao and G. Gomez Gallinato were involved. Apparently they also killed the Dean of the cathedral, Pedro Alverez, who, when he discovered the fate of the archbishop, ran back into the cathedral. The killers and a third person, Pedro el Cruel, chased him around the triforium before catching him. Pedro later denied any involvement.

Let us now leave the exotic world of *O Botafumeiro*, and return to the generic pendulum. We first enhance our simple model of the linearized pendulum, of the previous chapter, with the addition of various physical factors. With each new factor the mathematics becomes more complex and, eventually, reaches the point of intractability. At that point one must resort to numerical solution of the equations on a computer. In order to keep the analysis manageable, we will first treat many of the factors separately. In the second half of the chapter, we consider the full large amplitude, nonlinear, case.

3.2 The linearized pendulum with complications

3.2.1 Energy loss—friction

A common observation is that the periodic motion of a pendulum gradually diminishes and that, eventually, a pendulum will come to rest. In fact all large systems that are not continually energized lose energy . There

is no such thing as perpetual motion. In a mechanical system, the causes of energy loss are multitudinous, and include friction between solid surfaces and drag on the system from fluids and gases. Objects that travel through the atmosphere or other "fluids" at relatively high speeds experience a drag force that is proportional to the square of the velocity. For slower objects, the drag force may be realistically modeled as proportional to the first power of the velocity, a relationship named after the nineteenth century Cambridge University mathematician and physicist, Sir George Stokes (1819–1903). (Stokes, like Newton, Airy and the present day cosmologist Stephen Hawking, was, in his time, the Lucasian Professor. Like many other prominent scientists, Stokes was drawn to the study of the pendulum. He was particularly interested in the motion of pendulums within a fluid where friction would be important. His work on pendulums led to the study of geodesy and by the 1850s he had become the foremost British authority on the subject.) What constitutes a relatively high or low speed depends on the physical properties of the medium. But for a slow pendulum travelling in air, the linear dependence of drag on velocity is a reasonable approximation. Furthermore, other frictional effects for real pendulums seem also to be accounted for with the same velocity dependence. (However, O Botafumeiro travels fast enough that a velocity squared dependence is more realistic.) For now, we approximate the aggregate effect of drag or friction for typical pendulum as

$$F_D = -2\gamma \frac{d\theta}{dt}, \tag{3.1}$$

where γ is a constant. The equation of motion for the linearized pendulum now has an added term and becomes

$$\frac{d^2\theta}{dt^2} + 2\gamma \frac{d\theta}{dt} + \frac{g}{l}\theta = 0. \tag{3.2}$$

The general solution of this second-order differential equation has the form

$$\theta(t) = Ae^{r_1 t} + Be^{r_2 t},$$

where A and B are constants to be determined from initial conditions, and r_1 and r_2 are the two roots of the quadratic equation created by substitution of a trial solution, e^{rt}, into Eq. (3.2):

$$r^2 + (2\gamma)r + (g/l) = 0$$

$$r_1 = -\gamma + \sqrt{\gamma^2 - \omega_0^2} \tag{3.3}$$

$$r_2 = -\gamma - \sqrt{\gamma^2 - \omega_0^2}. \tag{3.4}$$

The angular frequency of undamped oscillations is $\omega_0 = \sqrt{g/l}$. The strength of the damping now determines the time-dependent pendulum behavior. Three distinct regimes exist.

Underdamped $\gamma^2 < \omega_0^2$
For this case, define a new frequency

$$\omega^2 = \omega_0^2 - \gamma^2. \tag{3.5}$$

Then the two roots are complex quantities which can be written

$$r_1 = -\gamma + i\omega$$
$$r_2 = -\gamma - i\omega.$$

The negative real part of the roots implies exponential decay, while the imaginary parts ($\pm i\omega$) yield oscillations at a new frequency that is slightly smaller than the undamped value ω_0. Combining these components, the angular motion can be expressed in the form

$$\theta = Ce^{-\gamma t}\cos(\omega t + \phi). \tag{3.6}$$

The canonical solution given earlier contained two constants A and B. An illustration of this form of damped oscillation is given in Fig. 3.4

Two constants remain in the new form of solution as expressed in Eq. (3.6)—one (C) defines the amplitude; the other (ϕ) appears as a phase shift. As noted before, specification of initial conditions for the pendulum will explicitly determine C and ϕ. For example, suppose it is known that at $t=0$, $\theta=\theta_0$ and the pendulum is at rest. Then

$$\theta_0 = C\cos(\phi)$$

and

$$\omega\sin(\phi) + \gamma\cos(\phi) = 0.$$

From these two equations C and ϕ are easily calculated.

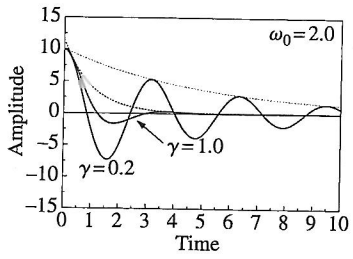

Fig. 3.4
Illustation of an underdamped oscillation in which the amplitude slowly decays under control of the exponential prefactor. The pendulum is released from rest at an angle of 10°. Two different damping values are shown. The dotted lines indicate the decay of the respective amplitudes.

Critically Damped $\gamma^2 = \omega_0^2$
In this special case, the two roots become equal and the method described above cannot be applied . The solution to the equation of motion is instead

$$\theta(t) = e^{-\gamma t}[A + Bt]. \tag{3.7}$$

The two constants can be determined as before from given initial conditions. If at $t=0$ the pendulum is at rest at a displacement θ_0, then

$$\theta_0 = A$$

and

$$B - A\gamma = 0.$$

A critically damped response using the previous choice $\omega_0 = 2$ is included in Fig. 3.5.

As can be seen in the figure, for critical damping the decay is optimum in the sense that the angle asymptotically approaches zero without overshoot (underdamping) or undershoot (overdamping).

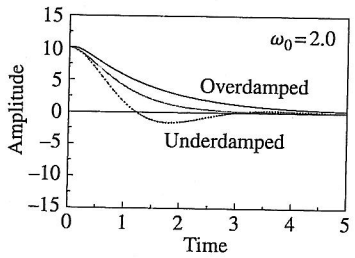

Fig. 3.5
Decay of the pendulum for three regimes: underdamped (lower curve: $\gamma=1$); critically damped (middle curve: $\gamma=2$); overdamped (upper curve: $\gamma=3$).

Overdamped $\gamma^2 > \omega_0^2$

For the overdamped case, both roots are real, so the decay is entirely exponential. With

$$k = \sqrt{\gamma^2 - \omega_0^2}, \tag{3.8}$$

which is of course a real quantity in this situation, the solution is

$$\theta(t) = e^{-\gamma t}\left[Ae^{kt} + Be^{-kt}\right]. \tag{3.9}$$

As in the previous two cases, the constants A and B will be fixed by the initial conditions of the problem.

The time dependence of the pendulum's angular displacement for this case is also included in Fig. 3.5. Furthermore, each of these motions may also be represented in phase space. The underdamped case is illustrated in Fig. 3.6.

In the ideal case of the completely undamped simple pendulum, the total energy of the system is conserved. The energy flows alternatively between kinetic and potential energy. But for the damped pendulum the energy dissipates exponentially. We calculate the energy of the pendulum as follows. Starting with Eq. (2.7);

$$E = \frac{1}{2}ml^2\dot{\theta}^2 + \frac{1}{2}mgl\theta^2, \tag{3.10}$$

we obtain the total energy of the linearized pendulum. The θ and $\dot{\theta}$ terms are replaced by Eq. (3.6) and its derivative. The final result is cumbersome and contains several terms,

$$E = \frac{1}{2}ml^2\theta_0^2 e^{-2\gamma t}[(\gamma^2 + \omega_0^2)\sin^2\alpha + \omega^2\cos^2\alpha - \gamma\omega\sin 2\alpha], \tag{3.11}$$

where $\alpha = \omega t + \phi$, but, unlike the nondissipative case, each term contains a decreasing exponential factor

$$f(t) = e^{-2\gamma t} \tag{3.12}$$

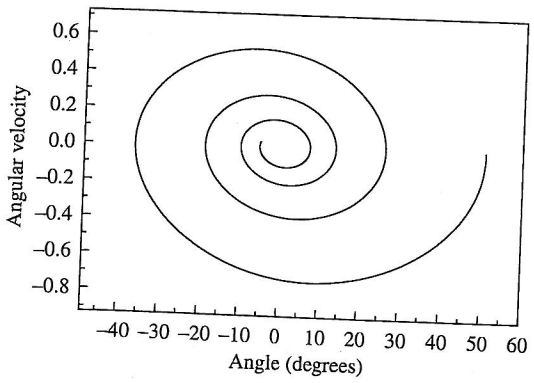

Fig. 3.6
Phase portrait of the underdamped linearized pendulum.

that decays at twice the rate of either the angular displacement or velocity time series. The remaining parts of each term in the expression are periodic with either the fundamental frequency ω or double that frequency.

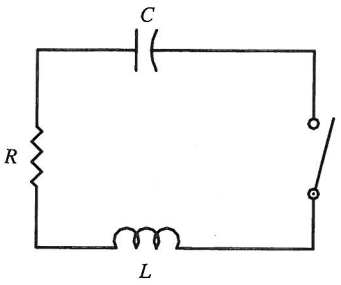

Fig. 3.7
Tuned circuit with resistance.

Example 4 *The electrical analog of pendulum damping is the presence of resistance R now added to the tuned LC circuit of Fig. 2.13. Figure 3.7 shows the modified schematic diagram for the tuned circuit. Eq. (2.20) is now augmented with a term proportional to the current, the simple Ohm's law term , as follows:*

$$L\frac{d^2q}{dt^2} + R\frac{dq}{dt} + \frac{q}{C} = 0. \tag{3.13}$$

Substitution of the trial solution $q = q_0 e^{-\gamma t}\sin(\omega t + \phi)$ *yields the frequency and the damping as*

$$\omega = \sqrt{\omega_0^2 - \gamma^2}, \tag{3.14}$$

where

$$\omega_0 = \sqrt{\frac{1}{LC}} \quad \text{and} \quad \gamma = \frac{R}{2L}. \tag{3.15}$$

We know from electrical theory that the power dissipation occurs only in the resistance R, and is given by the formula

$$\text{Power} = i^2 R. \tag{3.16}$$

Again the time dependent expression is cumbersome, but it does contain the exponential decay factor

$$f(t) = e^{-(R/L)t} \tag{3.17}$$

as expected. The quantity L/R is sometimes referred to as the decay constant or time constant or ring time of the circuit. It is the time during which the energy decays by a factor of 1/e from the original amount.

Example 5 *There are many examples of the decay of oscillations found in nature. For example, in magnetic resonance imaging, large numbers of tiny nuclei are momentarily energized by radio frequency electromagnetic radiation. Once the radiation is turned off, the nuclei "relax" to their equilibrium state. The relaxation time (equivalent to the decay time) tells the observer something about the environment and, in medical applications, the relaxation time can help with diagnosis.*

Example 6 *A more obvious example is found in the "ring" time of a large room, such as a concert hall. Each hall has its own damping constant (the inverse of the ring time) which will depend on many properties of the hall, including the size of the audience and the materials on the inside surfaces of the hall. A conductor can sometimes make dramatic use of the ring time. Suppose a large choir and orchestra are performing at a high volume and then have a sudden rest in the music. The musicians all stop playing very abruptly. The conductor can then draw out the pause—the time when the musicians are*

silent—such that the music will still 'linger' in the air even while the musicians are quiet. This phenomenon is sometimes used with powerful effect just prior to a grand finale. Conductors of the famous choral work "Messiah" by George Handel exploit this bit of physics just before the last few chords of the popular "Hallelujah" chorus.

3.2.2 Energy gain—forcing

The addition of dissipation to the pendulum causes energy decay and, strictly speaking, the motion continues at increasingly reduced energy for an infinite time. However, except for very long, massive pendulums with heavy masses, the oscillations do not actually last more than a few moments. Therefore continuous operation of most pendulums necessitates that some kind of forcing be applied to provide an energy infusion that compensates for the energy loss caused by the damping. In this section, we discuss several types of forcing: sinusoidal forcing, pulsed forcing, and parametric forcing.

3.2.2.1 Sinusoidal forcing

Sinusoidal forcing is simply a force with a constant amplitude and a sinusoidal time variation and it is inserted into the equation of motion as

$$\frac{d^2\theta}{dt^2} + 2\gamma\frac{d\theta}{dt} + \frac{g}{l}\theta = F\sin\Omega t. \tag{3.18}$$

(Note that in Eq. (3.18) F does not have the units of a force, but that its dimensions are $(\text{time})^{-2}$). This differential equation may be solved by standard methods (See, for example, chap. 5 of (Zill and Cullen 1993)). The complete solution consists of a general solution to the corresponding homogeneous equation and a particular solution appropriate to the full inhomogeneous equation. Assuming that the damping is relatively light, the solution is a linear combination of (a) an exponentially decaying, periodic solution of the corresponding homogeneous differential equation and (b) a periodic, particular solution due to the forcing term. It has the form

$$\theta(t) = \sqrt{c_1^2 + c_2^2}e^{-\gamma t}\sin(\omega t + \phi_1) + \frac{F}{\sqrt{4\gamma^2\Omega^2 + (\omega_0^2 - \Omega^2)^2}}\sin(\Omega t + \phi_2), \tag{3.19}$$

where

$$\phi_1 = \tan^{-1}\left(\frac{c_1}{c_2}\right) \quad \text{and} \quad \phi_2 = \tan^{-1}\left(\frac{2\gamma\Omega}{\omega_0^2 - \Omega^2}\right) \tag{3.20}$$

and

$$\omega_0 = \sqrt{\frac{g}{l}} \quad \text{and} \quad \omega = \sqrt{\omega_0^2 - \gamma^2}. \tag{3.21}$$

The constants c_1 and c_2 depend on the initial conditions for the pendulum. If we assume that the pendulum is a rest when the clock is started, then $\theta(0) = 0$ and $d\theta(0)/dt = 0$. These conditions lead to the following expressions for the constants:

$$c_1 = \frac{-2F\gamma\Omega}{[4\gamma^2\Omega^2 + (\omega_0^2 - \Omega^2)^2]}$$
$$c_2 = \frac{-F\Omega}{\omega}\left[\frac{(\omega_0^2 - \Omega^2) + 2\gamma^2}{4\gamma^2\Omega^2 + (\omega_0^2 - \Omega^2)^2}\right]. \tag{3.22}$$

The general solution, Eq. (3.19), has (a) a term that decays—a *transient solution*— and (b) a *steady state solution* that predicts long term periodic motion of the pendulum at the forcing frequency, Ω. It is interesting to note that while the frequency of the sinusoidal term of the decay part is ω, which depends on the resonant frequency ω_0 and damping γ, the frequency of the steady state sinusoidal term depends only on the frequency of forcing, Ω.

The *amplitude* of the steady state periodic motion depends on the size of the damping term. If the damping is quite small and if the forcing frequency Ω is close to ω_0 then the amplitude of the motion is relatively large. In fact, the expression goes to infinity if there is no damping at all. This case is described below. But for finite damping the shape of the amplitude curve as a function of Ω for several values of damping coefficient, γ, is given in Fig. 3.8. Each curve has a finite maximum that indicates the frequency value for maximum absorption of energy. In the previous chapter we discussed the concept of *resonance* as a periodic exchange of kinds of energy. We can also talk about resonance as the state of a system of maximum energy absorption. When Ω equals ω_0 the system is in the *resonant* state: and absorbs energy most easily. Furthermore, the resonant state is characterized by a certain width in frequency units that depends on the amount of damping. If the system is lightly damped then the resonant state is narrow but very absorbent with an extremely efficient transfer of energy from the forcing mechanism to the pendulum. On the other hand, if the damping is relatively strong, then the resonance is broad band and not very sensitive to frequency changes near ω_0, but neither is the transfer of energy very efficient because much energy is dissipated as heat. Additional details on resonance and the *quality* of the resonance as measured by the "Q" factor are discussed in Appendix A.

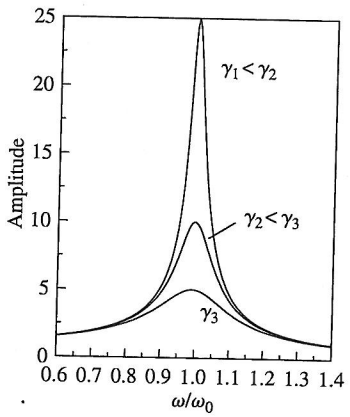

Fig. 3.8
Amplitude as a function of forcing frequency for various amounts of damping.

The study of periodic motion is at least partially motived by the fact that its mathematical form is relatively simple and the resulting differential equation of motion may be readily solved. To actually build a mechanical model of a pendulum (even a linearized pendulum) that is driven by the simple sinusoidal forcing function is not trivial. We discuss a similar (but nonlinear) pendulum later in this book but for now simply note that in most cases, simple mechanical pendular forcing is not well modeled by this function. However, there is one widely used application that does fit the linearized model of sinusoidal forcing very well; that is, the tuned electrical circuit that is subject to a sinusoidal electromagnetic field.

Pendulums less simple

We have already analyzed the LRC electrical circuit and found that, like the unforced, damped, linearized pendulum, the motion of charge among the elements gradually dies away as the energy is dissipated in the heating of the resistor. However, a periodic electromagnetic energy field impinging on the circuit will induce a time varying voltage across the circuit elements. This voltage will sustain the flow of charge through the circuit. In more exotic applications, such as radio and television, the electromagnetic field in the circuit may then be amplified to reproduce messages that were transmitted as a modulation of the original periodic electromagnetic field. This chain of events is the essence of radio and television reception. Returning to the basic mathematics of sinusoidal forcing in the circuit we find that, with the addition of the periodic electromagnetic field, the balance equation for the voltage across the circuit is

$$L\frac{d^2q}{dt^2} + R\frac{dq}{dt} + \frac{q}{C} = V\sin\Omega t. \tag{3.23}$$

This equation is identical in form to Eq. (3.18) and therefore all the mathematics derived from that equation of motion apply to this differential equation for the charge. We observe transient and steady state solutions, and we observe resonance. In a radio or television, we tune the circuit elements so that they will resonate with the carrier field of the desired transmitting station. In this way the radio or television receiver discriminates among transmitting stations and is able to select a particular station with its particular carrier frequency, ω_0

Let us conclude this section on sinusoidal forcing by looking at what happens if the system is forced *without* damping. Intuition suggests that the effect of an energy input from forcing without a corresponding dissipation of energy through damping will result in an oscillatory pendulum whose amplitude of motion will grow without limit. But this result is not obvious from simply setting the damping equal to zero in the solution of the general case. Therefore we begin again with the equation of motion from which the damping term is removed:

$$\frac{d^2\theta}{dt^2} + \frac{g}{l}\theta = F\sin\Omega t. \tag{3.24}$$

Using standard techniques, we find the general solution to be

$$\theta(t) = b_1\sin\omega_0 t + b_2\cos\omega_0 t + \frac{F}{\omega_0^2 - \Omega^2}\sin\Omega t. \tag{3.25}$$

As before we note that two sinusoidal terms contain the natural frequency ω_0, while the other sinusoidal term has the forcing frequency, Ω. Again, we assume that the pendulum is initially at rest; $\theta(0) = 0 = \theta'(0)$, and thereby determine the $b_{1,2}$ coefficients. This calculation results in the solution

$$\theta(t) = \frac{(F/\omega_0)[\omega_0\sin\Omega t - \Omega\sin\omega_0 t]}{(\omega_0^2 - \Omega^2)}. \tag{3.26}$$

This solution is only defined when the forcing frequency is *not equal* to the resonant frequency. In this case, and perhaps somewhat surprisingly, the nonresonant forcing does not lead to an unlimited growth in displacement.

For resonant forcing the case is different. We can determine the behavior when the frequencies *are equal* by a limit process whereby Ω is allowed to approach ω_0 Application of L'Hopital's rule results in

$$\lim_{\Omega \to \omega_0} \theta(t) = \frac{F}{2\omega_0^2}[\sin \omega_0 t - \omega_0 t \sin \omega_0 t]. \tag{3.27}$$

The second term of this solution grows without limit, as our intuition suggested. A sketch of the solution is shown in Fig. 3.9.

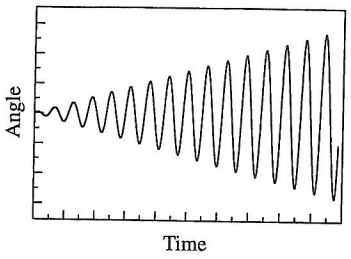

Fig. 3.9
Angular displacement as a function of time due to forcing at the resonant frequency.

3.2.2.2 Pulsed forcing

The common playground swing is one of the most ubiquitous examples of the driven pendulum. One pictures a small rider on the swing being pushed by an older child or adult. We might be tempted to model the periodic pushing by the second person as sinusoidal forcing. But, in reality, the rider receives a push or *impulse*, as the swing moves forward through the bottom of its arc, rather than sinusoidal forcing. Thus, a realistic model of the pushed swing will incorporate pulsed forcing. The profile of the push may be simply modeled as a rectangular pulse. Of course, any real pulse will have "soft" edges, but in either case the periodicity of the forcing and its nonsinusoidal form will guarantee that any realistic shape will have many Fourier components. We therefore expect complexity beyond that observed for sinusoidal forcing. While the mathematics is more complex, the final results are similar to the case of sinusoidal forcing. The fundamental frequency component of the forcing is a dominant factor in the resultant motion.

Let us assume that the swing starts from rest and that the periodic pulsing occurs at the beginning of each cycle at the bottom of the arc. In this first attempt at a model we ignore damping and let the amplitude of the motion be small in order that the swing may be treated as a linearized pendulum. The push function is illustrated in Fig. 3.10 and is written as

$$\begin{aligned} F(t) &= F, \quad 0 < t < \tau \\ &= 0, \quad \tau < t < T = n\tau. \end{aligned} \tag{3.28}$$

For simplicity of solution we choose the push time to be an integer fraction of the period of the pendulum. Furthermore, the period T is made to coincide with the resonant motion of the pendulum, as is the common practice in pushing a swing. That is

$$T = 2\pi\sqrt{\frac{l}{g}} \text{ with an angular frequency of } \omega_0 = \sqrt{\frac{g}{l}}. \tag{3.29}$$

With the pulsed forcing term , the equation of motion is now

$$\frac{d^2\theta}{dt^2} + \omega_0^2\theta = F(t) \text{ with initial conditions } \theta(0) = 0, \frac{d\theta(0)}{dt} = 0. \tag{3.30}$$

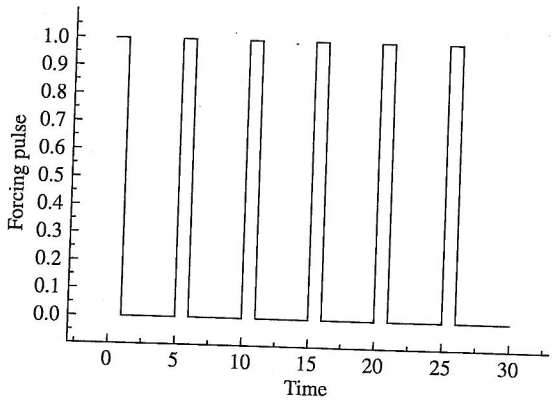

Fig. 3.10
Pulsed drive as a function of time.

The nature of the forcing function is such that the differential equation is readily solved by Laplace transform techniques. (For the uninitiated, we cryptically note that the Laplace transform technique consists of (a) converting a differential equation to an algebraic equation, (b) solving the algebraic equation, and (c) by the appropriate inverse transform operation, converting that algebraic solution into the desired solution of the differential equation. Its name comes from its originator, the French mathematician and astronomer, Pierre Simon Laplace (1749–1827). For a standard treatment see, for example, chapter 7 of (Zill and Cullen 1993).) The following definition of the transform provides the notation:

$$\mathcal{L}\{\theta(t)\} = \Theta(s) = \int_0^\infty e^{-st}\theta(t)\,dt. \tag{3.31}$$

The transformed version of the equation of motion is then

$$s^2\Theta(s) + \omega_0^2\Theta(s) = \frac{F(1-e^{-s\tau})}{s(1-e^{-sT})}, \tag{3.32}$$

with the transformed solution being

$$\begin{aligned}\Theta(s) &= \frac{F(1-e^{-s\tau})}{s(s^2+\omega_0^2)(1-e^{-sT})} \\ &= \frac{F}{s(s^2+\omega_0^2)}\begin{bmatrix}1+e^{-sn\tau}+e^{-s2n\tau}\ldots \\ -e^{-s\tau}-e^{-s(n+1)\tau}\ldots\end{bmatrix}.\end{aligned} \tag{3.33}$$

The inverse transform may be found with the help of the following identities:

$$L^{-1}\left[\frac{1}{s(s^2+\omega_0^2)}\right] = \frac{1}{\omega_0^2}(1-\cos\omega_0 t) \tag{3.34}$$

and

$$L^{-1}[e^{-as}L\{\theta(t)\}] = \theta(t-a)U(t-a), \tag{3.35}$$

where $U(t-a)$ is the unit step function equal to zero for $t<a$ and equal to one for $t>a$. The full solution to the equation of motion is then

$$\theta(t)=\frac{F}{\omega_0^2}\Big[1-\cos\omega_0 t+U(t-n\tau)-U(t-n\tau)\cos\omega_0(t-n\tau)$$
$$+U(t-2n\tau)-U(t-2n\tau)\cos\omega_0(t-2n\tau)\cdots\Big]$$
$$+\frac{F}{\omega_0^2}\Big[-U(t-\tau)+U(t-\tau)\cos\omega_0(t-\tau)-U(t-\{n+1\}\tau$$
$$+U(t-\{n+1\}\tau)\cos\omega_0(t-\{n+1\}\tau)\cdots\Big], \qquad (3.36)$$

where we have utilized our original assumption that $n\tau=T$, and the periodic properties of trigonometric functions. We can also write the solution for each time interval, either during a pulse, or between pulses. For example (in units of F/ω_0^2),

$$\begin{aligned}
\theta(t)&=[1-\cos\omega_0 t] && 0<t<\tau\\
&=[\cos\omega_0(t-\tau)-\cos\omega_0 t] && \tau<t<T\\
&=[1+\cos\omega_0(t-\tau)-2\cos\omega_0 t] && T<t<T+\tau\\
&=[2\cos\omega_0(t-\tau)-2\cos\omega_0 t] && T+\tau<t<2T\\
&=[1+2\cos\omega_0(t-\tau)-3\cos\omega_0 t] && 2T<t<2T+\tau\\
&=[3\cos\omega_0(t-\tau)-3\cos\omega_0 t] && 2T+\tau<t<3T\\
&=[1+3\cos\omega_0(t-\tau)-4\cos\omega_0 t] && 3T<t<3T+\tau
\end{aligned} \qquad (3.37)$$

and so on in the same pattern. Every second piece of the solution can be written as a simple sine or cosine function with a suitable amplitude and fixed phase angle. The alternative pieces are similar except that each has the additional factor of $(1-\cos\omega_0 t)$. The overall result is a sinusoidal function with a linearly increasing amplitude as seen in Fig. 3.11. For that illustration the forcing pulse occupies ten percent of the period of the motion. Note that Fig. 3.11 is very similar to Fig. 3.9, which illustrates sinusoidal forcing. Our intuition that the two types of forcing would lead to similar results has been vindicated. As usual, the model becomes unrealistic when the angular displacement becomes large.

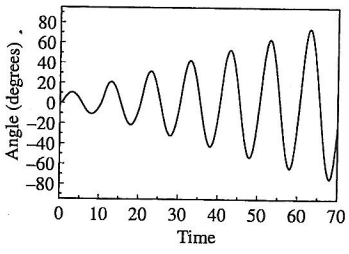

Fig. 3.11
Increasing angular displacement due to pulsed resonant forcing.

We have ignored two effects: damping and the actual sinusoidal dependence of the gravitational restoring force. For the moment we defer treatment of the latter effect and just add damping to our linearized, pulsed pendulum. With damping, the motion of the pendulum no longer diverges but is bounded, and depending on the damping factor, can be made to have a relatively small amplitude. The equation of motion now becomes

$$\frac{d^2\theta}{dt^2}+2\gamma\frac{d\theta}{dt}+\omega_0^2\theta=F(t) \qquad (3.38)$$

with the same initial conditions. Following the methodology of the undamped case we find the Laplace transform of the solution to be

$$\Theta(s) = \frac{F}{s\left((s+\gamma)^2+\omega^2\right)}\left[1 - e^{-s\tau} + e^{-ns\tau} - e^{-(n+1)s\tau} + e^{-2ns\tau} - e^{-(2n+1)s\tau}\right], \tag{3.39}$$

where

$$\omega^2 = \omega_0^2 - \gamma^2.$$

The solution to this equation is proportionately more complex than that of the undamped equation of motion. Computation of the inverse transform is left as an exercise for the persistent reader. It is illuminating to view the graphical representation of the solution shown in Fig. 3.12. Note that the time series is asymmetric and that the pulse causes the pendulum to be strongly displaced during and after the pulse, but that the pendulum loses energy, due to damping, between pulses.

The rather cumbersome form of the solutions to the pulsed pendulum equations of motion can motivate the search for a model that will produce less complex solutions. It turns out that some simplification can be achieved by letting the pulse become very strong during a very short time period. We consider the limit for which the pulse strength approaches infinity while the pulse duration approaches zero. This mathematical wizardry is achieved with the Dirac delta function, defined (Hundhausen 1998) as

$$\delta(t - t_0) = 0 \text{ for } t \neq t_0, \quad \text{and} \quad \int_{-\infty}^{\infty} \delta(t - t_0)\, dt = 1. \tag{3.40}$$

This function was invented by the theoretical physicist Paul Adrien Maurice Dirac (1902–1984) in order to deal with certain mathematical difficulties in the formulations of quantum mechanics. It has proved useful in a variety of contexts. Sometimes it is referred to as the "needle" function. We may think of the shape as being that of an infinitely thin vertical spike based at the coordinate t_0. Although this sort of infinitely quick, infinitely

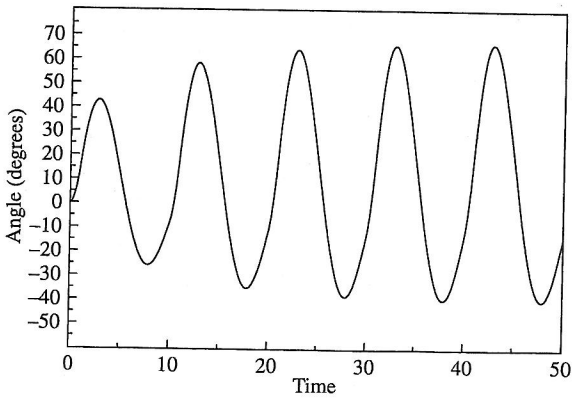

Fig. 3.12
Angular displacement due to pulsed forcing, but with added damping.

hard push on a pendulum is a little unrealistic, the use of the delta function leads to some simplification of the analysis. We rewrite the equation of motion as

$$\frac{d^2\theta}{dt^2} + 2\gamma\frac{d\theta}{dt} + \omega_0^2\theta = F[\delta(t) + \delta(t-T) + \delta(t-2T) + \delta(t-3T)\cdots], \tag{3.41}$$

where F is now a constant and $T = 2\pi/\omega_0$. The Laplace transform of this equation is

$$\Theta(s) = \frac{F}{[(s+\gamma)^2 + \omega^2]}\left[1 + e^{-sT} + e^{-2sT} + e^{-3sT} + \cdots\right], \tag{3.42}$$

where $\omega^2 = (\omega_0^2 - \gamma^2)$. Using various inverse transform relations, the solution to the equation of motion becomes

$$\theta(t) = \frac{F}{\omega}\left[e^{-\gamma t}\sin\omega t + U(t-T)e^{-\gamma(t-T)}\sin\omega(t-T)\cdots\right]. \tag{3.43}$$

Since $\omega \neq 2\pi/T$, it is cumbersome to write this solution as a set of piecewise solutions. The general effect is that while the amplitude decays slightly during the interval between each pulse, the next pulse provides a strong jump in the amplitude. The sharpness of the push causes a slight discontinuity in the slope of the time series at the moment of the pulse. Eventually the decay caused by the dissipative term, and the energy input caused by the Dirac function pulse balance each other and the system arrives at a steady periodic state. For a lightly damped swing, the motion is periodic. A simulation of the swing's motion for the first few pushes is shown in Fig. 3.13.

If the equation of motion does *not* include damping, then the solution in each interval is almost trivial:

$$\theta(t) = \frac{Fn}{\omega_0}\sin\omega_0 t \qquad (n-1)T < t < nT. \tag{3.44}$$

The amplitude grows linearly with n, as it does for the finite pulse width case, shown in Fig. 3.11.

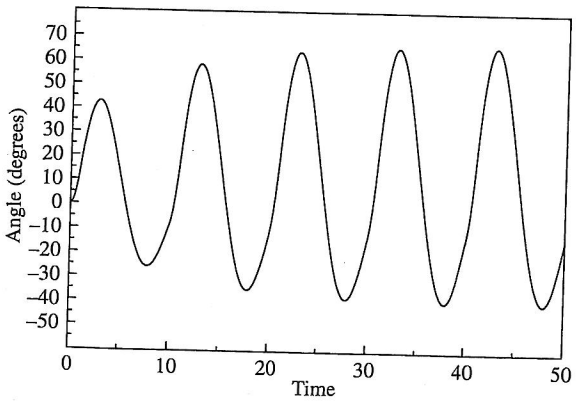

Fig. 3.13
Angular displacement due to Dirac delta function forcing (and damping). Note the slight discontinuity in the slope of the angle at the point of forcing.

Delta-function forcing is, of course not entirely realistic, but the motion it promotes is quite similar to that provided by forcing from finite width pulses. And the delta function has the huge advantage of providing simpler mathematics for the motion of the pendulum. Therefore, as a model, delta function forcing is a viable alternative to the more complex problem of finite width forcing.

3.2.3 Parametric forcing

Parametric forcing is any method of forcing that varies some parameter of the pendulum's configuration in a periodic manner such that the forcing energy becomes at least partially converted to motional energy for the pendulum. An ubiquitous example of periodic parametric forcing is the pumping of a playground swing performed by the rider in order to build and then maintain the swing's motion. In the case of the playground swing the rider's pumping action involves movement of his or her body so that the effective length of the swing is periodically altered. A more exotic example is found with the pumping of *O Botafumeiro* by the team of priests. The actual length of the pendulum is varied as the rope is periodically wound up and wound down around the rollers high above the transept. In both cases, the energy input periodically changes the *effective* length (parameter) of the pendulum. These changes also provide a change in the effective gravitational field on the pendulum bob due to the momentary forcing. The energy of motion along the length converts to angular motion of the pendulum. Both of these applications of parametric forcing will be discussed more fully after the nonlinear pendulum has been introduced. For now, we develop a simple model of a linearized parametric pendulum.

In complex systems, determination of the correct equations of motion may be a daunting task. It is not always easy to specify, with precision or confidence, the applicable forces in systems with several degrees of freedom. Another approach, commonly termed the Lagrangian approach after Joseph Louis Lagrange (1736–1813) , may often be less perilous even though the initial equations seem abstract.[1] The justification for this method is based upon an optimization and may be found in texts on advanced mechanics. See, for example, (Goldstein 1950) or (Chow 1995). Here we simply provide the prescription for its use. Let us define the excess of kinetic energy over potential energy as

$$L = T - V, \tag{3.45}$$

where L is called the Lagrangian , T is the kinetic energy, and V is the potential energy of the system. The system position is specified by generic coordinates that form the set (q_i) and therefore the Lagrangian, and particularly the potential energy are both functions of the q_i coordinates. The kinetic energy will depend upon velocity coordinates $(\dot{q}_i)$. Because only

[1] Lagrange's most famous treatise "Mécanique Analytique" contained not a single diagram. Lagrange took pride in employing only "algebraic operations." He went on to say that, "Those who love Analysis will, with joy, ... be grateful to me for thus having extended its field." (Quoted on p. 333 in Dugas (1955)).

energies are involved in the creation of the Lagrangian, it is relatively easy to write the appropriate Lagrangian. The required equations of motion are found by taking certain derivatives of the Lagrangian such that

$$\frac{d}{dt}\left(\frac{\partial L}{\partial \dot{q}_i}\right) - \left(\frac{\partial L}{\partial q_i}\right) = 0. \tag{3.46}$$

This expression gives one equation of motion for each of the coordinates. We now demonstrate this approach with the linearized parametric pendulum.

A typical parametric pendulum, whether a swing or a pumped incense burner has a time varying length. Polar coordinates relative to the pivot point are a good choice. The length of the pendulum may be represented by $r(t)$ and the angular displacement of the bob by $\theta(t)$. The Lagrangian for the linearized pendulum becomes

$$L = \frac{1}{2}m\dot{r}^2 + \frac{1}{2}mr^2\dot{\theta}^2 - mgr\left(\frac{\theta^2}{2}\right), \tag{3.47}$$

which, through use of Eq. (3.46), gives the equations of motion:

$$\begin{aligned} \frac{d}{dt}\left(\frac{\partial L}{\partial \dot{r}}\right) - \left(\frac{\partial L}{\partial r}\right) &\Rightarrow \ddot{r} - r\dot{\theta}^2 + g\theta^2 = 0 \\ \frac{d}{dt}\left(\frac{\partial L}{\partial \dot{\theta}}\right) - \left(\frac{\partial L}{\partial \theta}\right) &\Rightarrow r^2\ddot{\theta} + 2r\dot{r}\dot{\theta} + gr\theta = 0. \end{aligned} \tag{3.48}$$

The advantage of the Lagrangian approach becomes clear with the appearance of the nonintuitive middle terms in each differential equation. Our primary concern is the swinging motion as described by the second equation. Division by r^2 yields

$$\ddot{\theta} + 2\frac{\dot{r}}{r}\dot{\theta} + \frac{g}{r}\theta = 0, \tag{3.49}$$

an equation very similar to that of the simple linearized pendulum. We anticipate that the middle term will provide the forcing and thereby create the increasing amplitude of the motion. The natural angular frequency of the pendulum is given by $\omega_0 = \sqrt{g_0/r_0}$ where r_0 is the unperturbed length of the pendulum and g_0 is the acceleration due to gravity.

For parametric pumping the optimum effect is achieved by pumping at twice the natural frequency of the pendulum as shown by the path of the bob of O Botafumeiro in Fig. 3.14.Therefore, a possible time variation of the pendulum length may be expressed as

$$r(t) = \left(r_0 - \frac{\Delta r}{2}\right) + \frac{\Delta r}{2}\cos 2\omega_0 t, \tag{3.50}$$

where Δr is twice the amplitude of the rope length variation which, in turn, changes the effective field of gravity on the bob. Thus, the effective gravitational field becomes

$$g(t) = g_0 - \ddot{r} = g_0 + \frac{\Delta r}{2}4\omega_0^2\cos 2\omega_0 t. \tag{3.51}$$

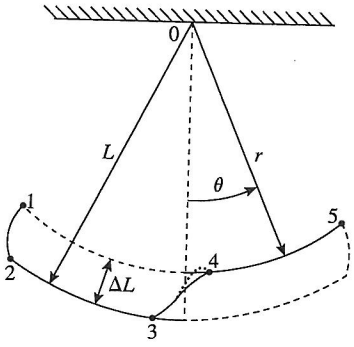

Fig. 3.14
Schematic diagram of the path of O Botafumeiro during a cycle. (Reprinted with permission from Sanmartin (1984, p. 940). ©1984, American Association of Physics Teachers.)

Numerical solution of the equation of motion subject to the time variations of r and g gives rise to the time series shown in Fig. 3.15.

As we will show, the frequency of the *nonlinear* pendulum is amplitude dependent. Optimum forcing requires that the forcing frequency track the pendulum's natural frequency, and therefore optimum forcing of a *nonlinear* parametric pendulum requires that the forcing frequency be adjusted downward as the amplitude increases. For O Botafumeiro, the adjustment is made by the *tiraboleiros* as the censer swings toward its maximum amplitude of about 80 degrees. Fig. 3.16 shows a monotonic increase in O Botafumeiro's amplitude.

We now temporarily leave the question of forcing and turn to the difficult problem of the nonlinear pendulum with its sinusoidal restoring force. Its mathematics becomes significantly more complex than that of the linear case. For the general case, with damping and even simple periodic forcing, there is no analytic solution and therefore the equation of motion cannot be solved without the help of a computer. As noted above, our analysis will reveal the important result that the natural frequency

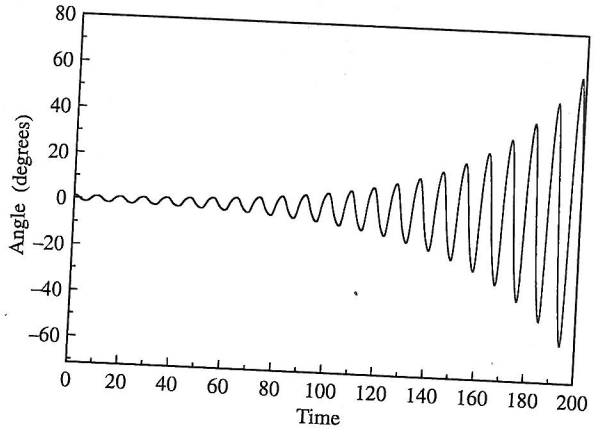

Fig. 3.15
Time series for the angular displacement as calculated by the computer simulation.

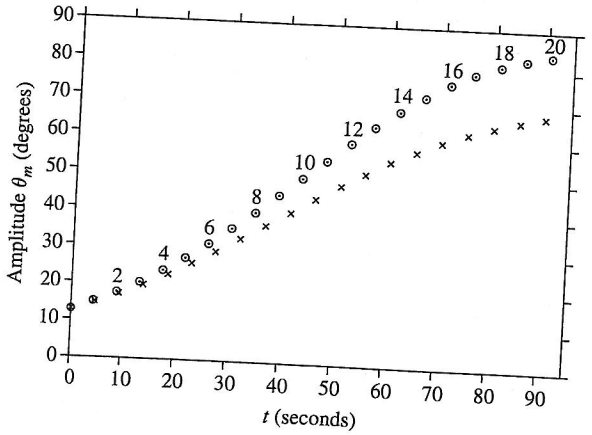

Fig. 3.16
Oscillation amplitude for each pumping cycle. Both sets of points are due to mathematical models, the circles representing a more complex model that yields an accurate representation of actual motion of O Botafumeiro. (Reprinted with permission from Sanmartin (1984, p. 942). ©1984, American Association of Physics Teachers.)

decreases with amplitude, a finding that counters Galileo's original observation of approximate isochronism.

3.3 The nonlinearized pendulum

We have seen that the linearized pendulum is a suitable model for many applications. But once the amplitude of oscillation gets past the point where $\sin\theta \cong \theta$, perhaps 10 degrees, the linearization approximation is no longer valid. Certainly the motion of *O Botafumerio*, with its amplitude of over 80°, requires modeling with the complete sinusoidal restoring force. Therefore it is necessary to return to the nonlinearized equation of motion, Eq. (2.1) for the simple pendulum. The mathematical machinery of linear differential equations and linear systems is no longer available to us. Solutions of nonlinear equations require a variety of less straightforward methods of solution, including power series expansion and, when all else fails, numerical solution by computer. Furthermore, the harmonic oscillator approximation of the pendulum is no longer true, and the various analogs of the harmonic oscillator such as the LRC electrical circuit no longer correspond to the large amplitude, nonlinear pendulum.

3.3.1 Amplitude dependent period

One of the most important differences between the linearized pendulum and the nonlinear pendulum is that while the former has a constant natural frequency, the period of the nonlinear pendulum decreases with increasing amplitude. Galileo's original hypothesis of isochronism is found only in an approximation of this equation ($\sin\theta \simeq \theta$). More generally, the period of the motion *does* vary with the amplitude. Derivation of this result is a nontrivial exercise (MacMillan 1927). We begin again with the undamped, unforced equation of motion,

$$\frac{d^2\theta}{dt^2} + \frac{g}{l}\sin\theta = 0. \tag{3.52}$$

Using

$$d\theta = \frac{d\theta}{dt}dt, \tag{3.53}$$

the equation of motion becomes

$$\frac{d\theta}{dt}\frac{d^2\theta}{dt^2}\,dt = -\frac{g}{l}\sin\theta\,d\theta. \tag{3.54}$$

The integral of this equation—the so-called *first integral of motion*—is a conservation of energy equation

$$\left(\frac{d\theta}{dt}\right)^2 = \frac{2g}{l}\cos\theta + \text{Constant}. \tag{3.55}$$

The constant of integration may be determined from the total energy, E, thereby yielding the following result,

$$\left(\frac{d\theta}{dt}\right)^2 = \frac{2g}{l}\cos\theta + \frac{2E}{ml^2} - \frac{2g}{l}, \tag{3.56}$$

which simply expresses the fact that the total energy is the sum of the kinetic and potential energies. At this point, three cases are distinguished by their respective regimes of total energy. In the first case the energy is less than a critical value, $2mgl$, the energy required for the pendulum bob to reach the upper vertical position. The second case corresponds to the total energy being equal to the critical value, and the third case occurs in the regime where the energy is greater than the critical value and is therefore sufficient to make the pendulum execute hindered rotary motion.

Case I: $E < 2mgl$. In this regime, the constant in Eq. (3.55) can be determined by letting the angular velocity be zero at some maximum displacement (or angular amplitude α) Then Eq. (3.55) becomes

$$\left(\frac{d\theta}{dt}\right)^2 = \frac{2g}{l}(\cos\theta - \cos\alpha). \tag{3.57}$$

This equation describes the behavior of the low energy pendulum in phase space $(\theta, \dot{\theta})$ when $\alpha \prec \pi$. For very small amplitudes, the phase orbit is approximately elliptical, as is the case for the linearized pendulum shown in Fig. 2.5. For higher values of α the ellipse becomes horizontally stretched. Let us continue to solve the differential equation. Use of the trigonometric identity $\cos\theta = 1 - 2\sin^2(\theta/2)$ leads to the expression

$$\frac{d\theta}{dt} = \pm 2\sqrt{\frac{g}{l}\left[\sin^2\left(\frac{\alpha}{2}\right) - \sin^2\left(\frac{\theta}{2}\right)\right]}. \tag{3.58}$$

We introduce two further variables, φ and k, with the substitutions

$$\sin\frac{\theta}{2} = \sin\frac{\alpha}{2}\sin\varphi \quad \text{and} \quad k^2 = \sin^2\left(\frac{\alpha}{2}\right). \tag{3.59}$$

An integral equation is now formed in which the variables t and φ are now separated:

$$\int_0^{t_0} dt = \sqrt{\frac{l}{g}}\int_0^{\varphi} \frac{d\varphi}{\sqrt{1 - k^2\sin^2(\varphi)}}. \tag{3.60}$$

The zero of time is set when the pendulum is at the bottom of its arc and t_0 occurs when the pendulum reaches the maximum angular displacement, α. The time t_0 then represents one quarter of the period, T. Also, when the pendulum is at its maximum angular displacement, α, then the new angular

variable φ is equal to $\pi/2$. Therefore the period of the motion is

$$T = 4\sqrt{\frac{l}{g}}\int_0^{\pi/2} \frac{d\varphi}{\sqrt{1 - k^2 \sin^2(\varphi)}}. \tag{3.61}$$

The integral in the above expression is called an elliptic integral of the first kind. Its value was first calculated by the French mathematician Adrien-Marie Legendre(1752–1833). Legendre worked extensively on elliptic functions and elliptic integrals for over forty years culminating in his book "Traite des fonctions elliptiques," published in 1830 (Hellemans and Bunch 1991). The integrand may be expanded according to the binomial theorem:

$$\begin{aligned}(1 - k^2 \sin^2(\varphi))^{-1/2} = 1 &+ \frac{1}{2}k^2 \sin^2\varphi + \left(\frac{1 \cdot 3}{2 \cdot 4}\right)k^4 \sin^4\varphi + \cdots \\ &+ \frac{1 \cdot 3 \cdot 5 \cdots (2n-1)}{2 \cdot 4 \cdot 6 \cdots 2n}k^{2n} \sin^{2n}\varphi \cdots,\end{aligned} \tag{3.62}$$

and integrated term by term. For the integration we use the formula

$$\int_0^{\pi/2} \sin^{2n}\varphi \, d\varphi = \frac{1 \cdot 3 \cdot 5 \cdots (2n-1)}{2 \cdot 4 \cdot 6 \cdots 2n}\frac{\pi}{2}, \tag{3.63}$$

and the previously defined value for k to obtain the final value for the period:

$$T = 2\pi\sqrt{\frac{l}{g}}\left[1 + \left(\frac{1}{2}\right)^2 \sin^2\left(\frac{\alpha}{2}\right) + \left(\frac{1 \cdot 3}{2 \cdot 4}\right)^2 \sin^4\left(\frac{\alpha}{2}\right) + \cdots\right]. \tag{3.64}$$

The graph of period versus angular amplitude is shown in Fig. 3.17. Note that when the amplitude is zero that the period is exactly equal to the period determined from the linearized version of the pendulum. As the amplitude approaches π radians, the bob approaches verticality and the factor $\alpha/2$ approaches $\pi/2$. The series now diverges and the period becomes infinitely large, as expected. This behavior is treated as the second case.

For *O Botafumeiro* with its angular amplitude of over 80°, the period of motion is longer than that found from a calculation that assumes a small angle of oscillation. One wonders what Galileo would have discovered if he had been sitting in the cathedral in Santiago de Compostela rather than (reportedly) sitting in the cathedral at Pisa. Would he have observed the difference in the pendulum's period as the team of priests gradually built up the amplitude of the censer's motion? Would his pulse have been a sufficiently accurate timer to quantify the difference? From Fig. 3.17 it is apparent that the period for an amplitude of 80° is about 15% more than that of the small amplitude approximation. With O Botafumeiro the formula for the period is not exactly applicable because of a variety of other effects. Use of the small amplitude formula for the period of oscillation leads to $T = 9.1$ seconds. Measurements taken from a graph found in

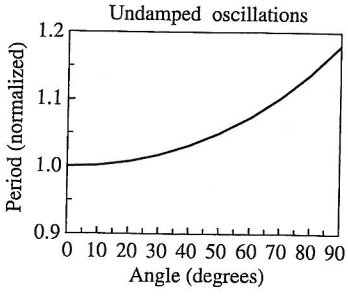

Fig. 3.17
Period of oscillation versus amplitude.

(Sanmartin, 1984) suggest that for maximum swing the period is about 10.2 seconds, a 12% difference. It seems unlikely that Galileo would have attributed much significance to either a 12% or 15% change.[2]

There is another important consequence of the nonlinearity of the pendulum's equation of motion. For the linearized pendulum, the angle and angular velocity of the pendulum behaved as a single sine or cosine wave,

$$\theta = A \sin \omega_0 t. \tag{3.65}$$

where $\omega_0 = \sqrt{g/l} \equiv \omega$. Such is not the case for the nonlinear pendulum. In order to gain some understanding we partially solve the equation of motion, Eq. (3.52), by a method of approximation. We first assume a trial solution, then substitute it into the differential equation, and finally discover a better trial solution. The process is repeated with each increasingly better solution. In this way, the general character of the solution is revealed. We begin with the trial solution Eq. (3.65) and through substitution into Eq. (3.52) obtain

$$\frac{d^2\theta}{dt^2} = -\omega^2 \sin (A \sin \omega t). \tag{3.66}$$

The outer sine function may be expanded such that the angular acceleration includes powers of the trial solution:

$$\frac{d^2\theta}{dt^2} = -\omega^2 \left[A \sin \omega t - \frac{(A \sin \omega t)^3}{3!} + \frac{(A \sin \omega t)^5}{5!} \cdots \right]. \tag{3.67}$$

Each of the powers of the trig functions can be shown to contain a harmonic that corresponds to that particular power. Therefore there are sinusoidal terms in the time series with frequencies that are odd harmonics of the fundamental frequency, ω. If the amplitude of oscillation is relatively small we might only keep the first two terms in the power series expansion and therefore the next approximate trial solution might have the form,

$$\theta = B \sin \omega t + C \sin 3\omega t. \tag{3.68}$$

This process would be repeated with ever better refinements of the amplitudes of each harmonic. The point is that while the motion of the pendulum is oscillatory, it is no longer described by the simple harmonic motion of a single sinusoidal function. A complete description would require a Fourier spectrum of the form (depending on initial conditions)

$$\theta = \sum_{i=0}^{\infty} A_{2i+1} \sin (2i+1)\omega t. \tag{3.69}$$

For the nonlinearized pendulum the natural frequency changes with amplitude and therefore the response curve is not static with continued forcing at a certain frequency. If a system is initially forced at its low amplitude resonant frequency, the increase in amplitude will eventually

[2] There is some evidence to suggest that Galileo would have not been inclined to regard any difference as credible—at least for an ideal pendulum. Isochronism may have been a matter of faith as well as of imperfect observation (Drake 1978).

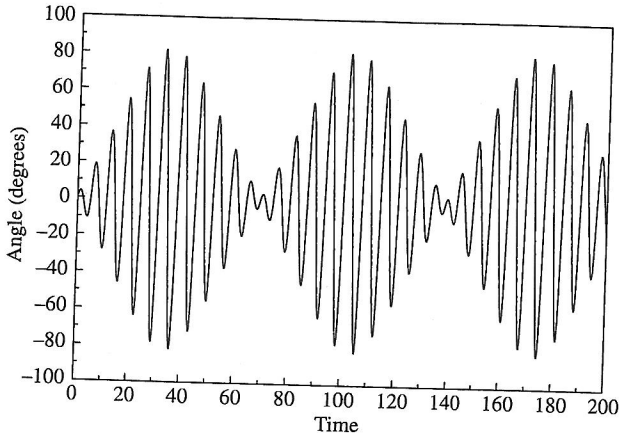

Fig. 3.18
Response of the pendulum to forcing at its small angle resonant frequency. For larger amplitudes, the forcing frequency is increasingly different from the pendulum's natural frequency and the forcing becomes counterproductive.

detune the pendulum, and thereby lower its resonant frequency from that of the originally tuned driving frequency. The forcing goes out of step with the momentary resonant frequency. As the forcing becomes further out of synchronization with the pendulum, the pendulum's amplitude of motion will diminish back to zero. The phenomenon gives rise to a periodic amplitude modulation of the pendulum's motion, as shown in Fig. 3.18. Therefore the rider on a swing must automatically account for the varying response by adjusting her pumping rate to achieve maximum response. In essence, the rider's efforts form part of a feedback loop with the swing, a phenomenon known as *autoresonance* . Similar considerations hold true for the pumping of the large amplitude oscillations of O Botafumeiro. The team of priests form a feedback loop such that their pumping frequency must slow as the amplitude increases.

Let us now consider the case for which the pendulum has just sufficient energy to reach an inverted position.

Case II: $E=2mgl$. For this condition, the expression for energy simplifies considerably. We start with Eq. (3.57) and using the same trigonometric substitution, obtain the result,

$$\left(\frac{d\theta}{dt}\right)^2 = \frac{4g}{l}\left(1-\sin^2\left(\frac{\theta}{2}\right)\right), \tag{3.70}$$

which may be simplified to

$$\frac{d\theta}{dt} = 2\sqrt{\frac{g}{l}}\cos\left(\frac{\theta}{2}\right). \tag{3.71}$$

Therefore the time interval t between the pendulum being at the bottom of its arc $\theta=0$ and being at some finite angular displacement, θ, is found by integration,

$$t = \frac{1}{2}\sqrt{\frac{l}{g}}\int_0^{\theta}\sec\frac{\theta}{2}d\theta = \sqrt{\frac{l}{g}}\ln\left[\tan\left(\frac{\theta}{4}+\frac{\pi}{4}\right)\right]. \tag{3.72}$$

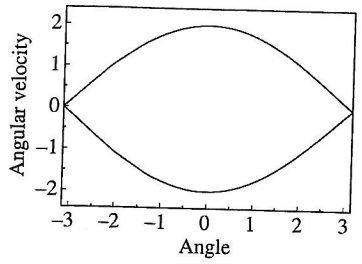

Fig. 3.19
Phase diagram for a pendulum with just enough energy to reach the upright vertical position.

Pendulums less simple

The pendulum approaches verticality as θ approaches π radians and therefore the time interval becomes infinite. We expected this result from the discussion of the previous case. Eq. (3.71) can also be used to plot the trajectory of this special orbit in phase space as shown in Fig. 3.19 when the phase orbit passes through $\theta = \pm\pi$. This is a unique orbit since it characterizes the pendulum's behavior at the critical energy. Note that there is a discontinuity in the derivative of the phase orbit at $\theta = \pm\pi$. This special phase orbit is called the *separatrix*; it marks the boundary between oscillatory and hindered rotary motion of the pendulum.

Case III: $E \rangle 2mgl$. The total energy is

$$E = \frac{1}{2}ml^2\left(\frac{d\theta}{dt}\right)^2 + mgl(1 - \cos\theta). \tag{3.73}$$

The angular velocity term may then be isolated such that

$$\begin{aligned}\left(\frac{d\theta}{dt}\right)^2 &= \frac{2E}{ml^2} - 2\frac{g}{l}\left(1 - 1 + 2\sin^2\frac{\theta}{2}\right) \\ &= \frac{2E}{ml^2} - 4\frac{g}{l}\sin^2\frac{\theta}{2}.\end{aligned} \tag{3.74}$$

Therefore

$$\frac{d\theta}{dt} = \sqrt{\frac{2E}{ml^2}}\sqrt{1 - k^2\sin^2\frac{\theta}{2}}, \tag{3.75}$$

where

$$k = \sqrt{\frac{2mgl}{E}}. \tag{3.76}$$

The differential equation is inverted and put in integral form. The integral over angular displacement, from 0 to π, describes motion for one half an orbit and therefore the integral gives the time for one half rotation. The period of the motion is then double this time. The integral is

$$t = \sqrt{\frac{2ml^2}{E}}\int_0^{\pi} \frac{d\left(\frac{\theta}{2}\right)}{\sqrt{1 - k^2\sin^2\frac{\theta}{2}}}. \tag{3.77}$$

Finally the period of the motion may be expanded, as before, to give

$$T = 2t = \pi\sqrt{\frac{2ml^2}{E}}\left[1 + \left(\frac{1}{2}\right)^2 k^2 + \left(\frac{1\cdot 3}{2\cdot 4}\right)^2 k^4 \cdots\right]. \tag{3.78}$$

The motion is that of a hindered rotation—faster at the bottom and slower at the top. If E is very large compared to the critical energy of $2mgl$, then the expression for the period reduces considerably. Suppose $E = Nmgl$ where N is a very large number; then k becomes very small and we can ignore all

but the first term in the expansion. The period then behaves as

$$T = \pi\sqrt{\frac{2l}{Ng}}, \tag{3.79}$$

which approaches zero for large N. The behavior of the period over the entire range of energies is sketched in Fig. 3.20.

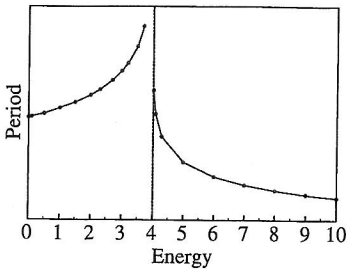

Fig. 3.20
Graph of period versus the energy of the pendulum. The vertical line represents the critical energy.

3.3.2 Phase space revisited

In Chapter 2 we introduced phase space as a means of visualizing the totality of the pendulum's motion. With the nonlinear frictionless pendulum phase space becomes more complex. Phase space naturally divides into two parts that correspond to the two regimes of energy, $E < 2mgl$, and $E > 2mgl$, as indicated by the boundary region (critical energy) shown in Fig. 3.19. For $E \ll 2\ mgl$, (inside the critical orbit or *separatrix*) the phase orbit is somewhat elliptical because the pendulum is reasonably approximated by its linearization. However, for larger energies that are still less than the critical energy, $E = 2mgl$, the ellipses become slightly squashed even as they become bigger. At the critical energy, the phase orbit (*separatrix*) has a discontinuity in slope at $\theta = \pm\pi$, where the period of the pendulum becomes infinite. Now, the pendulum's motion in time is always clockwise around the subcritical orbits. For supercritical orbits, the motion will just continue to the right as the angular displacement grows monotonically. Thus, the flow of the motion may be indicated by arrows, and for the critical orbit, we may think of arrows going into and coming out of the points where $\theta = \pm\pi$ and $\dot{\theta} = 0$. Because some of the arrows are going into these points and others are pointing away, these special points are called *saddle points*, and the arrows indicate whether the pendulum tends to go toward or away from the saddle point along the particular orbit. Trajectories that point toward the saddle point are called *stable* and those that point away are called *unstable*. Once the energy is greater than $E = 2mgl$, then the motion becomes that of a hindered rotor and the pendulum's motion is no longer confined to a finite region of phase space. (A non-hindered rotor would have a constant angular velocity $\dot{\theta}$ and its phase portrait would be a horizontal line.)

The addition of damping creates a new scenario. Now the motion of the pendulum decays and, for small amplitude oscillations the ellipse becomes a spiral toward the center as the motion dies away. For larger amplitudes the motion also decays and therefore the final state of any of the pendular motions is one of rest. The motion is always attracted to the center and therefore the center is called an *attractor*. Each center with coordinates $[\theta = 2n\pi, \dot{\theta} = 0]$ is an attractor, and which attractor the pendulum motion goes to depends upon the region of phase space from which the motion originates. The attractors alternate with the saddle points. The region of phase space that corresponds to a particular attractor is called its *basin of attraction*. Figure 3.21 illustrates a typical phase space for the damped pendulum.

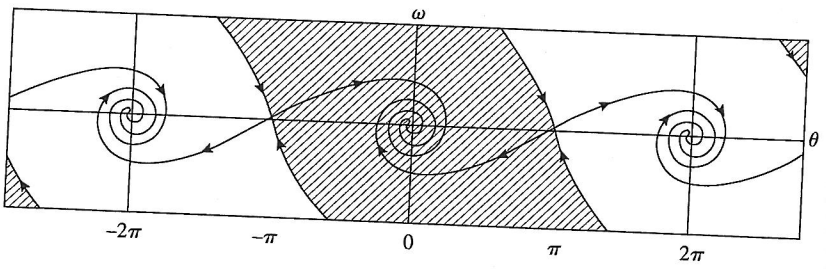

Fig. 3.21
Phase space diagram for the damped pendulum. The shaded and unshaded regions are basins of attraction. All points within a particular region are attracted to the central focal point within the basin. (From (Baker and Gollub 1996). Reprinted with the permission of Cambridge University Press.)

The attractors and the saddle points are located at what are called *fixed points* . These points are coordinates of phase space for which the derivatives of the coordinates vanish. For example, a typical second order differential equation for the damped pendulum

$$\frac{d^2\theta}{dt^2} + 2\gamma\frac{d\theta}{dt} + \frac{g}{l}\sin\theta = 0 \tag{3.80}$$

can be rewritten as two coupled first order differential equations

$$\begin{aligned}\frac{d\dot{\theta}}{dt} &= -2\gamma\dot{\theta} - \frac{g}{l}\sin\theta \\ \frac{d\theta}{dt} &= \dot{\theta}\end{aligned} \tag{3.81}$$

in the variables $\dot{\theta}$ and θ. The fixed points occur when the left side derivatives are zero at coordinates $[\theta = n\pi, \dot{\theta} = 0]$. These are the saddle points $(n = odd)$ and the attractors $(n = even)$. The arrows in Fig. 3.21 indicate whether the fixed point is stable.

Finally, if a small amount of constant or periodic forcing is added to a damped pendulum, an equilibrium state will be reached in which the added energy from the forcing just compensates for the energy dissipation. Equation (3.80) is then augmented by a forcing term $F(t)$, such that

$$\frac{d^2\theta}{dt^2} + 2\gamma\frac{d\theta}{dt} + \frac{g}{l}\sin\theta = F(t). \tag{3.82}$$

The phase space orbit will again be a closed curve, although not necessarily elliptical in shape. The closed orbit is sometimes called a limit cycle. Since the phase orbit tends to this motion—for a particular set of system parameters—no matter what the initial conditions, the orbit is also an *attractor*.

A graph of the intensity of the pendulum's response to mild periodic forcing as a function of forcing frequency is shown in Fig. 3.22 (see, for example, fig. 1 in (Miles 1988*b*)). In creating this diagram the nonlinear potential has been approximated by its linear term θ and the first nonlinear term $-\theta^3/6$ in the expansion of the pendulum's $\sin\theta$ restoring torque. For mild forcing and light damping the nonlinear approximation adequately portrays the pendulum's behavior. The cubic term provides

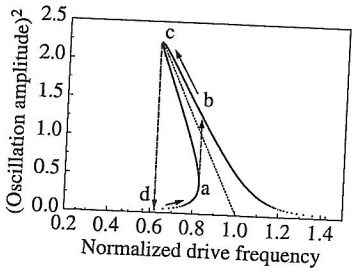

Fig. 3.22
A pendulum's response to change in forcing frequency. The response is different depending on whether the forcing starts well above the resonance or from well below resonance as explained in the text.

anharmonicity and the negative sign for the nonlinearity indicates that the equivalent linear spring has been effectively "softened" such that the natural frequency is lowered, and the peak response is shifted to the left of the small amplitude natural frequency. (A positive sign indicates that the spring has "hardened" with a commensurate shift to the right in the response peak.) A decrease in forcing frequency from above the small amplitude frequency follows the upper curve, whereas an increase from below follows the lower curve. But when each curve reaches its endpoints as indicated by the vertical dashed line the pendulum's response to forcing will change abruptly and move to the correspondingly opposite curve. Thus there is *hysteresis* in the response curve.[3]

On the other hand, strong nonresonant forcing—at a frequency different from the natural frequency—will precipitate a host of motions whose phase trajectories are complex. Some of these motions are periodic as in Fig. 3.23 and, as we will see in Chapter 6, some of the motions do not repeat and are therefore called *chaotic*.

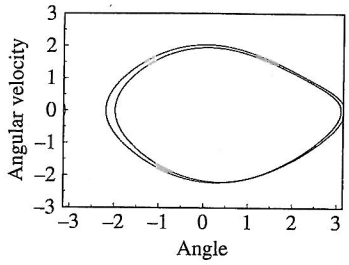

Fig. 3.23
Phase plane diagram of a pendulum whose period is twice that of the forcing period. Note that the boundary conditions on the angle are periodic and therefore there are discontinuities at $\theta = \pm\pi$.

3.3.3 An electronic 'pendulum'

Earlier in this chapter, we showed that the undamped, unforced, *linearized* pendulum was equivalent to a simple LC circuit. With the addition of damping of the pendulum, a resistance R was added to the LC circuit. Finally, the electronic circuit was augmented by a forcing voltage and the corresponding differential equation for the circuit was given by Eq. (3.23) which, in turn, is the electronic analog of Eq. (3.38) for the pendulum. In the same spirit we now present an electronic analog of the *nonlinear*, damped, forced pendulum, Eq. (3.82). It will be evident that the existence of nonlinearity adds considerable complexity.

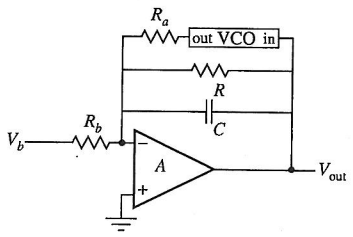

Fig. 3.24
Single op-amp circuit which is an electronic analog of a driven pendulum. The block labelled VCO is a voltage controlled oscillator (note the orientation of the input and output terminals).

Consider the apparently simple circuit depicted in Fig. 3.24. Fundamentally, this is an electronic integrator (see any standard electronics text such as (Sedra and Smith 2004)) to which is added a voltage controlled oscillator (VCO) subcircuit whose complete schematic is given in Fig. 3.25.

To analyze the overall operation of the simulator, we begin with the VCO. Operational amplifier A_1 is configured as an integrator, so its output is governed by the usual expression

$$V_1 = -\frac{1}{(20\ \text{k}\Omega)(0.1\mu\text{F})}\int V_X\, dt, \tag{3.83}$$

where V_X is the output of the multiplier module. Notice that V_X will be the product of the input voltage and either $+8$ V or -8 V, depending on the state of switch $SW1$. As can be seen in the figure, the other voltage-controlled switch, $SW2$, is set by the polarity of the input voltage.

For the purpose of this discussion, let us take a positive input voltage. $SW1$ and $SW2$ are set as shown in the diagram. The input to A_1 will be $+8 \times V_{\text{in}}$; hence according to Eq. (3.83), its output will be a linear ramp

[3] See (Jackson 1989, p. 310).

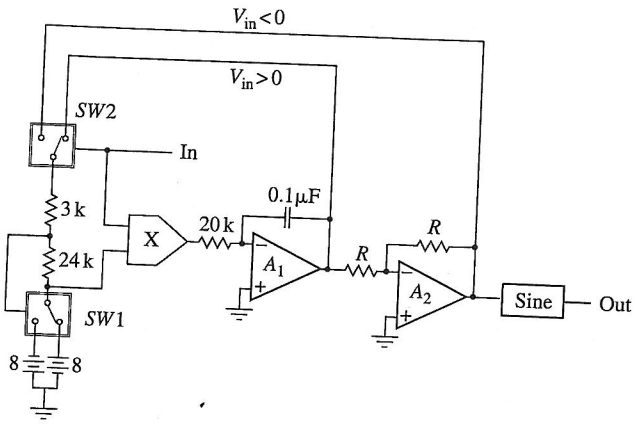

Fig. 3.25
Schematic of the VCO subcircuit. The block marked with an X is a voltage multiplier module. *SW*1 and *SW*2 are voltage-controlled switches.

with slope $-500 \times 8 \times V_{in}$ (V/s). This is fed to the top node of the 3 kΩ/24 kΩ resistor chain; the bottom of the chain is for the moment at +8 V. Note that the point between the 3 kΩ resistor and the 24 kΩ resistor will reach zero volts when the top of the chain drops to exactly −1 V. Therefore, when the negative-going ramp from amplifier A_1 reaches −1 V, switch *SW*1 will flip, now applying −8 V to the multiplier and causing the slope of the integrator ramp to change sign. This positive going linear output from A_1 will continue until it reaches +1 V, at which point *SW*1 will flip back to its original position as depicted in Fig. 3.25.

To summarize then, the output of A_1 will be a sawtooth voltage waveform with an amplitude ±1 V and a period which is twice the time required for a ramp to cover the range ±1 V (that is, a change of 2 V). From an earlier remark, the reciprocal of the slope of the output ramp is $(4000 \times V_{in})^{-1}$ (s/V) and so the *period* is $2 \times 2 \times (4000)^{-1} = 1$ ms for an input of 1 V. Altering the input voltage correspondingly changes the period (or frequency) of the oscillation.

Operational amplifier A_2 is a simple inverter which, combined with the action of *SW*2, guarantees proper operation of the VCO whenever a negative input voltage is present. The block labelled sine in Fig. 3.25 denotes a subcircuit whose purpose is to convert the sawtooth waveform to a sinusoidal waveform. Typically, such a function can be achieved by means of an array of resistors and diodes.[4]

Taking all these facts together, the VCO can be characterized by the functional relation

$$V_{out} = a \sin\left(2\pi k \int V_{in} dt\right), \tag{3.84}$$

where, for the component values used here[5], $k = 1000$ Hz/V.

[4] See, for example (Sedra and Smith 2004, fig. 13.31, p. 1204).
[5] The value of the amplitude coefficient a depends on the internal details of the sine converter circuit. A typical value might be approximately 0.7. For comparison, the amplitude of the fundamental Fourier component of a symmetric triangle waveform is $8/\pi^2 = 0.81$.

Turning now to the first circuit Fig. 3.24 and noting that the inverting input is a virtual ground, it is apparent that the conditions at the summing point of the op-amp dictate

$$\frac{V_b}{R_b} = -C\frac{dV_{\text{out}}}{dt} - \frac{V_{\text{out}}}{R} - \frac{VCO_{\text{out}}}{R_a}. \tag{3.85}$$

If we define $\theta(t) = 2\pi k \int VCO_{\text{in}}\, dt$, then noting that VCO_{in} is the same as V_{out},

$$\frac{1}{2\pi k}\frac{d\theta}{dt} = V_{\text{out}} \tag{3.86}$$

in which case Eq. (3.85) becomes

$$\frac{C}{2\pi k}\frac{d^2\theta}{dt^2} + \frac{1}{2\pi kR}\frac{d\theta}{dt} + \frac{a\sin\theta}{R_a} = -\frac{V_b}{R_b}, \tag{3.87}$$

which has the same form as the equation for a driven, damped, pendulum.

It is sometimes useful to simplify Eq. (3.87) by choosing a normalizing time

$$t^* = \left[\sqrt{\frac{2\pi ka}{CR_a}}\right] t \tag{3.88}$$

in which case

$$\ddot{\theta} + \left[\frac{1}{R}\sqrt{\frac{R_a}{2\pi kaC}}\right]\dot{\theta} + \sin\,\theta = -\frac{V_b}{a}\frac{R_a}{R_b}, \tag{3.89}$$

where the dot indicates differentiation with respect to t^*. Clearly, the right hand term assumes the role of a normalized torque.

The results of a PSpice[6] simulation of this circuit are shown in Fig. 3.26. Because of the negative sign on the right-hand side of Eq. (3.89), a negative-going ramp in bias voltage V_b corresponds to a positive applied torque. The upper trace is the voltage V_{out} which is proportional to the phase velocity. Thus the figure illustrates the circuit equivalent of a pendulum with slowly increasing torque. As the critical value of bias is reached, the pendulum just goes over the top, after which it rotates with the expected fast-slow modulation—a hindered rotational motion.

As this analysis demonstrates, the analog circuit of Fig. 3.24 will replicate the dynamics of a pendulum, but at a much faster time scale—milliseconds in contrast to seconds. The output voltage is proportional to the time derivative of the pendulum phase angle according to Eq. (3.86). The various circuit components can be selected to give any desired equivalent values of pendulum parameters, including the Q (see Appendix A) which for light damping turns out to be

$$Q = R\sqrt{\frac{2\pi kaC}{R_a}}. \tag{3.90}$$

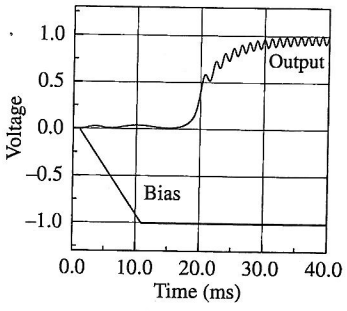

Fig. 3.26
PSpice results for the pendulum simulation circuit. The slowly ramping bias is equivalent to a slowly increasing torque applied to a pendulum.

[6] PSpice is software for simulating electronic circuits and is a product of Cadence Design Systems, Inc. Further information about PSpice may be found at www.orcad.com.

While this electronic analog is more complex than the LRC circuit for the linearized pendulum, there is an even more complex electrical analog which we describe in Chapter 9. This second electrical analog to the nonlinear pendulum is a superconducting, quantum mechanical device known as a Josephson Junction.

3.3.4 Parametric forcing revisited

We have already provided a simple model of parametric pumping for the case of the linearized pendulum. Let us now look at some of the complications provided by the nonlinear pendulum for the self-pumped swing and for parametric pendulums such as *O Botafumeiro*.

Pumping a swing

In the case of the playground swing , the rider's pumping action involves movement of his or her body so that the effective length of the swing is periodically altered. One method requires the rider to alternately stand and squat on the swing such that the effective length of the swing shortens and lengthens periodically. The other common method is for the rider to remain seated but to alternately rock his body, again so that the effective length of the swing changes periodically. Variations on either of these methods make use of pulling and pushing on the ropes of the swing to further enhance the motion. A further distinction can be made between methods of (a) initiating the motion, and (b) enhancing and maintaining the motion. In the last three decades a flurry of scholarly analysis has appeared on the physics of pumping a swing. Examples are given in the following references: (Tea and Falk 1968; Siegman 1969; Gore 1970, 1971; McMullan 1972; Walker 1989; Case and Swanson 1990; Wirkus et al. 1998).

In 1968 Tea and Falk of City College of the University of New York analyzed the case of a standing rider pumping the swing by alternately standing and squatting on the swing (Tea and Falk 1968). This activity periodically changes the center of mass of the swing and thereby its effective length in a manner very similar to that shown in Fig. 3.14. The swing may be treated as a simple pendulum with all its mass concentrated at the center of mass. The rider is squatting when the swing descends and then quickly stands as the swing passes through its lowest point. He can choose either to repeat the pattern on the return half of the cycle or simply to remain standing until the beginning of a new cycle.

Energy considerations help us discover the effects of the pumping action. In going from a squatting to a standing position at the point of lowest arc, the force provided by the pumper is radial, and therefore does not provide a torque that changes the angular momentum of the swing and rider. Thus, the angular momentum is conserved, while the center of mass and therefore the effective length of the pendulum are changed. Conservation of angular momentum prescribes that the decrease in length is compensated by an increase in angular velocity. In turn, the increased angular velocity leads to

a rapid increase in kinetic energy at the bottom of the arc that converts to an increase in potential energy at the maximum height of the swing. Therefore the objective of increased amplitude of the swing is achieved by the pumping action. Following (Tea and Falk 1968) we develop an equation for the increase of the swing's angular amplitude as a result of the pump action.

Assuming negligible friction, both angular momentum and energy are conserved at various points in the motion. In making the transition from the squatting to the standing position, angular momentum is conserved as follows:

$$ml_0^2\omega_A = ml_1^2\omega_B, \tag{3.91}$$

where ω_A and ω_B are respectively the angular velocities before and after the rider stands up and l_0 and l_1, respectively, are the effective lengths of the pendulum before and after the rider stands. Similarly, total energy is conserved prior to the rider standing, and then an increased energy level (from the work done by the rider) is obtained after the rider stands. That is,

$$mgl_0(1-\cos\theta_0) = \frac{1}{2}ml_0^2\omega_A^2 \text{ and } mgl_1(1-\cos\theta_1) = \frac{1}{2}ml_1^2\omega_B^2. \tag{3.92}$$

With some algebraic manipulation it is possible to show that these equations lead to an increase in the maximum angular displacement of the swing:

$$\cos\theta_0 - \cos\theta_1 = \left(\frac{l_0^3 - l_1^3}{l_1^3}\right)(1-\cos\theta_0). \tag{3.93}$$

Since $l_0 > l_1$ the maximum displacement is indeed increased by the pump action. Eq. (3.93) can be rearranged to generate a map of θ_1 in terms of increasing θ_0 values. Figure 3.27 (amplitude versus no. of cycles from Eq. (3.93)) shows the increase in the swing's angular amplitude as a function of the number of pumping cycles, assuming that the center of mass shortens by 10% during each pump action.It is apparent that the pumping action becomes more effective as the angular displacement increases. (The difficulty of getting the swing started is well known to swing riders.)

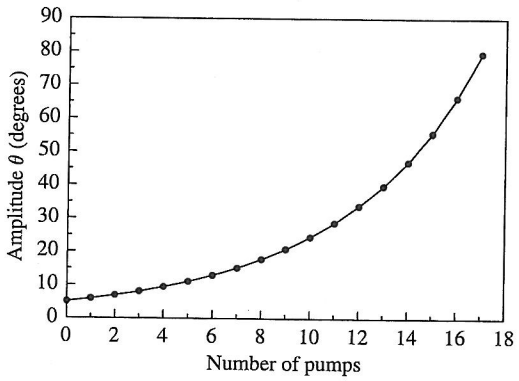

Fig. 3.27
Amplitude versus number of pumps using Eq. (3.93).

The amplitude increases as a result of the rider standing up. Is this amplitude increase lost when the rider squats? While some amplitude is lost, the fact that the squatting occurs at the extremes of the swing motion means that the change in potential energy of the center of mass is less than during the standing motion at the bottom of the arc and therefore the energy change in standing is less by a factor of sin θ.

It is interesting to determine how much energy is required of the rider during the action of standing. The work done is equal to the change in kinetic and potential energy as the center of mass goes from point A to point B. Therefore the expression for the work is

$$W_{AB} = -\int_{l_A}^{l_B} m(g + \omega^2 r)dr. \tag{3.94}$$

Again, we use conservation of angular momentum through the rising motion such that

$$\omega = \frac{r_A^2}{r^2}\omega_A. \tag{3.95}$$

Substitution of this result into the expression for the work and carrying out the integration eventually leads to

$$W_{AB} = -mg(l_A - l_B)\left[1 + l_A\frac{(1 - \cos\theta_0)(l_A + l_B)}{l_B^2}\right]. \tag{3.96}$$

The work done increases as the swing goes higher because of the cosine factor, again a common experience. This increased work is due to greater centrifugal force at the bottom of the arc from the higher velocity of the swing. The force and therefore the work done in rising requires an increasingly greater expenditure of energy by the rider. On the other hand, the graph in Fig. 3.27 suggests that this extra work also produces larger increments in the swing's amplitude.

This simple analysis applies to both standing and sitting pumping although in the latter case the change in the center of mass is smaller and therefore the predicted change in swing amplitude will be less for each cycle. In this analysis, we have not included frictional effects that might be found in the suspension point of the swing or in the surrounding air. We expect, however, that these effects are relatively small and that our discussion gives a reasonable picture of the underlying physics. In 1969, (Siegman 1969) Siegman of Stanford University showed that the model of pumping the swing by changing its center of mass is equivalent to the action of the common notion of a parametric pendulum; namely a pendulum that is energized by the periodic variation of the vertical position of its pivot point. The connection of the pumped swing with parametric devices opens new vistas of related phenomena (Strarrett and Tagg 1995; Louisell 1960).

In 1990, Case and Swanson of Grinnel College took a somewhat different approach (Case and Swanson 1990). They modeled the rider and swing as a compound pendulum, with a massive bob, m_1, at the rider's

position on the seat and the rest of the body by two other bobs, m_2 that account for the extension of the body due to the rest of the body parts—arms, legs, head and so on. For simplicity, the two other bobs of equal mass are represented as dumbbells that are positioned symmetrically about the seat of the swing, as shown in Fig. 3.28. Using the notation in this figure, the Lagrangian for the system is, to within a constant, as follows;

$$L = T - V = \frac{1}{2}(m_1 + 2m_2)l_1^2\left(\frac{d\phi}{dt}\right)^2 + m_2 l_2^2\left(\frac{d\phi}{dt} + \frac{d\theta}{dt}\right)^2 + (m_1 + 2m_2)l_1 g\cos\phi. \tag{3.97}$$

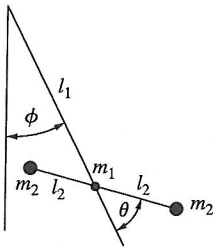

Fig. 3.28
Person on a swing modeled by a pair of point masses.

Our interest is in the motion of the swing itself. The motion of the rider, relative to the position of the swing seat, is that of a periodic dumbbell and satisfies an equation of the form

$$\theta = \theta_1 + \theta_0\cos\omega t, \tag{3.98}$$

where ω is the angular frequency of the pumping. The "at-rest" angle is θ_1 and the amplitude of the variation in orientation of the "dumbbell" is θ_0. Because the pendulum is nonlinear, the resonant frequency of the swing decreases as the amplitude of the motion increases. Therefore the rider will naturally vary the pumping frequency in order to match the resonant frequency of the swing. Lagrange's method provides the equations of motion for the swing:

$$\frac{d}{dt}\frac{\partial L}{\partial\dot{\phi}} - \frac{\partial L}{\partial\phi} = [(m_1 + 2m_2)l_1^2 + 2m_2 l_2^2]\ddot{\phi} + [m_1 + 2m_2]l_1 g\sin\phi + 2m_2 l_2^2\ddot{\theta} = 0, \tag{3.99}$$

with substitution from Eq. (3.98). The result is the equation of motion for a harmonically driven, undamped, nonlinear, pendulum,

$$[(m_1 + 2m_2)l_1^2 + 2m_2 l_2^2]\ddot{\phi} + [m_1 + 2m_2]l_1 g\sin\phi = 2\omega m_2 l_2^2\theta_0\cos\omega t. \tag{3.100}$$

While this equation looks complex, its essence is expressed by

$$\alpha\ddot{\phi} + \beta\sin\phi = \gamma\cos\omega t,$$

which is simply an undamped pendulum with sinusoidal forcing. The rotational motion of the dumbbell provides the pumping action and therefore increases the amplitude of the swing. We emphasize that the period of the pendular motion will increase with amplitude since the linearization approximation for small angle is not applied in this equation, and therefore the rider will need to decrease the frequency of the pumping action as the swing's amplitude increases.

Since the model uses a symmetric dumbbell, the center of mass of the swing is always at the position of the central mass, and therefore the parametric mechanism described earlier—periodically varying the center

of mass relative to the pivot—does not apply. However, if the dumbbell is allowed to be asymmetric, then the center of mass will change and the parametric energizing mechanism does come into play. But interestingly, Case and Swanson found that the parametric mechanism only dominates as the amplitude becomes large. We might have suspected this from a study of Fig. 3.27 where the amplitude of the swing grows slowly at first and then more rapidly at larger angular displacements.

Finally, Wirkus et al. of Cornell university (Wirkus et al. 1998) incorporated the work of both Falk and Tea, and Case and Swanson to determine an optimum mix of pumping techniques. They concluded that the rider should begin with sitting pumping, and progress to standing pumping at larger amplitudes for the most rapid accumulation of swing amplitude. In the full asymmetric dumbbell case the analysis becomes very complicated. The interested reader is referred to their work for the details. This brief survey of 40 years of study of the motion of playground swings illustrates the continuing fascination and inherent complexity of the subject. Yet the self pumping of playground swings is just one application of parametric forcing. Let us now return to parametric pumping through change in the length of the pendulum. Our example is *O Botafumeiro*.

O Botafumeiro: A simple model

Like the self-pumped swing, O Botafumeiro is a parametric pendulum whose length is periodically shortened. This pumping modifies the effect of gravity such that the downward force on the censer is increased as the pendulum is shortened, and decreased as the pendulum regains its full length. We begin with a nondissipative Lagrangian L, then develop equations of motion for the conservative system, and finally, insert the pumping and dissipative effects to complete the equations of motion. The Lagrangian for the appropriate conservative system is

$$L = T - V = \frac{1}{2}m\dot{r}^2 + \frac{1}{2}mr^2\dot{\theta}^2 - mgr(1 - \cos\theta). \tag{3.101}$$

The censer is approximated by a point mass (m) and the radial distance r is measured from the pivot to the center of mass of the censer. The equations of motion follow from standard operations on L,

$$\frac{d}{dt}\left(\frac{\partial L}{\partial \dot{r}}\right) - \frac{\partial L}{\partial r} = 0 \text{ and } \frac{d}{dt}\left(\frac{\partial L}{\partial \dot{\theta}}\right) - \frac{\partial L}{\partial \theta} = 0, \tag{3.102}$$

that lead to radial and tangential components, respectively, of the motion of the pendulum. These computations yield the following equations of motion,

$$\begin{aligned} m\ddot{r} - mr^2\dot{\theta} + mg(1 - \cos\theta) &= 0 \\ mr^2\ddot{\theta} + 2mr\dot{r}\dot{\theta} + mgr\sin\theta &= 0. \end{aligned} \tag{3.103}$$

The first equation is the radial equation and includes a centrifugal term $mr^2\dot{\theta}$, whereas the second equation is the tangential equation and describes

the angular acceleration and the torques causing that acceleration. (The term $2mr\dot{r}\dot{\theta}$ is due to Coriolis force, which is discussed in the next chapter.) We focus on the tangential equation and add a dissipative torque that is proportional to the square of the tangential velocity, $v_T = r\dot{\theta}$. For an extended object moving swiftly in air, the frictional force is typically given by

$$F_{\text{Friction}} = \frac{1}{2}\rho_A S C_D v^2. \tag{3.104}$$

The friction parameters are the density of air ρ_A, the equivalent surface area that the censer presents as it moves through the air S, and the drag coefficient of the censer C_D. The latter two parameters are provided by Sanmartin (1984) as well as other necessary parameter values. See the table below. The modified equation of motion then becomes

$$mr^2\ddot{\theta} + 2mr\dot{r}\dot{\theta} + \frac{1}{2}\rho_A S C_D (r\dot{\theta})^2 r + mgr\sin\theta = 0. \tag{3.105}$$

Dividing Eq. (3.105) by mr^2 yields a new equation

$$\ddot{\theta} + 2\dot{r}\dot{\theta}/r + \frac{1}{2m}\rho_A S C_D \dot{\theta}^2 r + g/r\sin\theta = 0. \tag{3.106}$$

The pumping action is now added. We note that g is affected by the radial acceleration of the censer and therefore both r and g are functions of time. Figure 3.12 shows the approximate path of the censer as caused by the pumping action of the *tiraboleiros*. The period of the pumping is twice the period of the pendulum and the time variation of the pendulum length may be crudely modeled by

$$r(t) = \left(r_0 - \frac{\Delta r}{2}\right) + \frac{\Delta r}{2}\cos\omega_F t. \tag{3.107}$$

The variation in $r(t)$ modifies the effective gravitational field as

$$g(t) = g_0 - \ddot{r} = g_0 + \frac{\Delta r}{2}\omega_F^2 \cos\omega_F t. \tag{3.108}$$

The parameter values provided by Sanmartin (1984) are given in the following table.

ρ_A	1.29 kg/m^3
S	$\pi(l/3)^2 = \pi(1.2/3)^2 = 0.503$ m^2
C_D	0.59
m	57 kg
r_0	20.9 m
Δr	2.9 m
$\omega_F(0)$	1.37 rad/s (zero amplitude)
g_0	9.8 m/s^2
ω_0	$\sqrt{g/r_0} = \sqrt{9.8/20.9} = 0.685$ rad/s

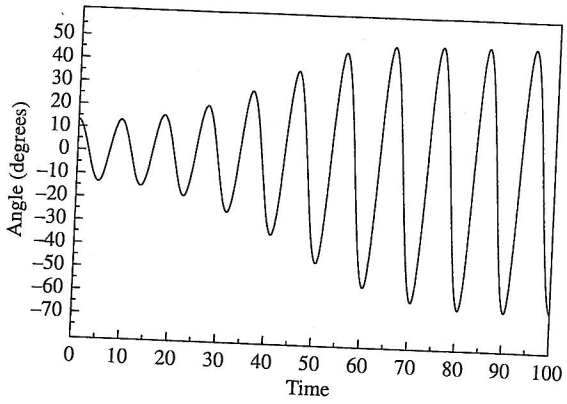

Fig. 3.29
Time series of the angular displacement of O Botafumeiro based upon the model described in the text.

The zero amplitude value of the pumping frequency ω_F is determined by noting that O Botafumeiro requires two pumping cycles for each oscillation. Of course, the pumping team will need to adjust their frequency of forcing as the amplitude increases, and therefore our model incorporates adjustment in the frequency according to a first order approximation of Eq. (3.64):

$$\omega_F = \frac{\omega_F(0)}{[1 + \theta_0^2/16]}.$$

As the amplitude changes the *tiraboleiros* need to modify the amount of pulling on the rope. This factor is more difficult to model. Relatively simple feedback mechanisms tend to lead to instability, and therefore we do not carry the process further. The resulting simulation shown in Fig. 3.29 illustrates the general features of the motion of O Botafumeiro's motion. Like the real pendulum the simulation starts at about 13° where a priest initially pushes the censer. It takes about 80 s to reach full amplitude in about 17 forcing cycles, in agreement with the real pendulum. However, there are two points of discrepancy between the model results and the reality. For the real pendulum the final amplitude is about 82° whereas in the model the amplitude is considerably less. Furthermore the amount of forcing in the model is $\Delta r = 0.9$ which is only about one third of the actual forcing stated in the table. Unfortunately, the model becomes unstable for strong forcing. These difficulties might be somewhat resolved by a feedback mechanism that would tie the forcing strength to the amplitude. As noted, simple feedback mechanisms seem to be unstable and therefore we leave the model with only the forcing frequency adjustment. However, the agreement of many facets of the real pendulum's motion with that exhibited by the simple model is gratifying, and modest deviation in the parameters' values from those given in the table yield results that more closely approximate the buildup in the real pendulum.

As well as the noted discrepancies with the motion of the real pendulum, we also note that the physical complexity of O Botafumeiro is considerably simplified in the model. The mass of the rope is a significant factor at

15.7 kg. The pendulum is not rigid and is perhaps more properly treated as a double pendulum. The thickness of the rope at 4.5 cm is also important and contributes to friction effects beyond those modeled for the censer alone. Sanmartin has included many of these effects in his analysis and consequently achieves a better agreement of theory and experiment. Nevertheless our simple model adequately represents many of the features of O Botafumeiro, one of the world's most unique pendulums.

At this point we defer further technical analysis of the nonlinear pendulum until Chapter 6 in which we discuss the chaotic pendulum. Let us end this chapter with a literary note.

3.4 A pendulum of horror

In 1842, the first American author of tales of horror, Edgar Allen Poe (1809–1849) wrote a short story entitled, *The Pit and the Pendulum* (Poe 1966). Poe's stories often contained a strong element of terror, in part, because he left many of the details quite vague, just as a standard technique of psychological terror is to keep the victim in ignorance as to his ultimate fate. The *Pit and the Pendulum* does exactly that to both the reader and the protagonist. The main, and practically only character, whose name we never know, is brought as a prisoner before the court of the Spanish inquisition in Toledo, Spain. The trial is recalled by the prisoner during a confused dreamlike state. Subsequently, he is carried into the bowels of the earth and flung into a damp and dark dungeon. He attempts to investigate the physical condition of his cell but exhaustion forces sleep upon him. When our hero awakes, he is tied to a low cot with only one hand free with which to feed himself the spiced meat that is mysteriously laid beside the cot. (Fig. 3.30) He now notices a large pendulum high above the cot and observes the start of its oscillations. However, the presence of rats attempting to steal his food distracts his attention from the pendulum. Meanwhile the pendulum continues to swish by overhead and, with each arc, the pendulum bob, now seen to be in the shape of a large sharp metal blade, comes ever closer to his person. The descent of the pendulum is tortuously slow giving our hero a chance to assess his situation. The strap by which he is held to the cot is a long single piece that is wound many times around his body. His first thought is that the pendulum might eventually cut the strap and allow him to free himself before he suffers his apparently inevitable fate. But, to his chagrin, he notes that the only place where the strap does not cover his body lies in the path of the pendulum. Therefore he needs to devise some other method of regaining freedom of movement.

The story continues as the pendulum draws ever closer with increasingly larger amplitudes for its swing. Like O Botafumerio, this pendulum can also be heard to make an ominous swishing sound as it describes its increasing arc. As the pendulum nears the prisoner's body he estimates the total range of the pendulum's motion to be about thirty feet. Given that the room itself is only about forty feet high, this pendular motion is of very large amplitude, again similar to O Botafumerio. At this point we refer

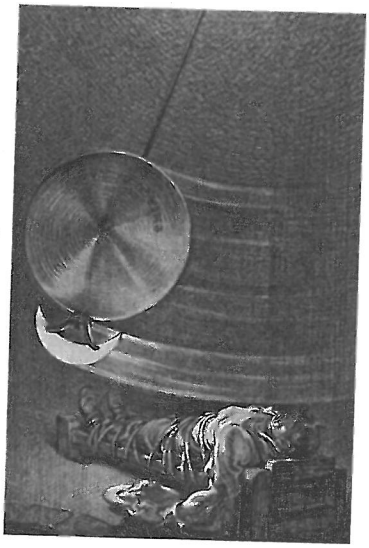

Fig. 3.30
Depiction of the victim in Poe's story "The Pit and the Pendulum." This drawing is actually a political cartoon drawn by Udo Keppler in the 1920s, highlighting the effect of inflation during that decade. Note "Cost of Living" on the blade/bob. (Political Cartoon Collection, Public Policy Papers, Department of Rare Books and Special Collections, Princeton University Library. Reprinted with permission.)

readers to the original story in order to learn the fate of the prisoner. However, it is of interest to ask whether Poe's tale is realistic. Does it seem likely that the inquisition would have used something like a motorized pendulum in this context? The answer is probably no. The time frame of the story is not clear but we may impose some limitations. The Spanish inquisition ended in the early nineteenth century and the story itself refers to capture of the city by a certain French General La Salle. Perhaps this allusion is to the Napoleonic wars, but the time could also be much earlier. Scholars (LLorente 1823; Lea 1907) suggest that while torture was a standard and accepted means of learning truth in matters both secular and religious, it was not likely to be used gratuitously by the inquisition once sentence had been passed. And, in the story, there had been a trial and a sentence pronounced. Furthermore, instruments of torture were fairly simple and direct. A driven pendulum that would slowly and noiselessly descend, and slowly increase its amplitude of motion, all inside and above a small dungeon, is relatively complex and hardly worth the effort even if craftsmen could be found to build such a machine. Therefore Poe's story is somewhat unrealistic in this regard. Some believe that the inspiration for Poe's tale was actually a large swinging bell that Poe had observed. Nevertheless, realistic or not, the image of a sharp-edged pendulum makes it frightening. It is the regularity and inexorability of the pendulum's motion that contributes to the climate of terror found in this story. The pendulum's periodicity, that is so important in other contexts, is here made to serve the cause of literary suspense.

With Poe's pendulum we conclude our discussion of the conventional classical physics of the pendulum. This discussion, beginning with the undamped linearized pendulum of the previous chapter, and progressing in complexity to the nonlinear pendulum of this chapter, will help our understanding of the pendulum as we meet more of its facets in the following chapters. In the next two chapters, we discuss important applications of what are, for the most part, linearized pendulums. The nonlinear pendulum is especially important for understanding the chaotic pendulum (Chapters 6 and 7) and the quantum pendulum (Chapter 8).

3.5 Exercises

1. Consider the effect of *constant* forcing of the damped driven pendulum. Start with Eq. (3.18) and let the forcing term be simply Υ.

   (a) Write the new equation of motion.
   (b) One way to think about this system is to make the force (aside from friction) acting on the pendulum to be $F = -mgl\sin\theta + \Upsilon$ and find a "potential" $V = -\int F\,d\theta$. Write the expression for the potential and sketch its graph as a function of θ. Because of the shape of the graph this potential is sometimes called a "washboard" potential.

   If the constant torque is slowly increased from zero the pendulum bob rises (with negligible angular velocity) up to the critical angle of 90°. In this regime the local minima in the washboard potential will keep the pendulum bob from moving out of the local minimum. At $\theta_c = 90°$ the torque is at its critical value of $\Upsilon_c = mgl$.

The washboard potential is now sufficiently steep that the local minima disappear and the pendulum bob can fall out of the local minimum, accelerate and rotate almost freely. Thus there is a sudden jump in the pendulum's angular velocity. (The rotation is slightly hindered by the bumps in the washboard, corresponding to the pendulum slowing as it goes over the top of its motion.) If the constant torque is now gradually decreased, then the pendulum continues the hindered rotational motion because it now has sufficient momentum. Even at relatively low values of the torque where, for increasing torque, the pendulum was previously stationary, it now still rotates. The phenomenon of different behaviors with increasing and decreasing torque is another example of *hysteresis*, and a graph is shown in Fig. 3.31.

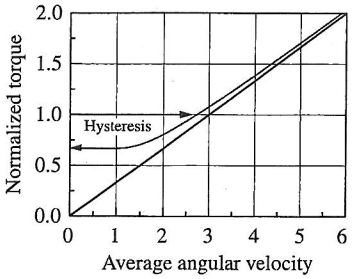

Fig. 3.31
Slowly varying constant torque versus angular velocity. Another example of hysteresis.

2. (a) Substitute the solution given by Eq. (3.6) into Eq. (3.2) and thereby verify Eq. (3.6). (b) Determine the phase angle ϕ in terms of the initial angle $\theta(0)$ and the initial angular velocity, $\dot{\theta}(0)$.
3. With the forced, damped linearized pendulum, the amplitude of the steady state part of Eq. (3.19) $F/\sqrt{4\gamma^2\omega^2 + (\omega_0^2 - \omega^2)^2}$ varies with both frequency ω and damping strength γ. Sketch a few curves of Amplitude versus ω, each being at different values of damping strength. (See the Appendices for samples of such curves.)
4. Physical systems that are linear and dissipative all respond to periodic forcing as indicated in the curves developed in exercise 3. Such curves may be characterized by a "quality" factor Q that is calculated in the following manner. First, we note that the "power" of the pendulum's response is proportional to the *square* of the steady state solution time series, $F^2/((4\gamma^2\omega^2) + (\omega_0^2 - \omega^2)^2)$. Find the value of the power $P(\omega_0)$ when $\omega = \omega_0$. (For light damping, this value of the power should be very close to the maximum value.) Now observe that when $4\gamma^2\omega^2 = (\omega_0^2 - \omega^2)^2$, the power is reduced by one-half. For light damping, where $\omega \approx \omega_0, \omega + \omega_0 \approx 2\omega_0$, we define the half-width of the resonant peak as $\Delta\omega = |\omega - \omega_0|$. The quality factor Q gives a measure of the sharpness of the resonant peak in terms of the relative size of the resonant frequency and the width of the curve at the half power points. That is we define $Q = \omega_0/2\Delta\omega$. Using the information given in this exercise show that $Q = (1/2)(\omega_0/\gamma) = (1/2)\omega_0\tau$. Thus, a sharp resonant curve with light damping has a high Q. Find Q for a pendulum with a period of 1 s and a ring time of 10 s. (Remember the factor of 2π in these calculations.) See Appendix A.
5. The amount of damping is inversely proportional to the "ring time" τ of a pendulum or spring or electric LRC circuit. That is, the less damping the longer the time that the system oscillates. Mathematically, $\tau \approx 1/\gamma$. The calculations made in the previous exercise lead to a very simple relationship between the linewidth $2\Delta\omega$ and the ring time τ. Show that the linewidth of the resonance curve is related to the ring time as $\Delta\omega \cdot \tau \approx 1$. This relationship is similar to the energy version of the Heisenberg uncertainty principle in quantum physics whereby the lifetime of an unstable energy state is inversely proportional to the uncertainty in energy.
6. Eq. (3.13) has the same general form as Eq. (3.2). Make the former exactly match the latter and thereby find the corresponding value for γ. Show that the quality factor for this electrical circuit is given by $Q = \omega_0 L/R$. Find Q for a circuit that is resonant at 50 MHz, has an inductance of $L = 2\,\mu h$, and resistance of 2 Ω.
7. The Laplace transform technique is a powerful one for dealing with pulse systems. However, simpler techniques may be used at least during the time of the first pulse, $0 < t < \tau$. In the equation of motion as given, with initial conditions, by Eq. (3.30), try a solution of the form $\theta(t) = c_1 \sin\omega_0 t + c_2 \cos\omega_0 t + B$. Substitute this trial solution into Eq. (3.30), determine B, and the constants c_1 and c_2. Compare your result to the first term in the comprehensive solution given by Eq. (3.37).

The chaotic pendulum

6

6.1 Introduction and history

Much of the history of physics has been characterized by the effort to understand, in great detail, increasingly smaller pieces of nature; beginning with classical particles and waves, and progressing to molecules, atoms, nuclei, and elementary particles. This trend became especially pronounced in the twentieth century with the development of sophisticated experimental apparatus capable of probing deeply into nature's innermost parts. Aside from the sense that one is closer to reality at the deeper levels of nature, it is plausible to assume that a clear understanding of the small pieces of nature will lead to a clear view of the large picture. The whole is presumed equal to the sum of its parts. This approach is sometimes call *reductionism*.

More recently, in certain areas of physics, the opposite methodology has proved fruitful. New structure and organization may become evident when there is complexity, large numbers of parts, several degrees of freedom, or even just sufficient energy to make a discrete change in the system. Indeed, sometimes the whole is more than the sum of its parts. This creation of new richness of behavior often occurs in the study of processes that are pushed well beyond their equilibrium configurations. Researchers find new levels of organization, new complexity that does not seem to be obvious from a consideration of the individual parts of the process (Prigogine 1980). For example, if reactants are forced rapidly into certain chemical reactions, the resultant products may show spatial or temporal ordering (Zhabotinskii 1991). Or convective systems with large temperature gradients may exhibit new structural or dynamic organization of fluid motion. Even the motion of the humble pendulum achieves a new level of complexity if it is driven energetically at nonresonant frequencies. Why should this be? Part of the answer lies in the fact that when systems are well beyond equilibrium, they are often unstable, and instability can lead to new complex states. The entire field of chaotic dynamics is an important manifestation of a new order being achieved through instability. It is remarkable that the damped driven pendulum is an archetypical example of chaotic dynamics. The chaotic pendulum is therefore our next story of the pendulum.

The chaotic pendulum

6

6.1 Introduction and history

Much of the history of physics has been characterized by the effort to understand, in great detail, increasingly smaller pieces of nature; beginning with classical particles and waves, and progressing to molecules, atoms, nuclei, and elementary particles. This trend became especially pronounced in the twentieth century with the development of sophisticated experimental apparatus capable of probing deeply into nature's innermost parts. Aside from the sense that one is closer to reality at the deeper levels of nature, it is plausible to assume that a clear understanding of the small pieces of nature will lead to a clear view of the large picture. The whole is presumed equal to the sum of its parts. This approach is sometimes call *reductionism*.

More recently, in certain areas of physics, the opposite methodology has proved fruitful. New structure and organization may become evident when there is complexity, large numbers of parts, several degrees of freedom, or even just sufficient energy to make a discrete change in the system. Indeed, sometimes the whole is more than the sum of its parts. This creation of new richness of behavior often occurs in the study of processes that are pushed well beyond their equilibrium configurations. Researchers find new levels of organization, new complexity that does not seem to be obvious from a consideration of the individual parts of the process (Prigogine 1980). For example, if reactants are forced rapidly into certain chemical reactions, the resultant products may show spatial or temporal ordering (Zhabotinskii 1991). Or convective systems with large temperature gradients may exhibit new structural or dynamic organization of fluid motion. Even the motion of the humble pendulum achieves a new level of complexity if it is driven energetically at nonresonant frequencies. Why should this be? Part of the answer lies in the fact that when systems are well beyond equilibrium, they are often unstable, and instability can lead to new complex states. The entire field of chaotic dynamics is an important manifestation of a new order being achieved through instability. It is remarkable that the damped driven pendulum is an archetypical example of chaotic dynamics. The chaotic pendulum is therefore our next story of the pendulum.

The chaotic pendulum

What do we mean by chaotic dynamics? What are its characteristics? Chaotic systems are unstable deterministic systems whose trajectories are extremely *sensitive to the initial condition* of the system. The French mathematician Henri Poincaré is generally credited as being the first to articulate the behavior of such systems. In Chapter 1, we repeated his often quoted words that suggest how a deterministic system might behave in a probabilistic way. Let us give a larger version of that quotation.

> A very small cause that escapes our notice determines a considerable effect that we cannot fail to see, and then we say that the effect is due to chance. If we knew exactly the laws of nature and the situation of the universe at the initial moment, we could predict exactly the situation of that same universe at a succeeding moment. But even if it were the case that the natural laws had no longer any secret for us, we could still only know the initial situation *approximately*. If that enable us to predict the succeeding situation with the same approximation, that is all we require, and we should say that the phenomenon had been predicted, that it is governed by laws. *But it is not always so:* it may happen that small differences in the initial conditions produce very great ones in the final phenomena. A small error in the former will produce an enormous error in the latter. Prediction becomes impossible, and we have the fortuitous phenomenon.[1]

In this statement, Poincaré makes the distinction between two kinds of deterministic systems. He notes that we would consider a system to be deterministic if our prediction of its final state were accurate to approximately the same degree as our knowledge of its original state. This is our common experience. In science education we perform laboratory exercises in which variables are slightly uncertain. Yet we are satisfied that our calculations and observations have proved some physical law if the results give *approximately* the "right" numbers. That is, uncertainty is not amplified. (Technically, we allow uncertainty to increase only *linearly* with time if the process is time dependent. If the initial uncertainty is Δx_0 then after a time t the uncertainty has grown according to $\Delta x = \Delta x_0 \lambda t$, where λ is some constant growth rate.) On the other hand, Poincaré suggests that with certain systems the initial uncertainty increases quite rapidly and therefore the final outcome looks as if it is the result of a random process or probability. Systems that behave in this latter manner are *unstable*. Unstable systems have the ability to be affected by very small changes in their initial conditions. This property is referred to as *sensitivity to initial conditions* (SIC) and it is the hallmark of chaotic dynamics. (Technically, sensitivity to initial conditions occurs when an initial uncertainty grows *exponentially* in time. The uncertainty grows according to $\Delta x = \Delta x_0 e^{\lambda t}$.) Of course, if a system is deterministic and if the initial conditions are somehow known to an *infinite* degree of precision, then the final state of the system is completely predictable. In practice however, no real system is completely determined, and therefore it is the instability of the system coupled with the initial uncertainty that leads to the possibility of widely varying outcomes. Thus, the deterministic unstable system, the chaotic system, gives the appearance of being probabilistic.

[1] See (Poincaré 1913, p. 397).

Chaotic dynamics, or Chaos as it is popularly named, is not to be confused with the primordial chaos suggested by various mythologies to exist at the moment of creation, or with the chaos that might ensue in the wake of a parade of small children and active dogs being turned loose in a confined space. In fact, the term "chaos" was coined by James Yorke and Tien-Yien Li of the dynamics group at the University of Maryland. In 1975 Li and Yorke published a paper with the title "Period Three implies Chaos" (Li and Yorke 1975) and the name stuck. Thus, we now define chaotic systems as deterministic systems that are unstable enough to exhibit a probability-like nature through their sensitivity to initial conditions. While confusion of the technical meaning with the common meaning is unfortunate, *chaos* is now firmly entrenched in the scientific literature as the short form for *deterministic chaotic dynamics*.

The history of chaos might be arbitrarily divided into two segments: first, from the time of Poincaré's large work on dynamics in 1892 to Edward Lorenz's 1963 computer simulations of unstable convection and second, from the early 1960s to the present. This division provides an approximate distinction between the scattered efforts of individual researchers, and the later epoch in which chaos came to be an accepted field complete with journals and conferences dedicated to the subject. We briefly mention a few of these contributions from the first epoch. In his studies of celestial motions (Peterson 1993), Poincaré realized that analysis had limitations especially when it came to nonlinear dynamics and revived the use of geometric methods to study stability in such systems. The American mathematician George David Birkhoff (1884–1944) continued the geometric tradition of Poincaré and helped to develop the general aspects of the connection between unstable systems and probability. In 1932 he published the first chaotic attractor to appear in the literature. The Russian mathematician Aleksandr Mikhailovich Liapounov (1857–1918)[2] studied the question of stability in dynamical systems and his name is now associated with the exponent λ that is the rate of exponential growth of uncertainty. In 1944 Levinson suggested that a system with three degrees of freedom and forcing (like a driven pendulum) could produce a chaotic attractor. Other important pioneers include the English mathematician Dame Mary Cartwright (1900–1998) who, in collaboration with John Littlewood (1885–1977), analyzed the van der Pol nonlinear oscillator during World War II (Tattersall and McMurran 2001), the Russian mathematicians Kolmogorov, well known for his work in probability, and Arnol'd and Moser, the last three for whom the famous KAM theory of nonlinear systems is named. Stephen Smale produced a series of seminal theoretical papers in the 1960s that are important for more advanced treatment of the chaotic pendulum. On the experimental side Balthasar van der Pol (1889–1959) used (*c.*1927) an LRC electrical circuit with a nonlinear resistance to produce chaotic behavior. Georg Duffing (1861–1944) created mechanical devices, specifically oscillators, with spring

[2] The spelling "Liapounov" is slightly different from that typically used to describe the "Liapounov" exponent.

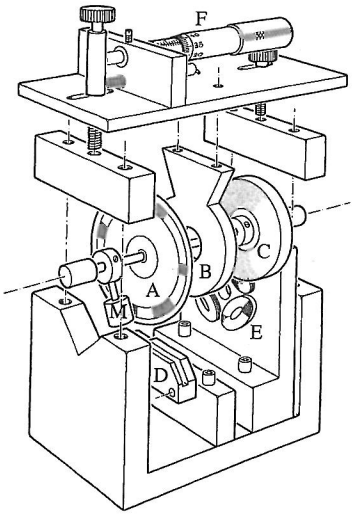

Fig. 6.1
Exploded view of an experimental forced, damped pendulum, designed by JAB and John Smith.

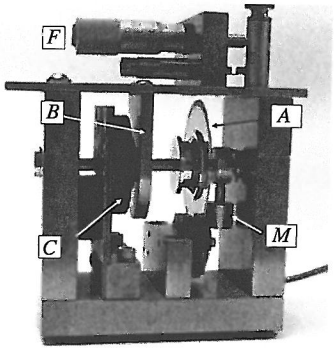

Fig. 6.2
Photograph of the Blackburn–Smith pendulum.

constants that depended upon position, to study nonlinear vibrations (*c.*1908). Finally we note the work of the mathematician Chihiro Hayashi (1911–1987) of Kyoto University in whose research group then (in 1961) graduate student Yoshisuke Ueda (born 1936) used an analog (as opposed to digital) computer to produce a strange attractor simulation of a nonlinear oscillator (Ueda 2000).

From the 1960s chaotic dynamics become a much more universal and active field. It is quite impractical to give anything like a complete history. We just note that many of the techniques and characterizations that we will discuss for the chaotic pendulum were developed in this period. The digital computer became a primary tool and an initial series of computer simulations of the chaotic pendulum were published by Gwinn and Westervelt from Harvard University during the mid-1980s (Gwinn and Westervelt 1985; 1986). Other researchers also saw the possibilities in a study of the pendulum. (See, for example (Bryant and Miles 1990).) The first physical model of the chaotic pendulum was built by one of us (JAB) in collaboration with John Smith of the University of Waterloo (Blackburn et al. 1989a). An exploded view of this design and a photograph of the actual system are shown in Figs. 6.1 and 6.2. Through the optical encoder, data giving the angular displacement of the pendulum is sent to a computer where it can be processed for further analysis. The fit of such data to the simple nonlinear dynamical model described below is remarkably good (see Fig. 6.3).

Variations on the basic chaotic pendulum have also been constructed and analyzed (See, for example, Starrett and Tagg (1995) and Shinbrot et al. (1992).) In 1990, one of us (GLB) with coauthor Jerry Gollub of Haverford College and the University of Pennsylvania gathered together many aspects of the behavior of the pendulum in an accessible undergraduate text. (Baker and Gollub 1996). Many of the figures in this chapter are from that book and further details of much of what we describe here may be found there.

Chapters 2 and 3 of this book provide a great many technical details about the mechanics of the pendulum. In order to introduce concepts gradually we used the linearized version of the pendulum to develop some sense of the pendulum's motions. The mathematics for the linearized pendulum is solvable by straightforward analytic techniques. However, the full nonlinear pendulum is more complex. As we discovered in Chapter 3, even an analysis of the natural frequency of the nonlinear pendulum becomes an involved calculation. While the linearized pendulum can be used to illustrate much of the expected behavior of the pendulum, only the nonlinear pendulum is capable of chaotic motion. This requirement of nonlinearity is actually a necessary condition for chaotic motion in any physical system. It is the nonlinearity which leads to instability and the possibility of an abrupt transition, a *bifurcation*, to a new kind of motion. A classic example of nonlinearity is the straw that breaks the camel's back. The camel may be loaded with increasing weights with only a slight proportional buckling of its legs. Yet there may come a point where the addition of just one small thing—a piece of straw—may be sufficient to

"break" the camel's back. The camel would then be completely prostrate and unable to carry any weight at all. Thus there is an abrupt transition from one "state" to a completely different state. A slightly more scientific illustration is the example of a weight suspended at the end of thin wire. As more weight is added the wire stretches proportionately (linearly)—the behavior predicted by Hooke's law. But at some point a small extra weight causes a disproportionately large stretch or even breakage in the wire. Again, this behavior reflects a nonlinear response by the wire. Similarly, nonlinearity allows the pendulum to exhibit corresponding transitions. For small amplitudes of forcing the driven pendulum exhibits the usual periodic behavior that characterizes the linearized pendulum's motion, but for larger amounts of forcing where nonlinearity becomes important, the picture may change completely. The motion may become chaotic.

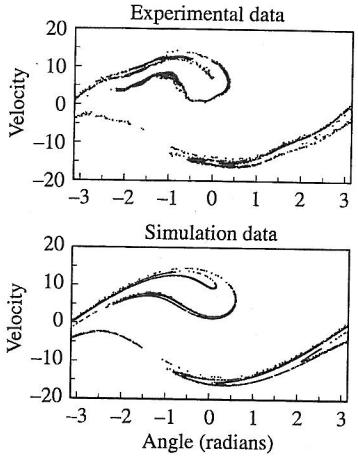

Fig. 6.3
Comparison of data from the experimental pendulum with simulated data computed from a mathematical model of the pendulum.

6.2 The dimensionless equation of motion

For a rigid compound pendulum of moment of inertia I, we may write the complete equation of motion for the sinusoidally driven, damped, nonlinear pendulum as

$$I\frac{d^2\theta}{dt^2} + b\frac{d\theta}{dt} + mgd\sin\theta = \Upsilon\cos\omega_F t, \tag{6.1}$$

where b is the friction parameter, mgd is the critical gravitational restoring torque, d is the distance from the pivot to the center of mass, Υ is the amplitude of the drive and ω_F is the angular driving frequency. The natural angular frequency of the corresponding linearized pendulum was given previously as $\omega_0 = \sqrt{mgd/I}$. The study of Eq. (6.1) can be simplified by reducing the number of adjustable parameters. This is achieved through the introduction of dimensionless parameters—those which have no physical units. Toward this end, we first introduce a dimensionless time parameter, $t' = \omega_0 t$. By appropriate use of the chain rule and the following conversions

$$\begin{aligned} Q &= \omega_0 I/b \\ A &= \Upsilon/(\omega_0^2 I), \\ \omega_D &= \omega_F/\omega_0 \end{aligned} \tag{6.2}$$

the nondimensional equation becomes:

$$\frac{d^2\theta}{dt^2} + \frac{1}{Q}\frac{d\theta}{dt} + \sin\theta = A\cos\omega_D t. \tag{6.3}$$

(For simplicity, the primes on the nondimensional time t have been omitted.) Instead of the seven parameters of the original equation of motion, this dimensionless equation has only three adjustable parameters, Q the inverse of the strength of the damping, A the strength of the forcing, and $\omega_D$the drive frequency relative to the natural frequency. Adjustments in any of the parameters can radically change the pendulum's motion. Thus, the value of each member of this minimal set of parameters will determine the dynamics.

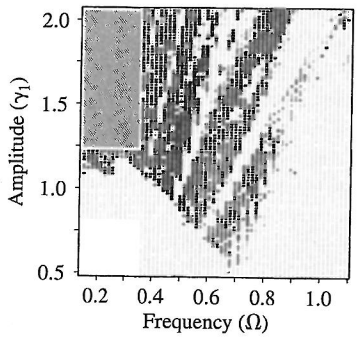

Fig. 6.4
Behavior of an experimental pendulum with fixed damping but variable normalized forcing amplitude (γ_1) and variable normalized forcing frequency (Ω). Filled squares represent chaotic motion and small dots represent periodic motion. Each point is derived from a single experiment and there are a total of 5250 points. Because of the time constraints, the large shaded rectangle was not covered experimentally, but the behavior in that region is mainly chaotic. The damping was fixed at $Q = 4.2$. See Blackburn et al. (1989*b*). The symbols used for the frequency and amplitude of the forcing are different from those found in this text.

The motion of the pendulum will either be periodic or chaotic. With periodic motion the pendulum repeats its behavior at regular intervals. In the simplest case, the period of the motion will coincide with the period of the forcing. But there are other possibilities. Periodic motion may also be more complex than a simple back and forth oscillation yet still be characteristically repetitive. To say that the motion of a driven pendulum is complex is an understatement. Much of the rest of this chapter describes tools that are used to display and characterize the wide variety of possible motions. Readers wishing to gain a quick impression of the possible complexity may look ahead to Figs. 6.9–6.11 in which the motions are schematically portrayed as the parameters A, ω_D, and Q, respectively, are varied. Ideally, one would like to study the pendulum's motion for every set of parameter values. That is, every state of the pendulum would be represented by a point with coordinates (A, ω_D, Q) and the actual motion might be indicated by the symbol placed at the point. Such a three-dimensional diagram would be very time consuming to produce and probably confusing to interpret. However, a two-dimensional version for which one parameter is held fixed is helpful. Such a diagram is shown here in Fig. 6.4. Unlike computer simulations, this figure was created with data obtained from a real driven pendulum.[3]

6.3 Geometric representations

There are a variety of ways to represent the pendulum's motion geometrically. Some of these we have already seen in other parts of the book. In Fig. 6.5 representative periodic motions are illustrated by sketches of the actual paths of the pendulum bob over several cycles. Situated beside the sketch of each motion is the corresponding phase plane diagram, first described in Chapter 2. The phase diagram or phase portrait is a graph of angular velocity versus angle. Each phase diagram or phase portrait is traced through many drive cycles and yet, in Fig. 6.5, the motion, although somewhat complex, remains periodic and therefore the phase portrait is fairly simple. As the amount of forcing increases complexity generally increases. For example, the period of the motion is sometimes twice or even four times that of the forcing motion. This phenomenon, known as *period doubling*, can be a mechanism that leads to chaotic motion. Thus, the understanding of chaotic motion is facilitated by using a variety of geometric representations.

[3] A small pendulum will have a period of perhaps one-half second. In Fig. 6.4, each data point is the result of a single experiment carried out under the following protocol: (a) the ac drive was switched off and the pendulum was allowed to come to rest (b) the drive amplitude and frequency were set electronically to the desired new values (c) the drive was turned on and the pendulum motion was allowed to stabilize (d) the pendulum motion was observed over a measurement interval using a data acquisition system. The information from this final stage was then interpreted to form a conclusion as to the type of motion that had occured. From start to finish, the protocol took several minutes. Obviously, more than 5000 points in the figure would require weeks of experiments.

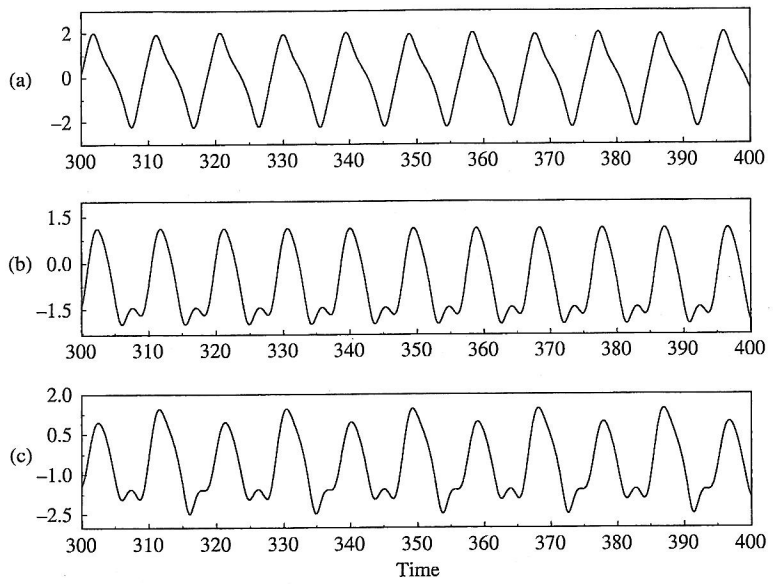

Fig. 6.6
Time series for the pendulum's angular velocity corresponding to parameters used in Fig. 6.5.

Thus we have several ways to represent the motion of the pendulum, time series, phase portraits, Poincaré sections, and Fourier analysis—although further elements of Fourier analysis or spectral analysis are needed for the discussion of chaotic motion.

Chaotic motion appears when the pattern of periodic motion is broken through instability. The motion then becomes nonrepetitive or nonperiodic. Another way of describing the motion is to say that it contains *all* periodic frequencies, but that none of them last very long. More technically, it is said that chaotic motion contains an infinite number of unstable periodic orbits. As the phase trajectory wanders around the phase space, it comes very close to lots of periodic orbits but it is unable to maintain itself for very long on any one of these orbits. Thus, time series seem to have no discernible pattern or periodicity, the phase plane is very congested, and even the Poincare section becomes complex. These features are illustrated for the chaotic pendulum in Fig. 6.7.

The simplification caused by the strobe effect of the Poincaré section now becomes apparent. Whereas the phase portrait is quite congested, the Poincaré section has an appearance which lends itself to characterization. We note first that (for a dissipative system) the Poincaré section is confined to a particular complex region in space. No matter what the initial conditions the points will eventually all lie in this region which has a special characteristic appearance. Thus, the creation of the Poincaré section requires that the system be allowed to run until any initial aberrations are no longer evident, and then data are saved for the diagram. In essence the pendulum's motion is *attracted* to the set of points that form the Poincaré section. The Poincaré section and the corresponding phase portrait are

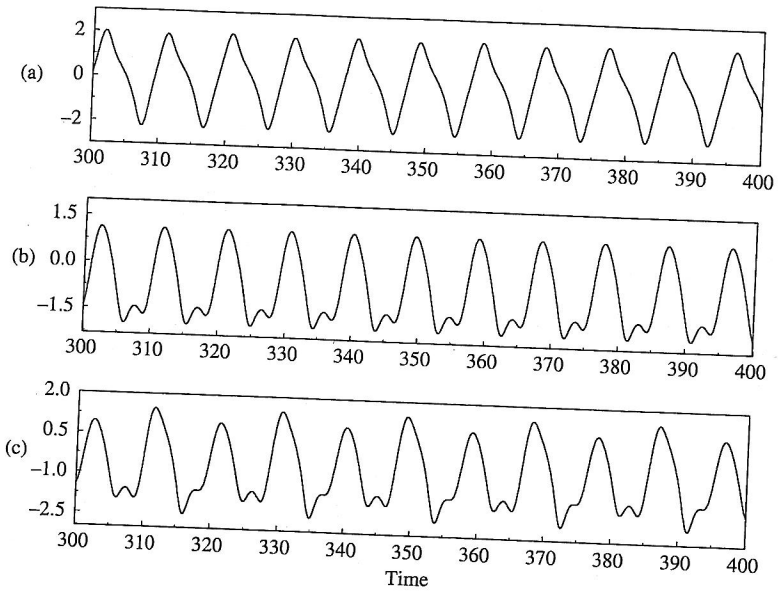

Fig. 6.6
Time series for the pendulum's angular velocity corresponding to parameters used in Fig. 6.5.

Thus we have several ways to represent the motion of the pendulum, time series, phase portraits, Poincaré sections, and Fourier analysis—although further elements of Fourier analysis or spectral analysis are needed for the discussion of chaotic motion.

Chaotic motion appears when the pattern of periodic motion is broken through instability. The motion then becomes nonrepetitive or nonperiodic. Another way of describing the motion is to say that it contains *all* periodic frequencies, but that none of them last very long. More technically, it is said that chaotic motion contains an infinite number of unstable periodic orbits. As the phase trajectory wanders around the phase space, it comes very close to lots of periodic orbits but it is unable to maintain itself for very long on any one of these orbits. Thus, time series seem to have no discernible pattern or periodicity, the phase plane is very congested, and even the Poincare section becomes complex. These features are illustrated for the chaotic pendulum in Fig. 6.7.

The simplification caused by the strobe effect of the Poincaré section now becomes apparent. Whereas the phase portrait is quite congested, the Poincaré section has an appearance which lends itself to characterization. We note first that (for a dissipative system) the Poincaré section is confined to a particular complex region in space. No matter what the initial conditions the points will eventually all lie in this region which has a special characteristic appearance. Thus, the creation of the Poincaré section requires that the system be allowed to run until any initial aberrations are no longer evident, and then data are saved for the diagram. In essence the pendulum's motion is *attracted* to the set of points that form the Poincaré section. The Poincaré section and the corresponding phase portrait are

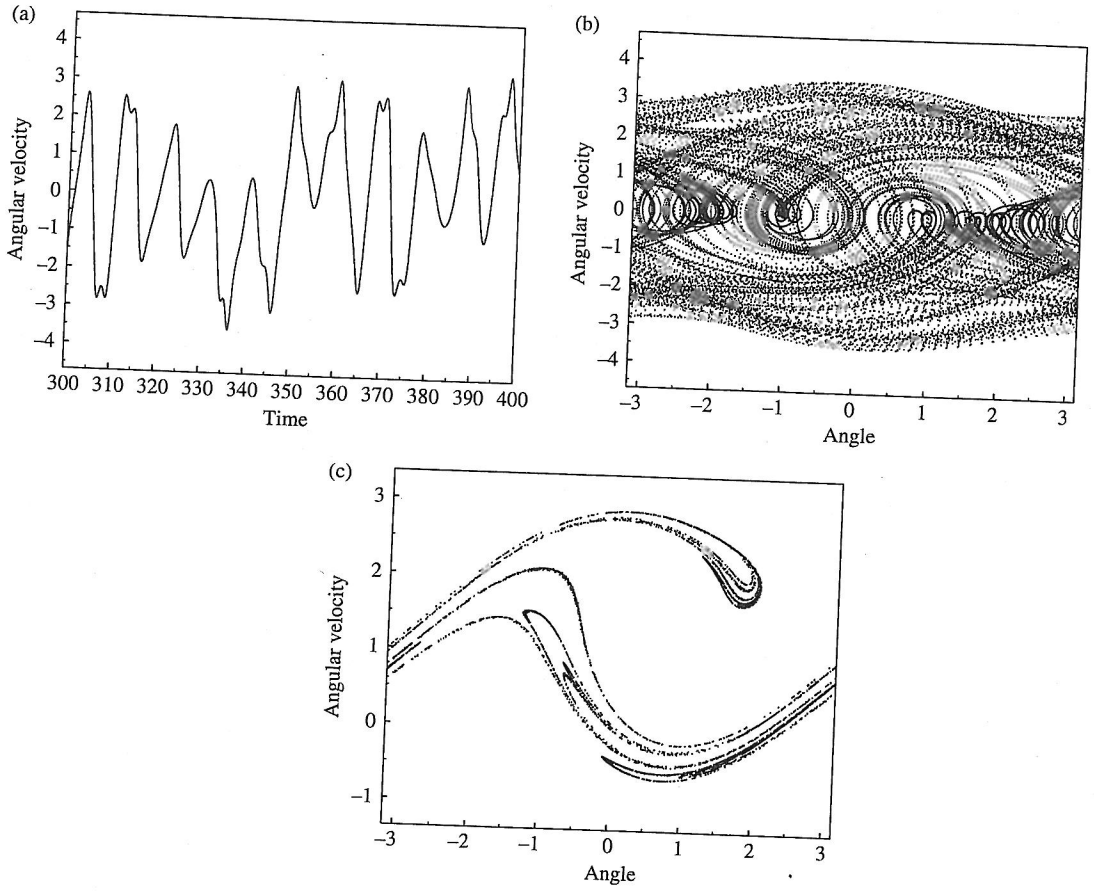

Fig. 6.7
Three geometric representations of the chaotic pendulum; (a) Time series of the angular velocity, (b) Phase plane diagram, and (c) Poincaré section.

said to be *strange attractors*. For nonchaotic motions, the attracting phase space set for periodic motion was referred to as an *attractor*. The word "strange" is related to the particular geometry of the attractor for chaotic motion. For chaotic systems in general and the chaotic pendulum in particular, the attractor is a *fractal*, about which more will be said later. Therefore, an attractor that is a fractal is called a "strange attractor".

Obviously chaotic motion is complex. This complexity suggests that nonlinear equations of motion are difficult and usually impossible to solve by analytic methods. The equation for the nonlinear driven pendulum has no analytic solution. Solutions are generated by numerical methods using computers to do repetitive calculations. It is not surprising that the bulk of the work in chaotic dynamics has occurred after the computer revolution. Edward Lorenz of MIT is generally credited with being the first to observe chaotic time series on a computer. Lorenz recounted the story of this bit of serendipity for a television program on chaos. During observation of the

computer solution of his model equations for convective air flow in 1963, he had occasion to restart his computer. In doing this, he failed to put in the precise numbers used to start a previous computer simulation and the computer gave him quite a different result for the system trajectory. This was the first recorded instance of sensitivity to initial conditions, and led to the actualization of Poincaré's oft quoted prediction for the unstable behavior of a set of deterministic differential equations.

The computer is now the primary tool in the theoretical study of chaotic systems. In an ideal application of the scientific method experimental apparatus should be constructed whose behavior approximates that of the computer simulation. The experimental apparatus may then be used to test the theoretical model. But while chaotic systems are believed to be ubiquitous in nature, they are difficult to construct as controlled systems suitable for laboratory experimentation. Fortunately, the chaotic pendulum is one of the few exceptions to this chronic difficulty and, as we have seen, can be realized experimentally.[4] Thus, aside from the pendulum and a few other experimental systems, the computer is essential for the bulk of the research in chaotic dynamics. We therefore ask, "Given the instability and sensitivity of chaotic systems, does the computer accurately represent the motion of chaotic systems?". The answer is both "yes" and "no." Because of sensitivity to initial conditions and the finite precision of computer calculations, the actual trajectory of a system may, after a relatively short time not be the same as that which would be provided by an "infinitely" precise calculation using infinitesimally small time steps for the calculation. But fortunately chaotic attractors possess a characteristic that mitigates the deleterious effect of the approximate nature of the computer simulation. Figure 6.7(b) shows that chaotic trajectories are densely packed in the sense that their orbits in phase space are close together. Therefore the computer tends to produce a phase trajectory that "shadows" a "true" trajectory for some time. Then, as the computer orbit drifts away from the true orbit, it comes close to another "true" trajectory and shadows the true motion again and so forth (Grebogi et al. 1990; Fryska and Zohdy 1992). In this way, the computer does not necessarily provide a true trajectory but rather a series of shadowings of true trajectories. On the other hand, all true trajectories that are being shadowed by the computer calculations lie on the "true" strange attractor and consequently the shadow trajectories also lie on or extremely close to the strange attractor. Hence the computer does provide a true Poincaré section or phase portrait if data is taken over a long time. Therefore we accept the computer as a primary tool, partly from necessity and partly because it really does give true results in many circumstances.

6.3.2 Spectral analysis

But let us return to geometric representations of the pendulum's motion. What about spectral analysis? Since chaotic motion is not periodic, the

[4] While the Blackburn/Smith pendulum seems to have been the first experimental chaotic pendulum, there are other configurations. See, for example, (DeSerio 2003; Peters 1999).

Fourier decomposition into components as described in Chapter 2 no longer holds. There is no fundamental frequency of motion on which to base the Fourier series expansion. However, there is a generalization of the process used to obtain Fourier series that works for nonperiodic functions. This process requires a mathematical transformation known as the *Fourier transform*. In developing this transform, we start with the Fourier series of Eq. (2.11)

$$f(t) = \sum_{n=-\infty}^{n=\infty} a_n e^{in\omega_0 t}, \text{ where } a_n = \frac{\omega_0}{2\pi}\int_{-\pi/\omega_0}^{\pi/\omega_0} f(t)e^{-in\omega_0 t}dt. \tag{6.4}$$

in complex form. If the time series is not periodic as is the case with chaotic motion, then the nonperiodic motion can be thought of as part of a single wave whose period is *infinitely* long. The fundamental period of a possible Fourier series now becomes infinitely long or, conversely, the fundamental frequency becomes infinitely short. Creation of the Fourier transform then becomes a limit process for several of the variables as shown by the following transformations:

$$T \Longrightarrow \infty$$
$$n\omega_0 \Longrightarrow \omega,$$

where ω is a continuos variable, and

$$a_n \Longrightarrow a(\omega)d\omega \tag{6.5}$$

$$f(t) = \sum_{n=-\infty}^{n=\infty} a_n e^{in\omega_0 t} \text{ becomes } f(t) = \int_{-\infty}^{\infty} a(\omega)\, d\omega e^{i\omega t}, \text{ and}$$

$$a_n = \frac{\omega_0}{2\pi}\int_{-\pi/\omega_0}^{\pi/\omega_0} f(t)e^{-in\omega_0 t}\, dt \text{ becomes } a(\omega)d\omega = \frac{d\omega}{2\pi}\int_{-\infty}^{\infty} f(t)e^{-i\omega t}\, dt.$$

From these transformations the *amplitude*, $a(\omega)$, of each of the uncountably infinite number of frequency components is found using the *Fourier transform*, given by the equation

$$a(\omega) = \frac{1}{2\pi}\int_{-\infty}^{\infty} f(t)e^{-i\omega t}\, dt. \tag{6.6}$$

While the graph of the spectral components, a_n, of a Fourier series is a set of *discrete* lines at harmonics of the fundamental frequency ω_0, a graph of the Fourier transform $a(\omega)$, or frequency density, is a continuous function of the *continuum* of frequencies present in nonperiodic motion. Similarly, the original function $f(t)$ is now expressed in terms of an integral with each member of the continuum of frequencies being weighted by the frequency density according to the formula

$$f(t) = \int_{-\infty}^{\infty} a(\omega)e^{i\omega t}\, d\omega. \tag{6.7}$$

The Fourier transform of the time series for the chaotic pendulum shown in Fig. 6.7(a) is illustrated in Fig. 6.8.

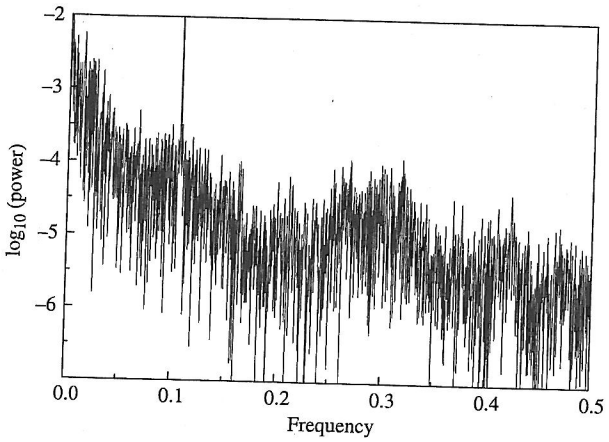

Fig. 6.8
Fourier spectrum for a chaotic pendulum. Aside from the strong component at the forcing frequency, the spectrum power diminishes inversely with increasing frequency.

It seems fairly clear that the idea for the Fourier transform stems from Fourier's 1811 paper (Kline 1972) although other mathematicians were working on similar ideas. But for the effective implementation of the transform in chaotic dynamics we rely on a modern approach. Toward this end we note that our development of the Fourier transform implies the use of a continuous function, $f(t)$. But the computer generates time series as a noncontinuous, discrete set of points and therefore chaotic times series generated by computers will be Fourier transformed, again by numerical integration. Furthermore, the discretization of the points requires that the appropriate Fourier transform is slightly modified and renamed as the *Discrete* Fourier transform (DFT). The process is essentially that of the continuous transform but the many integrations done in the transform process are performed by discrete numerical integration. (We also note in passing that the discrete nature of the sampling in the time series can cause subtle problems, but that is another story.) At any rate, for much of spectral analysis up until the mid-1960s the discrete transform was standard procedure. But in 1964, J. W. Culley and J. W. Tukey, at the urging of R. L. Garwin at the IBM research center, created a better method or "algorithm".[5] One way to assess an algorithm is by the number of computational steps required. A "better" algorithm therefore has fewer steps and computes faster. Thus was born the *Fast Fourier Transform* (FFT). This ingenious technique took advantage of certain symmetry properties of trigonometric functions at their points of valuation. The increase in speed over the discrete transform method is substantial. If the time series contains N points then the DFT requires a number of calculations that is of the order of N^2, whereas the FFT computation requires a number of calculations on the order of $N \log_2 N$. For $N = 1000$ points the efficiency is increased by a factor of more than 100 (Press et al. 1986). The spectrum shown in Fig. 6.8 was generated using the FFT algorithm. Let us now return to the application of spectral analysis to the chaotic pendulum.

[5] The FFT seems to have been discovered independently at different times, possibly as early as 1942, and implemented on hand calculators.

Periodic motions in time typically yield a small number of discretely spaced frequency components. Furthermore, even for periodic motions with very sharp corners that yield spectra with a large number of components or harmonics, the components are still spaced apart by a frequency interval equal to the fundamental frequency. But, as shown in Fig. 6.8, chaotic motion gives rise to an *infinite* number of *densely* packed frequency components. This observation reinforces the statement made earlier that chaotic motion contains an infinite number of unstable periodic orbits. The spectrum also shows a very strong component at the frequency of the pendulum forcing, together with a couple of harmonics, that characterize the forcing motion. By ignoring these components we see that, for the bulk of the components, the amplitude of the components is approximately proportional to the inverse of the frequency, $1/\omega$. This behavior points to much of the pendulum's motion as being in (unstable) periodic orbits of very long periods and is consistent with the notion that one route to chaos is through increasing complexity of the periodic orbits which, in turn, implies increasingly longer periodic orbits. A spectrum that is inversely proportional to frequency is also characteristic of a certain type of electrical noise, called "$1/f$" noise. This noise is above that which is inherent in an electrical system due to simple thermal agitation. "$1/f$" noise can be caused, for example, by fluctuations in the electrical resistance in a circuit. These fluctuations are quite prominent at low frequencies. In vacuum tubes—now largely a museum artifact—current was transmitted between the cathode and anode. The electron emission from the cathode is not strictly uniform and again, this generated noise whose spectrum exhibits $1/f$ behavior. The analogy between $1/f$ noise and a $1/\omega$ spectrum for chaotic time series is important. The processes that generate electrical $1/f$ noise are random. On the other hand, the governing rules for chaotic systems are deterministic. Therefore we once again witness a manifestation of Poincaré's statement that deterministic processes can sometimes appear to be probabilistic; that is, according to spectral analysis, the chaotic pendulum appears to behave randomly.

6.3.3 Bifurcation diagrams

Previously described geometric representations of chaotic motion all picture the development of a particular pendulum being driven with a particular forcing strength and frequency. We can also provide a more global picture, in the sense that the motion of a variety of pendulums can be represented on a single diagram. That is, we observe some aspect of the motion of the pendulum for a particular configuration, but then change slightly the configuration and repeat the process. This is done many times for incremental changes in one of the pendulum's parameters, (A, ω_D, Q). In this way, the motion is observed over a range of pendulum configurations. The bifurcation diagram shown in Fig. 6.9 is a typical example.

The vertical axis coordinate is the pendulum's angular velocity $d\theta/dt$ as determined at a single point during a drive cycle. It is essentially the vertical coordinate of the Poincaré section. The horizontal axis coordinate is one of the parameters of the system. In this example, it is the strength of the

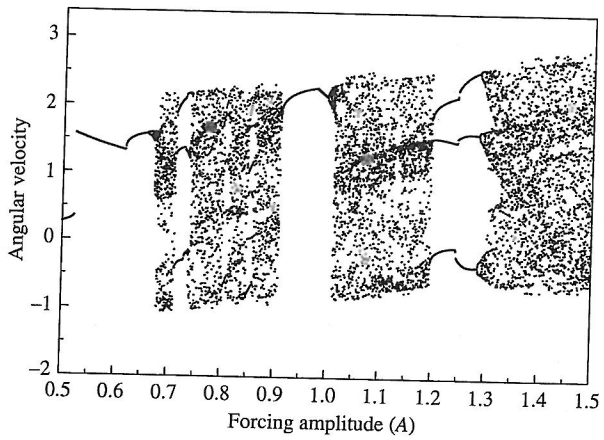

Fig. 6.9
Bifurcation diagram. A plot of the angular velocity, taken many times at a fixed point in the forcing cycle, versus the forcing amplitude.

forcing, A. In essence, each vertical segment of the diagram requires data equivalent to that of a Poincaré section and therefore the construction of the entire diagram is computationally intensive as it requires the creation of a Poincaré section for each value of A. The advantage of this sort of presentation is that it provides a summary of the possible types of motion over some range of the system parameter. Points where the pendulum's motion changes to a new kind of motion are called *bifurcations* and since this diagram is characterized by many such points, it is called a *bifurcation diagram*. At the left side, where the forcing amplitude is small, the motion has a period equal to the forcing period. Further to the right on the diagram the motion, still periodic, becomes more complex through successive *period doublings*. After a few such doublings the strobed angular velocity takes on many values and the motion is now chaotic. However, the motion does not remain uniformly chaotic but reverts to *windows* of periodicity throughout the range of forcing amplitudes. We see that there is often a certain sameness to the progression via period doubling from periodic motion to chaotic motion over the range of amplitudes. By looking at increasingly smaller ranges over which the system parameter is varied we magnify the bifurcation diagram and observe another phenomenon; namely, the number of periodic windows increases as the bifurcation diagrams are increasingly magnified. This property of increasing complexity under magnification is also found in phase portraits and Poincaré sections.

Similar bifurcation diagrams may also be created through variation of each of the other two parameters, ω_D the forcing frequency, and Q, the friction parameter. Examples of these are shown in Figs. 6.10 and 6.11.

The appearance of these figures is similar to that of Fig. 6.9. We noted earlier that, although impossible to draw, one might try to imagine a parameter space with coordinates (A, Q, ω_D) in which the various types of motion could be exhibited and thereby gain a comprehensive overview of the pendulum's behavior. Such a diagram would somehow contain in one figure all the information found in the two-dimensional representations of Figs. 6.9–6.11. Thus one could identify parameter sets of periodic (stable) and chaotic behavior (unstable).

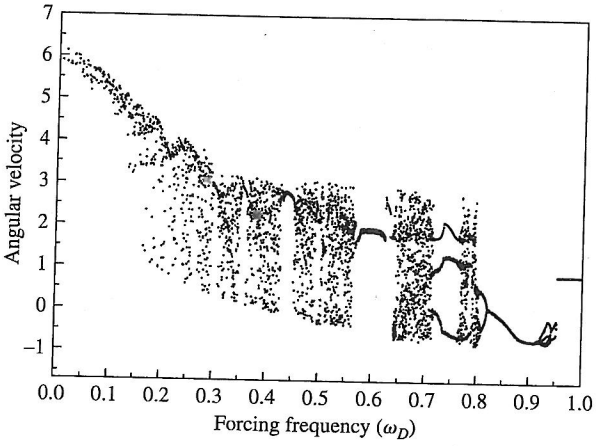

Fig. 6.10
A bifurcation diagram using the forcing frequency as the independent parameter.

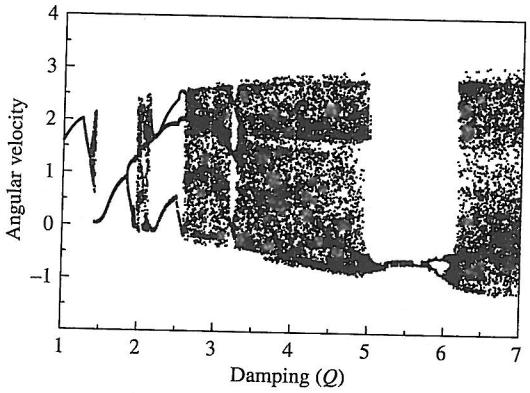

Fig. 6.11
Bifurcation diagram with the damping Q as the independent parameter.

6.4 Characterization of chaos

6.4.1 Fractals

The geometric representation of chaotic motion by, for example, the strange attractor of the Poincaré section, has an almost artistic quality. This representation is also a fruitful subject for mathematical analysis as an example of *fractal* geometry. As we will see, the quantitative description of the Poincaré section fractal is intimately related to the pendulum's dynamics. But let us first give some idea of the general properties of a fractal. The term "fractal" was coined by the mathematician Benoit Mandelbrot (Mandelbrot 1977). It comes from the Latin adjective "fractus" which means "broken". If we imagine the coastline of, say, Norway, and look at that country's map at ever increasing magnification, we would see that there is no characteristic length that can be applied. Any apparently straight lines are, upon further magnification, seen to break into smaller line segments. Hence any characteristic length is "broken". Fractals then are roughly defined as geometric sets that have

no characteristic length. Fractals also exhibit a property known as *self-similarity*. For example, viewed at one level the coast of Norway appears to be fairly jagged. If a portion of that coast is now magnified to the same size as the original view, it will have an appearance similar to that of the original stretch of coastline. This sameness under observation at increasing magnifications is called self-similarity. In summary, fractals typically have (a) no characteristic length and (b) some degree of self-similarity.

Yet long before the term "fractal" was invented, several mathematicians studied geometric configurations that later came to be known as fractals. Some of the mathematicians that are associated with these fractal precursors are the German mathematicians Georg Cantor (1845–1918) and David Hilbert (1862–1943) who proposed *space-filling* curves, the Italian Mathematician Guiseppe Peano (1858–1932), Helge von Koch, the Swedish mathematician who, in 1904, published the *Koch snowflake*, the Polish mathematician Waclaw Sierpinski (1882–1969) who published the *Sierpinski gasket* fractal in 1916, the French mathematician Gaston Julia (1893–1978) who gave us the family of fractals known as *Julia sets*, and the German mathematician Felix Hausdorff (1868–1942) with whom we associate the idea of dimension of a fractal. (During World War II Hausdorff and his wife, both Jewish, committed suicide in anticipation that they were within a week of being sent to a concentration camp.) Mandelbrot, born in 1924, entered the scene much later. Mandelbrot's uncle recommended Julia's 1918 paper to him around 1945. For various reasons Mandlebrot did not like the paper and he found his own path to Julia's work in about 1977. With the aid of the computer Mandelbrot greatly expanded Julia's work and showed the potential for creating beautiful pictures. The *Cantor* set (1883) is simple but popular, and its construction is indicated in Fig. 6.12.

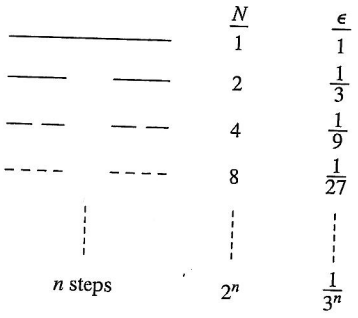

$$d = \lim_{\varepsilon \to 0} \frac{\log(N)}{\log(1/\varepsilon)} = \lim_{n \to \infty} \frac{\log(2^n)}{\log(3^n)} = \frac{\log(2)}{\log(3)} < 1$$

Fig. 6.12
Calculation of the fractal dimension for the Cantor set. (Reprinted from Baker and Gollub (1996, p. 113), with the permission of Cambridge University Press.)

The set is constructed by consecutively removing the middle third out of each line segment. After an infinite number of steps there are an infinite number of points but the pieces do not form a connected line. Clearly the Cantor set is self-similar—same appearance at varying magnifications—and has no characteristic length. The Poincaré section for the pendulum also has these properties in some measure. Figure 6.13 shows the Poincaré section under increasing magnification, and there is a sense that further structure is revealed with increasing magnification. This is especially the case in looking "across" the Poincaré sections.

We are quite used to the idea that objects have integer dimensionality—either one, two, or three dimensions. A single point or perhaps a finite collection of points have zero dimension. Lines are one-dimensional and consist of an infinite set of closely spaced points. Yet, one of the distinguishing features of most fractals is that they have noninteger values of dimension. This notion seems strange; but we see that while the Cantor set consists of an infinite number of points it has no parts that can be considered to be line segments. By some sort of intuitive interpolation, the

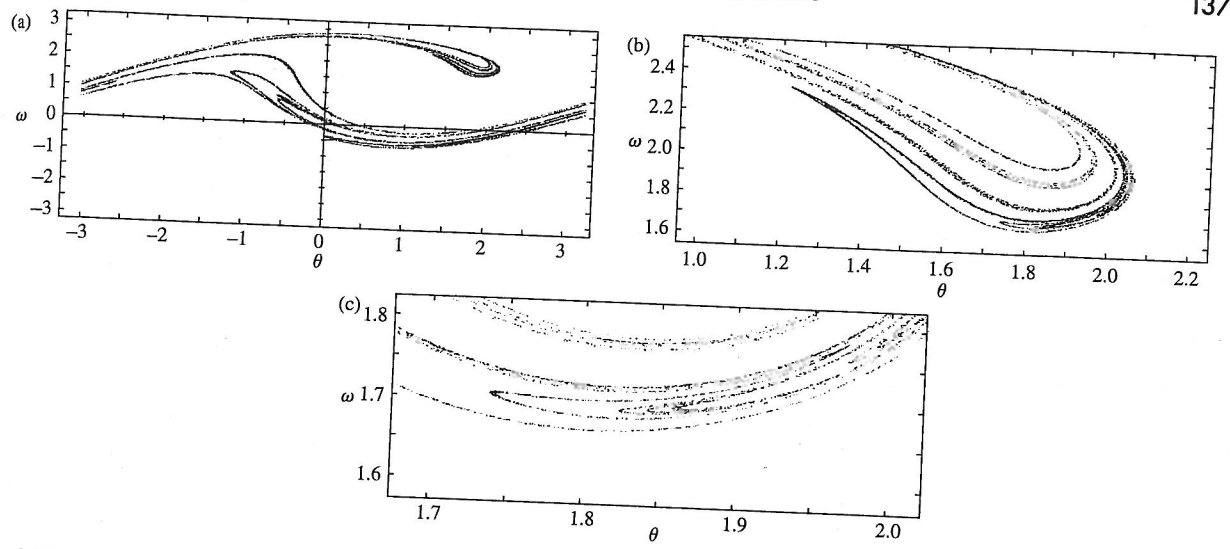

Fig. 6.13
Increasing magnifications of the Poincaré section of the chaotic pendulum that reveals the fractal structure of the attractor. (Reprinted from Baker and Gollub (1996, 56,57 pp.), with the permission of Cambridge University Press.)

Cantor set should have dimension somewhere between zero and one. To find the precise number requires a methodology for the calculation of dimension.

Perhaps surprisingly, there are several definitions of dimension. We will use a method that gives the *capacity dimension* d_C, introduced by Kolmogorov in 1959 (Kolmogorov 1959). As shown in Fig. 6.14, a line may be "covered" by a set of one-dimensional "boxes" of ever decreasing size, ϵ. If the length of the line is L then the number of boxes $N(\epsilon)$ is clearly equal to $L(1/\epsilon)$. Similarly the two-dimensional square in Fig. 6.14 can be covered by $N(\epsilon) = L^2(1/\epsilon)^2$ boxes. For a three-dimensional cube the exponent would be equal to 3. Therefore we define dimension as the exponent d in the expression

$$N(\epsilon) = L^d(1/\epsilon)^d \text{or, taking logs,}$$

$$d = \frac{\log N(\epsilon)}{\log L + \log(1/\epsilon)}. \tag{6.8}$$

In the limit as N gets very large and ϵ becomes very small the fixed term $\log L$ becomes negligible and the expression for dimension is simplified to

$$d = \lim_{\epsilon \to 0} \frac{\log N(\epsilon)}{\log(1/\epsilon)}. \tag{6.9}$$

This expression can be used to calculate the dimension, the *fractal* dimension, of the Cantor set as shown in Fig. 6.12. The result is found to be $(\log 2/\log 3) = 0.63093$, a number between zero (for a point) and one (for a line).

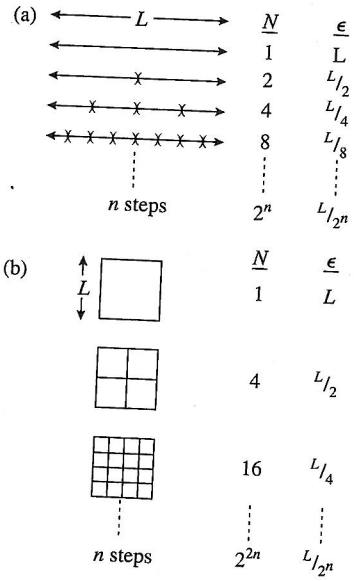

Fig. 6.14
Application of the box counting technique to calculate the capacity dimension. The scaling exponent gives the dimension. (Reprinted from Baker and Gollub (1996, p. 111), with the permission of Cambridge University Press.)

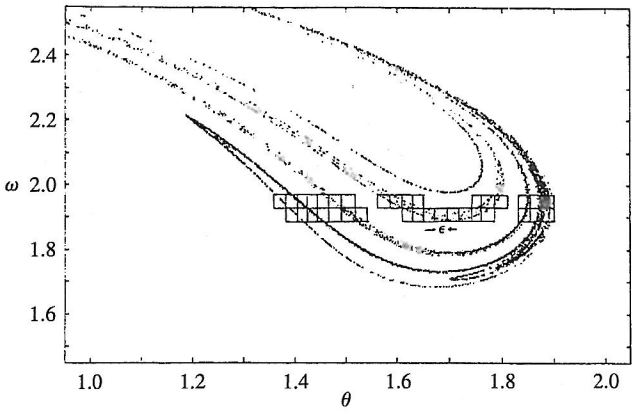

Fig. 6.15
A portion of the Poincaré section with some representative covering boxes. (Reprinted from Baker and Gollub (1996, p. 115), with the permission of Cambridge University Press.)

This procedure (or a similar one) may be used to calculate the fractal dimension for the Poincaré section of the chaotic pendulum. Figure 6.15 shows a set of boxes covering the Poincaré section.[6] Of course the process must now be done on a computer and is subject to some limitations. A close examination of the Poincaré section shows that its points do not cover an area, but are really a (possibly infinite) set of closely spaced lines. Therefore the Poincaré section is more than a line and less than an area. We expect its dimension to lie between one and two. Again, the methodology is indicated in Fig. 6.14.

A set of square boxes of side $1/\epsilon$ cover the Poincaré section. The logarithm of the number of boxes $N(\epsilon)$ is plotted against $\log(1/\epsilon)$ and the slope gives the fractal's dimension. For the parameter set $A = 1.5$, $Q = 4$, $\omega_D = 0.66$ the fractal dimension is about 1.3. The capacity or *box counting* dimension is the simplest measure of dimension. In this sort of work it is more common to use another, related but somewhat less intuitive measure of dimension, called the *correlation* dimension. For the details of this process as applied to the pendulum, see, for example, Baker and Gollub (1996).

The fact that the geometry of the Poincaré section has unusual fractal properties is itself an interesting and surprising feature. Even more striking is the fact that the fractal dimension is intimately and beautifully related to the dynamics of the pendulum through a measure of the pendulum's sensitivity to initial conditions. This measure is known as the *Lyapunov exponent*.

6.4.2 Lyapunov exponents

At the beginning of this chapter we introduced the notion of sensitivity to initial conditions and defined it in terms of the exponential separation in

[6] There exist many variations on the definition of dimension. For simple fractals there is a high degree of equivalency among them. But in some cases the more general definitions provide a higher degree of specificity of the fractal. For a concise summary see the table in Takayasu's book on page 150.

time of identical systems whose initial conditions are separated by an amount Δx_0. That is, the time dependence of this separation is given by $\Delta x(t) = \Delta x_0 e^{\lambda t}$. The parameter λ is called the Lyapunov exponent. By following the change in separation of an initial pair of coordinates one can determine the Lyapunov exponent. If the parameter is negative or zero then the separation either diminishes or stays constant. But if λ is positive then SIC holds and the system is chaotic.

For a one-dimensional system with the single variable $x(t)$, the interpretation of λ is relatively straightforward. However, the pendulum is a three-dimensional system, with angle, angular velocity, and time (or forcing phase) as the three variables. We need to think about a three-dimensional phase space and imagine following the growth or decay of a ball of coordinates (points) representing many identical pendulums in states that momentarily differ only slightly from each other. The evolution of this ball of coordinates is complicated. It may grow in some directions and shrink in other directions—becoming a kind of twisting and shape-changing football. In this process, the directions of growth and shrinkage are not constant but vary as the system evolves over the phase space in which the attractor is imbedded. If the initial volume of the ball is ΔV_0 then its volume a short time later is $\Delta V(t) = \Delta V(0) e^{(\lambda_1+\lambda_2+\lambda_3)t}$ where the three λ's—Lyapunov exponents—give the expansion or contraction rates in the three "directions" that define the football. (The time over which we follow these many points needs to be short because the attractor is limited in size and the evolving ball will fold back on itself for longer times. SIC is exhibited between foldings.)

For the chaotic pendulum, time, and thus the forcing phase, increases at a constant rate, and therefore there is no spread of the ball in the phase direction. The Lyapunov exponent corresponding to the forcing phase or time coordinate is, say $\lambda_2 = 0$. This leaves the exponents for contraction and expansion. The directions of expansion and contraction change as the ball moves along its central phase space orbit and therefore, unlike the orbit direction, no constant direction can be associated with contraction or expansion of the ball. Expansion implies the existence of a positive Lyapunov exponent, a necessary condition for SIC. Let us call this exponent λ_1. What about contraction of the phase ball of the damped driven pendulum? If millions of pendulums were started each at one of the millions of possible starting points in the entire phase space, these points would tend to collect on the attractor, and therefore there must be overall shrinkage of phase volume ball. Thus there will be a negative Lyapunov exponent, say λ_3. Shrinkage of the phase volume requires, not only that there be the negative Lyapunov exponent, but that it must be sufficiently negative so that

$$\lambda_1 + \lambda_2 + \lambda_3 < 0. \tag{6.10}$$

A schematic diagram of this shrinkage process is shown in Fig. 6.16. Algorithms for computation of the Lyapunov exponents are somewhat complex and beyond the needs of this book. (See, for example, Wolf et al. (1985) and Eckmann et al. (1986).) A computer program for the computation of the exponents for the pendulum is given in Baker and Gollub (1996).

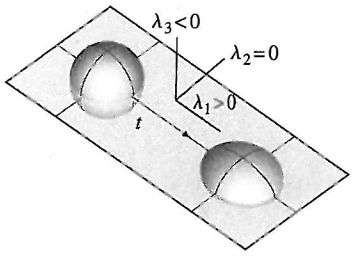

Fig. 6.16
Schematic of the process of shrinkage and stretch of an ensemble (ball) of phase coordinates for the chaotic pendulum.

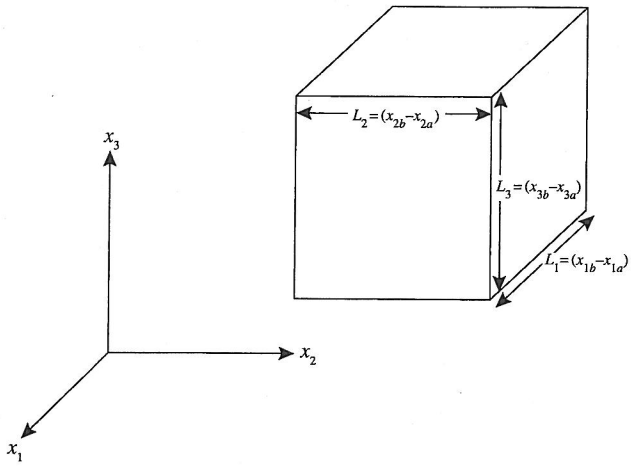

Fig. 6.17
Evolution of an initial volume of phase coordinates in phase space. (Reprinted from Baker and Gollub (1996, p. 13), with the permission of Cambridge University Press.)

What is the connection between Lyapunov exponents and the dynamics of the pendulum? The Lyapunov exponents measure the evolution of the phase space ball. Therefore we require some sort of analysis of how a phase volume changes in the general case. Consider the general three-dimensional phase space of Fig. 6.17 where the coordinates are the generic triplet of dynamical coordinates (x_1,x_2,x_3). The figure shows a rectangular box of sides

$$L_1 = x_{1b} - x_{1a}, \quad L_2 = x_{2b} - x_{2a}, \quad L_3 = x_{3b} - x_{3a}. \tag{6.11}$$

and the product of these sides gives the volume. Let us calculate the time rate of change of the volume. Using the product rule for differentiation we obtain

$$\frac{dV}{dt} = L_2L_3(\dot{x}_{1b} - \dot{x}_{1a}) + L_1L_3(\dot{x}_{2b} - \dot{x}_{2a}) + L_1L_2(\dot{x}_{3b} - \dot{x}_{3a}), \tag{6.12}$$

where $\dot{x}$ means dx/dt. Now the dynamical coordinates each have a rate, $\dot{x}_i$, that depends on the other coordinates and the various system parameters. In general these dynamical rates may be expressed as

$$\begin{aligned} \frac{dx_1}{dt} &= F_1(x_1, x_2, x_3) \\ \frac{dx_2}{dt} &= F_2(x_1, x_2, x_3) \\ \frac{dx_3}{dt} &= F_3(x_1, x_2, x_3) \end{aligned} \tag{6.13}$$

and are simply the equations of motion for the system expressed as a set of first order differential equations.

Therefore the rate of change of phase volume may be written in terms of the dynamics, as represented by the functions (F_1, F_2, F_3), as

$$\begin{aligned} \frac{dV}{dt} &= L_2L_3[F_1(x_{1b}, x_{2a}, x_{3a}) - F_1(x_{1a}, x_{2a}, x_{3a})] \\ &\quad + 2 \text{ similar terms.} \end{aligned} \tag{6.14}$$

For small evolution times with small change in phase volume we use a linear approximation by expanding the first term in a Taylor series as

$$F_1(x_{1b}, x_{2a}, x_{3a}) \approx F_1(x_{1a}, x_{2a}, x_{3a}) + \frac{\partial F_1(x_{1a}, x_{2a}, x_{3a})}{\partial x_1}(x_{1b} - x_{1a}) \quad (6.15)$$

and similarly with the other terms. This linearization means that our final result for the rate of change of volume is only valid for small periods of the system's evolution. Nevertheless, by averaging the changes over many small steps we obtain an average rate of shrinkage of the phase volume. Combining the above equations gives the rate

$$\frac{dV}{dt} = L_2L_3\frac{\partial F_1}{dx_1}(x_{1b} - x_{1a}) + L_1L_3\frac{\partial F_2}{dx_2}(x_{2b} - x_{2a}) + L_1L_2\frac{\partial F_3}{dx_3}(x_{3b} - x_{3a}), \quad (6.16)$$

which may be more compactly expressed as a logarithmic derivative

$$\frac{1}{V}\frac{dV}{dt} = \nabla \cdot \mathbf{F}. \quad (6.17)$$

Putting this expression together with the definition of the Lyapunov exponents leads to

$$\lambda_1 + \lambda_2 + \lambda_3 = \nabla \cdot \mathbf{F}. \quad (6.18)$$

Amazingly, the dynamics are now connected to the phase volume shrinkage.

Let us apply this general formulation to the pendulum. We simply transform the equation of motion for the pendulum into the form of a dynamical system—the collection of rate equations for each dynamical variable. We begin with the pendulum's equation of motion, Eq. (6.3)

$$\frac{d^2\theta}{dt^2} + \frac{1}{Q}\frac{d\theta}{dt} + \sin\theta = A\cos\omega_D t.$$

Rather than using just the single dependent variable we define new variables, ω for angular velocity, and ϕ for phase. These new variables, combined with Eq. (6.3) lead to the dynamical system

$$\begin{aligned} \frac{d\omega}{dt} &= -\frac{1}{Q}\omega - \sin\theta + A\cos\phi \\ \frac{d\theta}{dt} &= \omega \\ \frac{d\phi}{dt} &= \omega_D. \end{aligned} \quad (6.19)$$

In terms of Eq. (6.17) the logarithmic volume rate is $-1/Q = \lambda_1 + \lambda_2 + \lambda_3$. This equation makes the connection between the pendulum dynamics—in this case the rate of dissipation—and the phase space volume evolution as characterized by the Lyapunov exponents. Now that we know how phase

space volumes evolve, we will make one more connection between geometry and dynamics. That is, we connect the fractal dimension of the attractor with the Lyapunov exponents.

6.4.3 Dynamics, Lyapunov exponents, and fractal dimension

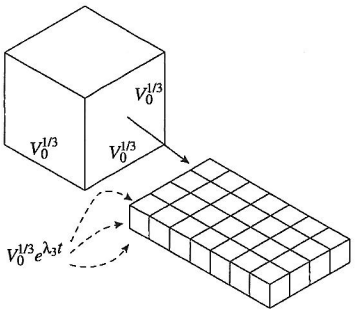

Fig. 6.18
Schematic illustrating the stretching and shrinkage of a small volume (ensemble) of phase points.

The relationship between Lyapunov exponents and fractal dimension was posited by Kaplan and Yorke in 1979 (Kaplan and Yorke 1979). In the following paragraphs, we provide an informal argument to make the conjecture plausible. Consider the schematic diagram, as shown in Fig. 6.18, of the simultaneous stretching and shrinking of a set of points that fills a small portion of a three-dimensional phase space. Like the pendulum this system is dissipative and therefore the volume occupied by the set shrinks in time.

Let the evolution of the unit volume be described by $V(t) = e^{(\lambda_1+\lambda_2+\lambda_3)t}$ where, as in Fig. 6.16, the stretching rate is described by the positive Lyapunov exponent $\lambda_1 > 0$, λ_2 may be positive or zero, and the shrinking rate is described by the negative Lyapunov exponent $\lambda_3 < 0$. Note that in the labeling the exponents decrease numerically as the index increases. Eq. (6.9) defines the fractal dimension in terms of $N(\epsilon)$, the number of boxes needed to cover the evolved volume, and $\epsilon(t)$, the time dependent length of one side of an elemental box. From the figure we see that

$$N(\epsilon(t)) = \frac{V(t)}{\epsilon^3(t)} = \frac{e^{(\lambda_1+\lambda_2+\lambda_3)t}}{e^{3\lambda_3 t}} = e^{(\lambda_1+\lambda_2-2\lambda_3)t} \tag{6.20}$$

and therefore

$$d_L = \frac{\log(N(\epsilon(t)))}{\log(1/\epsilon(t))} = \frac{(\lambda_1+\lambda_2-2\lambda_3)t}{-\lambda_3 t} = 2 + \frac{\lambda_1+\lambda_2}{|\lambda_3|}. \tag{6.21}$$

Dimension that is calculated in this way is sometimes called the *Lyapunov dimension* and in certain simple cases it will equal the box counting dimension. A discussion of the conditions under which the Kaplan-Yorke conjecture is true has been given by Grassberger and Procaccia (1983).

(The Kaplan-Yorke conjecture may also be used for the higher dimensional phase space of more complex systems. In these cases the formula becomes

$$d_L = j + \frac{\lambda_1+\lambda_2+\cdots+\lambda_j}{|\lambda_{j+1}|}, \tag{6.22}$$

where the λ_i are ordered from largest to smallest with λ_j being the smallest nonnegative exponent.)

Let us put all the pieces together. We are now thinking of the pendulum as a dynamical system that may be represented in a three-dimensional phase space with coordinates (ω, θ, t). The full attractor for the pendulum in this space is shown in Fig. 6.19. Side and end views are shown in Figs. 6.20 and 6.21.

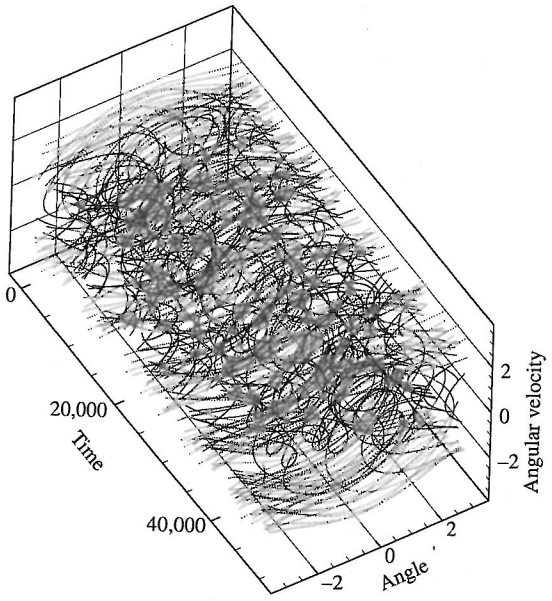

Fig. 6.19
Full three-dimensional attractor for the chaotic pendulum. The angle coordinate θ is constrained by periodic boundary conditions at $\pm\pi$.

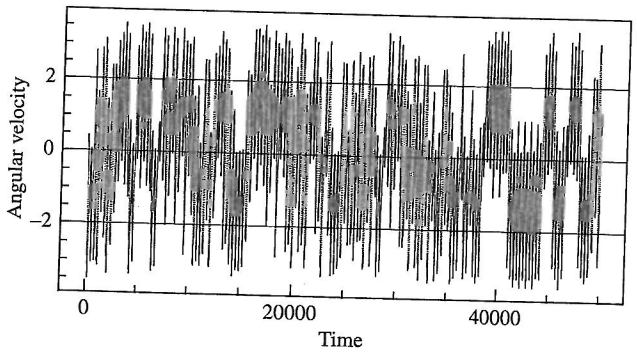

Fig. 6.20
Side view of the 3D attractor showing a time series similar to that of Fig 6.7(a).

The attractor is now embedded in three-dimensional space but is not space filling. Therefore we expect its dimension to be less than three. In this particular case it is computed to be about 2.4. The time coordinate t is a measure of the phase ϕ of the forcing function. Furthermore, motion along the time (phase) axis is represented by the second Lyapunov exponent λ_2. We noted that since time grows linearly and there is no change in phase volume due to time, then λ_2 is zero. The connections between Lyapunov exponents, fractal dimension, and dynamics, may now be summarized in two equations:

$$d_L = 2 + \frac{\lambda_1 + \lambda_2}{|\lambda_3|} \quad \text{and} \quad -1/Q = \lambda_1 + \lambda_2 + \lambda_3. \tag{6.23}$$

Baker and Gollub (1996) computed the various pertinent quantities for several values of the damping factor, Q. The results of that work are summarized in Table 6.1. Remember that $\lambda_2 = 0$. (We previously

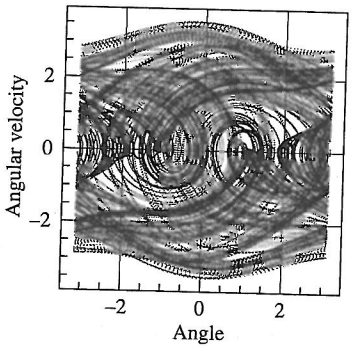

Fig. 6.21
End-on view of the 3D attractor (looking down the time axis) showing a phase plane diagram similar to that of Fig. 6.7(b)

Table 6.1 Lyapunov exponents and dimension for several values of damping

Q	λ_1	λ_3	$\sum_{i=1}^{3}\lambda_i$	$-1/Q$	$d_L = 2+\frac{\lambda_1+\lambda_2}{\lvert\lambda_3\rvert}$
4.0	0.16	−0.42	−0.26	−0.25	2.38
3.7	0.16	−0.43	−0.27	−0.27	2.37
3.0	0.11	−0.44	−0.33	−0.33	2.25
2.8	0.09	−0.45	−0.36	−0.36	2.2
2.0	0.12	−0.58	−0.46	−0.5	2.2

calculated dimension using the box counting technique for the two-dimensional attractor—see Fig. 6.14—and found that $d_c \approx 1.4$. For the three-dimensional attractor the corresponding dimension would be $d_c \approx 2.4$, a value that is similar to those shown in Table 6.1)

As Q increases the damping diminishes and the pendulum has freer motion in both real space and in phase space. Therefore the attractor is more open and fuller, and its dimension increases with less damping. We have seen that Lyapunov exponents, fractal dimension, and pendulum dynamics are all intimately connected. While our focus is on the pendulum it is useful to note that other nonlinear dynamical systems exhibit these same SIC properties and lead to fractal geometries that are susceptible to similar analyses. On a more speculative note, we might ask whether fractal geometry leads to SIC. Does the appearance of fractal geometry—such as in tree leaves, spiral galaxies, and coastlines—suggest a mechanism of nonlinear chaotic dynamics as the functional source of this geometry? The relationship of the pendulum's damping to geometry may indicate the operation of similar dissipative mechanisms in these other diverse phenomena.

However, we return to the pendulum and look at further connections between geometric properties and dynamics.

6.4.4 Information and prediction

The notion of information is related to the thermodynamic concept of entropy. Entropy is the measure of disorder or uncertainty in a closed system. Information, or more precisely *missing information*, is also a measure of uncertainty in a system. For example, suppose there is a system which may be in one of two states, A and B. If one knows that the system is in state B, then there is no missing information. On the other hand, if the state of the system is completely unknown, and one must assume that A or B is equally likely, then we say that there is 1 bit of missing information. Intermediate between these two possibilities might be a condition where we know that A is twice as likely as B. Then the associated probabilities are $p_A = 2/3$ and $p_B = 1/3$. In this case the missing information is equal to 0.918 bits. Again, if $p_A = 9/10$ and $p_B = 1/10$ then the missing information is equal to 0.465. All of these results may be calculated from the formula

$$I = -(p_A \log_2 p_A + p_B \log_2 p_B). \tag{6.24}$$

The use of the base 2 for the logarithm is typical of information theory. However, in nonlinear dynamics the base e is more commonly used. We follow that practice here and define the missing information as

$$I(t) = -\sum_{i=1}^{n} p_i(t) \ln p_i(t). \tag{6.25}$$

For a dynamical system, the probabilities for the system's configuration may change in time. Consider three cases. If the system is *deterministic* and *nonchaotic*, then if the system is known initially, it will be known for all time. For example, if the system's starting configuration is confined to a small number of states, W then its starting information is $\ln W$. As time goes on the state of the system is exactly predictable and therefore the time evolution of the small number of initial states is known precisely. Thus the entropy starts at a constant value and remains equal to that value, and therefore

$$I(t) = I(0) = \text{constant}. \tag{6.26}$$

The other limiting case is the *random* system. Again the system can be started in a specific state. But after some transient epoch, the system will randomly travel through all possible states. After these initial moments, the system's specific configuration always remains unknown. Therefore the missing information becomes and remains infinite for all time:

$$I(t) = I(0) + \infty. \tag{6.27}$$

The intermediate *deterministic* case is the *chaotic* system. As in the previous deterministic case, the initial state is known and the initial information is constant. This condition may be represented by a set of points in phase space all being located in a small region. However, SIC now causes a gradual increase in uncertainty. One can imagine the points in phase space beginning to spread and a measure of this spread is the system's positive Lyapunov exponent. Thus the spreading into other states after a time t is proportional to $e^{\lambda_+ t}$, where λ_+ is the positive Lyapunov exponent. (More generally the increase in possible (but unspecified) states would be proportional to $e^{\Sigma \lambda_+ t}$ where the sum is taken over all positive Lyapunov exponents.) If the "size" in phase space of the initial state, or equivalently the number of states, is taken as ϵ then after time t the number of states is $\epsilon e^{\lambda_+ t}$. Assuming all states are equally probable we see that the information develops in time according to

$$I(t) = \ln (1/\epsilon) + \lambda_+ t. \tag{6.28}$$

In general, it has been shown for many chaotic systems that the information change is linear (Atmanspacher and Scheingraber 1987)

$$I(t) = I_0 + Kt, \tag{6.29}$$

where K is called the *Kolmogorov entropy*. (Note that the Kolmogorov entropy is really a rate of change of entropy.) Under many circumstances (Grassberger and Procaccia 1983) it is reasonable to suppose that $K \approx \sum \lambda_+$

and therefore knowledge of the positive Lyapunov exponents can give some estimate of the time variation of the information content of a system. If $K = 0$ then the system is deterministic and nonchaotic, if $K =$ constant, then the system is deterministic and chaotic, and if $K = \infty$, then the system is random. For the chaotic pendulum, one typical set of pendulum parameters gave $\lambda_+ \approx 0.16$, thus providing some measure of the growth of uncertainty.

Growth in uncertainty implies a limitation on the ability to predict the future behavior of the chaotic pendulum. Such uncertainty is very familiar to all those who follow weather reports. In such reports we often see the initial uncertainty in the knowledge of present weather conditions amplified into a much larger uncertainty in what seems to be a relatively short time. While we probably do not know the values of the positive Lyapunov exponents for weather systems, we can make some predictions for simple systems like the pendulum.

Calculation of Lyapunov exponents for growth and decay of a phase volume are made over times that are short compared to the time required to traverse the phase space. Once the ball of initial conditions has stretched to a size comparable to that of the attractor, the ball typically folds over, and the stretching and shrinking process begins again. Thus the prediction time T is approximately the time taken for a set of points in small volume of phase space to diverge to the boundaries of the phase space of size, say L. In one dimension, $L \approx \Delta e^{\lambda_+ T}$ where Δ is the initial linear dimension of the phase volume. Therefore the prediction time, T is given by

$$T = \frac{\ln(L/\Delta)}{\lambda_+} = \frac{\ln(L/\Delta)}{K}. \tag{6.30}$$

We can obtain some idea of this prediction time for the pendulum. Suppose that the initial linear dimension, or uncertainty in the dynamical coordinates, is about one, one hundred millionth of the attractor size. With $\lambda_+ = 0.16$ we obtain a prediction time of about 115 in the dimensionless time units used in Eq. (6.3), which is about 12 forcing cycles. This prediction is tested by the simulation in Fig. 6.22 where two pendulums are started with the above, very small, difference in one of their initial coordinates. The figure shows that after about a dozen forcing cycles the two time series start to come apart, as predicted.

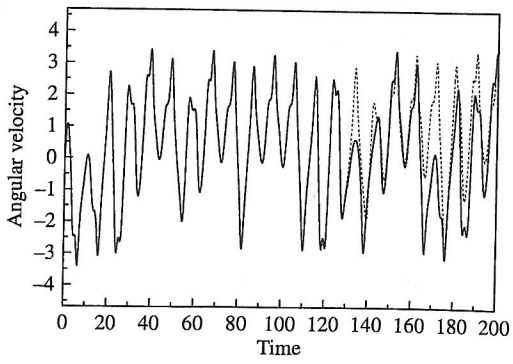

Fig. 6.22
Two angular velocity time series (one solid, one dotted) with a difference between their initial angles of one part in 10^8.

One goal of science is to develop models of reality that will predict the future. Some theories seem to work amazingly well. For example, astronomers can predict the motions of the planets hundreds of years into the future. On the other hand meteorologists seem unable to achieve anything more than approximate short term weather forecasts and very approximate long term forecasts. Similarly, accurate long term prediction of the future of chaotic systems is not possible. But within this constraint, scientists have built up a series of methods in their efforts to enhance the prediction of chaotic systems. There are two aspects to this problem. In our treatment of prediction of the pendulum's motion we have used the model provided by the deterministic differential equation. The accuracy of any prediction then depends strongly on the degree of specificity of the initial state, as indicated by Eq. (6.30). Such specificity can theoretically go well beyond that which is possible from experimental data. A more realistic approach is to consider the problem of prediction from a set of experimental data. This data may be such that there is no corresponding mathematical model or, if there is such a model, it may be approximate at best. This latter problem has led to a great deal of interesting work which is really beyond the scope of this book. (The interested reader is referred to the paper by Abarbenal et al. (1990) and the book by Weigend and Gershenfeld (1994).) For the pendulum, two of the simpler methods are discussed in Baker and Gollub (1996) and applied to data from the Blackburn pendulum. Ingenious as some of these methods are, the fundamental limitation described by Eq. (6.30) is still the best that can be done. Thus, despite the fact that chaotic systems are deterministic as to the causes of their motions, we have yet another confirmation that they are unpredictable.

6.4.5 Inverting chaos

Model equations, such as that for the pendulum, are often used to simulate chaotic data. But let us turn the process around and consider the more challenging task of fitting of model equations to chaotic data, especially real, experimental chaotic data. In this final section of this chapter, we briefly describe this "inverse" problem.

A real pendulum, such as the design of Blackburn and Smith, produces data which roughly approximates simulated data from a computerized solution of the model differential equation. Figure 6.3 shows simulated and experimental data for the pendulum. In order to obtain experimental data, the physical characteristics of the real pendulum are first calibrated according to the parameters (Q, A, ω_D) used in the model equation. Then the settings are adjusted so that the parameters of the real pendulum are as close as possible to those used in the model equation, (Q, A, ω_D). The real pendulum and the simulated pendulum then produce data sets for comparison. Minor discrepancies between the two pictures may be due to a variety of sources: perhaps the model equation does not exactly represent the dynamics of a real pendulum, or perhaps there are effects that result from flaws in the manufacture of the

pendulum, or perhaps there are limitations on the quality of the parts. Nevertheless, the agreement between the simple nonlinear simulation and the data produced by a complex mechanical and electronic pendulum is quite good.

Now let us suppose that one does *not* have a calibration of the real pendulum. Is there some way that the parameters of the model pendulum, given by the differential equation, could be determined? This question is part of a larger question in science. Can experimental data help to determine a theoretical model of some phenomenon? In chaotic dynamics, much effort has gone into such work. Sometimes the equations of motion are not known and one is starting only with the data (Brown et al. 1994). In other cases, information about the model is sufficient to suggest equations of motion but the values of the parameters of the equation set are not known (Parlitz 1996). This latter situation is the case for the driven pendulum. A good set of equations of motion is known. Thus one can test an inversion method, a method to obtain the equation parameters, by using data sets from a real chaotic pendulum. The statistical method of *least squares fitting* is the mathematical basis for the study of the pendulum inversion problem (Baker et al. 1996).

As we will see, the set of *three* parameters (Q, A, ω_D) is not sufficient for this work and therefore we use a modified dimensionless equation,

$$\omega' = -\alpha\omega - \beta \sin\theta + \gamma \sin(\delta t + \phi). \tag{6.31}$$

with *five* unknown parameters (α, β, γ, δ, ϕ). The two extra unknown parameters account for our lack of knowledge (a) of the pendulum's natural frequency and (b) of the initial phase of the pendulum. In the test of this inversion process, only the range of possible experimental values is known, as shown in Table 6.2

Table 6.2 Range of possible experimental parameters

$2 < \alpha < 10$
$60 < \beta < 100$
$80 < \gamma < 200$
$0 < \delta < 12$
$0 < \phi < 2\pi$

The real pendulum produces a set of data points $\{\omega_i, \theta_i\}$ each data pair being separated by a time of $\Delta t = 0.007$ s. The "experimental" angular acceleration ω'_i is calculated by a standard finite difference approximation defined as

$$\omega'_{i\text{Expt}} = \frac{-\omega_{i+2} + 8\omega_{i+1} - 8\omega_{i-1} + \omega_{i-2}}{12\Delta t} \tag{6.32}$$

Least squares fitting is a technique whereby one minimizes the sum of all the differences between the "experimental" value of $\omega'_{i\text{Expt}}$ and the value of ω'_i using the right side of Eq. (6.31). That is, the sum

$$S = \sum_{i=1}^{n} \left[\omega'_{i\text{Expt}} - (-\alpha\omega_i - \beta \sin\theta_i + \gamma \sin(\delta t_i + \phi))\right]^2 \tag{6.33}$$

is minimized with respect to each parameter by setting

$$\frac{\partial S}{\partial \alpha} = 0, \frac{\partial S}{\partial \beta} = 0, \text{ etc.} \tag{6.34}$$

Differentiation with respect to the set (α β γ) leads to linear equations in these parameters which may be solved to give complex but closed form

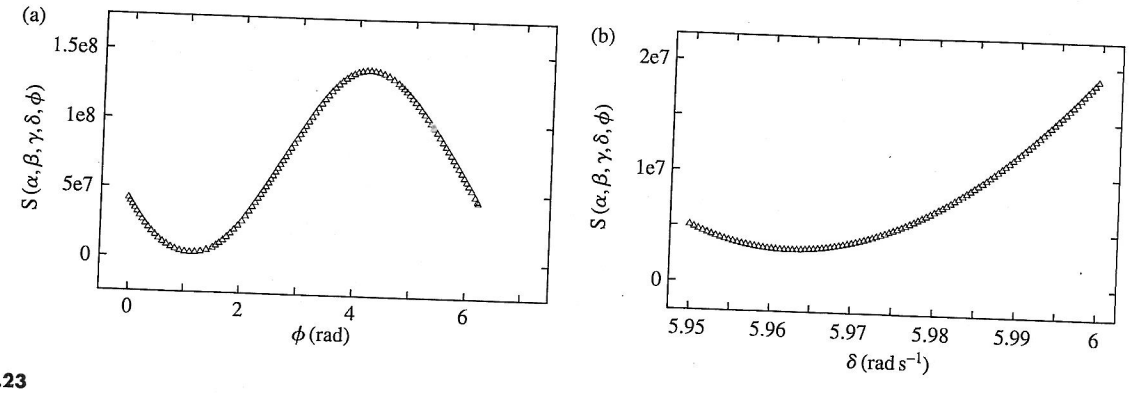

Fig. 6.23
Minima of the graphs are used to determine the best values for δ and ϕ. (Reprinted with permission from Baker et al. (1996, p. 531). ©1996, by the American Institute of Physics.)

expressions for these parameters in terms of the data sets $\{\omega_i, \theta_i\}$. On the other hand, equations involving the parameters δ and ϕ are nonlinear and it is not possible to find a closed form expression for these parameters. Therefore the process of determining all five parameters requires several steps.

As a first step the experimental time series is subjected to a fast Fourier transformation. The transform gives the spectrum of all frequencies present in the data and the experimental data has an appearance similar to the spectrum shown in Fig. 6.8. The forcing frequency δ is a strong component and therefore a first estimate of its value is provided by the spectrum. The other problematic parameter ϕ, the phase of the time series is not especially sensitive to values of α, β, and γ. Using the newly acquired estimate of δ and almost any reasonable values of (α, β, γ) it is possible to look for a minimum in S as a function of the phase ϕ. The estimates of δ and ϕ are then used together with the linear equations for (α, β, γ) to determine a first estimate for all five parameters. Now all parameter values can be further refined by iteration of the process of minimizing S as a function of each parameter. Figure 6.23 shows minimization graphs for δ and ϕ.

This procedure was followed by the authors in an effort to find parameters that would best fit real experimental data. The final results from the successive iterations are given in Table 6.3. The experimental values were known only to one of us (JAB) while the analysis was being carried out by the other (GLB).

The agreement between the two parameter sets is quite good although not perfect. In a previous section we discussed the Lyapunov exponents and fractal dimension of an attractor. Data from the real pendulum and data from a simulated pendulum with the "fitted" parameters both provide attactors. The corresponding Lyapunov exponents and dimensions of the attractors should match if the simulation accurately models the experiment. Table 6.4 provides a comparison of these geometric "invariants," and the agreement is very good. How well the fitting process works depends upon the number of points and upon the amount of noise on the data. Various tests involving both factors were conducted and, within certain

Table 6.3 Comparison of experimental and fitted parameters

Parameter	Exp. value	Fitted (from exp. data)
α(rad s^{-1})	2.24±0.1	2.12
β(rad s^{-2})	80.6±0.1	76.1
γ(rad s^{-2})	121±6	117
δ(rad s^{-1})	5.98±0.02	5.96
ϕ(rad)	unknown	1.05

Table 6.4 Comparison of experimental and simulated values of dimension and positive Lyapunov exponent

	Exp. data	Simulated data
Dimension	2.2±0.15	2.1±0.1
Positive Lyap. Exponent	0.9±0.1	0.9±0.1

limits, the fitting process is found to fairly robust against noise and small data sets. Thus the combination of Least Squares, FFT, and iteration led to a successful "inversion process." The data successfully "predicted" the model equations—or at least the parameter values.

The chaotic pendulum exhibits a variety of unusual and surprising phenomena, including beautiful strange attractors and felicitous connections between geometry and dynamics. Further effects appear when pendulums are coupled together as in the next chapter.

6.5 Exercises

1. Use the transformations of Eq. (6.2) to convert Eq. (6.1) to Eq. (6.3).
2. Periodic motion often changes to chaotic motion because of increased forcing of the dynamical system. In many cases, subharmonics of the original frequency of the forcing or even the natural frequency of the system become more prominent. With increased forcing, more and more subharmonics are created until the system destabilizes and becomes chaotic. The musical scale can also provide examples of subharmonics. For example, period doubling of middle C whose frequency is 256 Hz (scientific scale) leads to the first subharmonic of 128 Hz that is the C one octave below middle C. For 256/3 Hz there is period tripling and the musical note is the "F" below the lower C. Calculate the frequencies of all the subharmonics down to 256/16. Refer to the *Handbook of Physics and Chemistry* to determine which of the subharmonics correspond to real musical notes. Use the "scientific" or "just" scale.
3. Find the Fourier transform $a(\omega)$ of the function

$$\begin{aligned} f(t) &= 0, \quad t < -b \\ &= c, \quad -b \le t \le b \\ &= 0, \quad t > b. \end{aligned}$$

Sketch the graphs of $f(t)$ and $a(\omega)$. What is the width Δt of the graph of $f(t)$? Define the width $\Delta\omega$ of $a(\omega)$ as the distance between the two zeros on either side of the line, $\omega = 0$. Calculate $\Delta\omega$ and find the product of the two widths. Note that the product is independent of either separate width. This observation is generally true. This product illustrates the mathematical basis of the uncertainty principle of quantum physics.

4. *Fixed points* in phase space are important in the study of dynamics. These are points in phase space where the time derivatives of the variables vanish. Suppose we write the dimensionless equation for the damped, but not driven, pendulum as

$$\frac{d\dot{\theta}}{dt} = -\frac{1}{Q}\dot{\theta} - \sin\theta$$
$$\frac{d\theta}{dt} = \dot{\theta}$$

and consider the phase portrait which, for this system is given in Chapter 3 as Fig. 3.21. From that diagram or a consideration of the equations find the fixed points. Note that there are two kinds of points. One kind corresponds to the pendulum bob being at the top of its motion and therefore unstable, and the other kind corresponds to the pendulum bob being at the bottom of its motion and therefore stable. We noted in Chapter 3 that this latter point is called an *attractor* and the former point is called a *saddle point*.

5. A *Bifurcation diagram* shows that as the amplitude of the driving force for the pendulum is increased, more and more subharmonics occur. The transition

points are known as *bifurcation points*. While location of these bifurcation points are often impossible to predict, the following simple (nonpendulum) model illustrates their basic characteristics. Consider the curve in phase space

$$\dot{\theta} = f(\theta) = \theta^2 - h.$$

(a) Graph $f(\theta)$ in phase space. (b) For $h > 0$ what are the roots of $f(\theta)$? Note that these roots are the fixed points of the equation. (c) The behavior of $f(\theta)$ near the fixed points (roots) may be approximated by a linear Taylor series. For the ith root θ_i this approximation is $f(\theta) \approx f'(\theta_i)(\theta - \theta_i)$. Using your answers to (b) for θ_1 and θ_2, write the two linearized equations for $f(\theta)$. (d) Now let us examine the stability of the fixed points. First, near a fixed point, we define a new variable $\eta = \theta - \theta_i$ and look at whether this small deviation from the fixed point increases with time. If the deviation η does increase then the fixed point is unstable. If the deviation decreases then the fixed point is stable. Thus $d\eta/dt = d(\theta - \theta_i)/dt = \dot{\eta} \approx f'(\theta_i)\eta$. The sign of $f'(\theta_i)$ determines whether the system will regress toward or away from the fixed point. Find and solve the linearized differential equations for η near each of the fixed points. Determine the stability of each fixed point. (e) Now consider the changes in the model curve $f(\theta)$ and, particularly, in the fixed points as the parameter h tends toward zero. The parabola gradually moves upward, its roots (the fixed points) approach each other and the origin along the θ axis. As the roots coalesce when $h = 0$, the fixed points disappear and the system has undergone a distinct change or bifurcation. Therefore $h = 0$ specifies a *bifurcation point* (See, for example, Strogatz, (1994).)

6. Calculate the fractal dimension of a Cantor set where the middle *one-quarter* is removed rather than the middle third. Follow the process shown in the text. Prove that the length of the set is zero.
7. Construct a two-dimensional Cantor set as follows. Draw a square, one unit on a side. Inside the square remove a square of sides 1/3 from the center of the original square. The result is a square that contains 8 squares of size $1/3 \times 1/3$. Now, in each of those remaining squares, remove from the center a square of size $1/9 \times 1/3$, and so on. The look will be somewhat like Swiss cheese. Sketch a few iterations of this process. (a) Find the dimension by following the limiting process in the text. Note that ε is the length of the side of the appropriate covering squares. (b) Prove that the area of the resulting set is zero.
8. The first computer generated attractor is due to the pioneering work of Lorenz (1963) who modeled the atmosphere according to the equations

$$\dot{x} = -\sigma x + \sigma y$$
$$\dot{y} = -xz + rx - y$$
$$\dot{z} = xy - bz,$$

where σ, r, and b are positive constants. Calculate the logarithmic rate of change of the phase volume, $(1/V)dV/dt$ using the formula that connects Lyapunov exponents, volume change, and the equations of motion. If the result is negative then the system is dissipative and has an attractor. The attractor in question is shaped somewhat like a butterfly and is ubiquitous in the popular literature of chaos.
9. Consider a physical system that is capable of being in one of the n states. The missing information for the system is given by $I(t) = -\sum_{i=1}^{n} p_i(t) \ln p_i(t)$. Prove that if all states are equally likely then $I(t) = \ln n$.
10. Suppose a physical system can exist in one of two states whose probabilities are $p_1 = e^{-Kt}$ and $p_2 = 1 - e^{-Kt}$. At $t = 0$, what are the values of the probabilities? At $t = \infty$, what are the values of the probabilities? What are the values of the missing information at these two times? Write the missing information as a function of time. Using a plotting program, sketch the function. For what value

of t is the missing information a maximum? Prove this result in two ways: (a) by using calculus, and (b) using the result of problem 9.

11. If the positive Lyapunov exponent for a chaotic system is $\lambda_+ = 0.1$, how big would an initial relative uncertainty of one billionth grow to be in a time of 200 (dimensionless) units?

12. Suppose a dissipative system has Lyapunov exponents of $\lambda_1 = 0.10, \lambda_2 = 0.0$, and $\lambda_3 = -0.13$. (a) Calculate the relative change in phase volume, $(V_I - V_F)/V_I$, after a time T. (b) Using the Kaplan–Yorke conjecture, calculate the dimension of the system's attractor.

13. "Inverting" chaos in the case of the Lorenz equations (given in exercise 8) is relatively straightforward since all equations for the unknown parameters, σ, r, and b are readily solvable. Use the least squares method described in the text to develop equations for the parameters in terms of sums involving the data sets $[x_i, y_i, z_i]$ and $[\dot{x}_i, \dot{y}_i, \dot{z}_i]$. Show that $\sigma = (\sum \dot{x}_i y_i - \sum \dot{x}_i x_i)/(\sum x_i^2 - 2\sum x_i y_i + \sum y_i^2)$, $r = (\sum x_i \dot{y}_i + \sum x_i^2 z_i + \sum x_i y_i)/\sum x_i^2$, and $b = (-\sum z_i \dot{z}_i + \sum x_i y_i z_i)/\sum z_i^2$.

14. The Kaplan–Yorke conjecture may also be demonstrated using the time evolution of an initial sphere of radius r as it becomes an ellipsoid (see Fig. 6.16) with semi-axes, $a = re^{\lambda_1 t}, b = re^{\lambda_2 t}, c = re^{\lambda_3 t}$, where $\lambda_1 > 0, \lambda_2 = 0, \lambda_3 < 0$, as with the pendulum. Start from Eq. (6.20) and let the elemental volume be a sphere of volume $4\pi c^3/3$. Then follow the corresponding derivation in the text to arrive at the Kaplan–Yorke conjecture. (Hint: the volume of an ellipsoid is $V = 4\pi abc/3$.